THE UNIVERSITY OF NOTTINGHAM
DEPARTMENT OF ELECTRICAL AND ELECTRONIC ENGINEERING

Antenna Array Geometries and Algorithms for Direction of Arrival Estimation

by Hao Xiong, BEng.
Supervised by Dr. Kristof Cools

Thesis submitted to the University of Nottingham for the degree of Master of Science (by Research) in Electromagnetics Design

SEPTEMBER 2012

Abstract

Direction of arrival (DOA) estimation with the antenna array was a forever topic of scientist. In this dissertation, a detailed comparison of the direction of arrival (DOA) estimation algorithms, including three classic algorithms as MUSIC, Root-MUSIC and ESPRIT, was performed and an analysis of various array geometries' (configurations) properties in DOA estimation was demonstrated. Cramer-Rao Bound (CRB) was used for theoretic analysis and Root Mean Square Error (RMSE), which determined the best performance for a given geometry, regardless the specific estimation algorithm used, was implemented in simulation comparison.

In the first part, MUSIC, Root-MUSIC and ESPRIT were illustrated, where theoretic underlying of the algorithms were expressed by revisited, paseudo code algorithms, and compared in the aspects of accuracy and computational efficiency. Consequently, ESPRIT was found more efficient than the other two algorithms in computation. However, the accuracy of MUSIC was better than ESPRIT.

In the second part, four particular array geometries, including Uniform Circular Array (UCA), L Shaped Array (LSA), Double L Shaped Array (DLSA) and Double Uniform Circular Array (DUCA), were analyzed in the area of directivity, accuracy and resolving ability. A simulation comparison of DOA estimation with these four array geometries by MUSIC algorithm in two dimensions was made then, since MUSIC had the best accuracy in these three algorithms. According to the analysis and comparison, it was found that L

Shaped Array (LSA) and Double L Shaped Array (DLSA) were more accurate than others, considering both azimuth and elevation estimation. Also, in the case of two dimensional DOA estimation, the Double L Shaped Array (DLSA) was shown a theoretically relative isotropy to other array geometries. From the simulation, the detection ability of Double L Shaped Array (DLSA) was proved the best in the array geometries discussed in this dissertation.

These findings had significant implications for the further study of the array geometry in DOA estimation.

Acknowledgement

It is a pleasure to thank all of those who made this thesis possible. Firstly, I would like to thank my supervisors, Dr. Kristof Cools and Dr. Ana Vukovic, for their excellent guidance, support and encouragement. I have been greatly inspired by their insightful knowledge and expertise. Special thanks are owed to Professor Trevor Benson and Dr. Steven Greedy for their assistance and suggestions. It has been a great pleasure working with the people in GGIEMR. This thesis would not have been possible without the input from all of them.

The moral support from my friends and family has greatly motivated me and I would like to show my gratitude to them for their wonderful love and support. I sincerely thank my parents, Aiping Wu and Muchun Xiong, who have given me the chance to research.

List of Acronyms

1D	One dimensional
2D	Two dimensional
3D	Three dimensional
BER	Bit Error Rate
CRB	Cramer-Rao Bound
CRLB	Cramer-Rao Lower Bound
DLSA	Double L Shaped Array
DOA	Direction of Arrival
DUCA	Double Uniform Circular Array
ESPRIT	Estimation of Signal Parameters via Rotational Invariance Techniques
LSA	L Shaped Array
ML	Maximum-likelihood
MLM	Maximum-likelihood Method
MUSIC	Multiple Signal classification
MVDR	Minimum Variance Distortionless Response
QoS	Quality of Service
RA	Rectangular Array
RMSE	Root Mean Square Error
SNR	Signal to Noise Ratio
TD-SCDMA	Time Division-Synchronous Code Division Multiple Access
ULA	Uniform Linear Array
UCA	Uniform Circular Array
WSF	Weighted Subspace Fitting

YSA	Y Shaped Array

List of Symbols

A	Magnitude of the wave function
A_0	Peak magnitude of the oscillation
$\boldsymbol{A}$	Relation among array elements matrix
$\vec{a}(\varphi_d, \theta_d)$	Steering vector
$\vec{B}$	Magnetic field
$\boldsymbol{B}$	Configuration matrix
c	Speed of light
D	Number of resources
d	Ordinary Euclidean distance
E[ ]	Expectation operator
$\boldsymbol{E}$	Eigenvector matrix
$\boldsymbol{E_N}$	Noise subspace matrix
$\vec{E}$	Electric field
$\boldsymbol{F}$	Null-space matrix
$\boldsymbol{Fi}$	Incident signals matrix
$\boldsymbol{I}$	Identity matrix
Inf	Fisher information function
$\vec{K}$	Wave vector
k	Number of wave
$\vec{l}_m$	Location of elements vector
M	Number of array elements
n	Noise signal
p	Probability density function

$\boldsymbol{R}$	Covariance matrix
$\vec{r}$	Radius vector
T	Efficiency of CRB
$\boldsymbol{T}$	Transition matrix
$\boldsymbol{U}$	Incident angle matrix
$\boldsymbol{V}$	A random vector
$\vec{V}_d(\varphi_d, \theta_d)$	Unit vector pointing towards the dth source
$\boldsymbol{W}$	White random vector
$\boldsymbol{X}$	Received data complex vector
μ_0	Permeability
ε_0	Permittivity
λ	Wavelength of the wave
λ_e	Eigenvalue
ω	Wave's angular frequency
φ	Wave phase shift with the units of radians
θ	An unknown deterministic parameter
Δ	Inter element spacing
$\boldsymbol{\Delta}$	Subarray location matrix
$\Delta_m(\varphi_d, \theta_d)$	Propagation delay of source signal
σ^2	Variance
μ	Mean
s	Varying amplitude function
S	Power spectral density function
δ	Impulse function
var	Function of variance

(φ, θ)	Incident angle

Contents

Chapter 1 Introduction

In this chapter, we will introduce the development of smart antenna at first, and then demonstrate the outline of this dissertation.

1.1 The development of Smart Antenna

The static magnetic and electrostatic phenomenon was noted by human attention very early by Chinese ancient when the phenomenon that the magnet attracts iron and magnet guides friction electricity had been found. The system study of these phenomena began in the 16th century. In 1600s, British physician William Gilbert (William Gilbert, 1544 ~ 1603) concluded the previous research on magnetic thorough discussion of the nature of the geomagnetic records of a large number of experiments, and the magnetic transition formed experience to science.

Then, the basic theories of electromagnetism were developed by many physicists in the 19th century. The Maxwell equations were unified by a set of equations of all these work, and revealed the nature of light as an electromagnetic wave. J.C. Maxwell set the theoretical basis for the development of electromagnetism. He stated the theory of electric and magnetic fields travelling through space, and cleared the way for smart antenna.

We can never ignore Guglielmo Marconi, the Italian engineer. He specialized in the development of radio equipment and improvements and won the 1909 Nobel Prize in Physics. In the spring of 1895, the use of electromagnetic waves for communication was tested, but failed because of the unsuccessful funding request to the Italian government. In 1896, the 14.4 km communications test was successfully carried out in the UK and patented. In 1897, he conducted a series of radio communication experiment, and set up a wireless telegraphy Company named after Marconi in London. In 1901, Marconi's research team received the first transatlantic radio signal sent from the United Kingdom in Newfoundland. In 1932, he found high-frequency waves.

Besides the electromagnetic waves, the knowledge of antennas was essential in the development of smart antenna. Edison was one of the first to use antennas,

which are arrangements of conductors that generate a radiating electromagnetic field when an alternating voltage is applied [1]. The antenna was an instrument for transmitting or receiving radio waves, or in a more general work, it was a term of electronic devices of electromagnetic waves. The antenna was used in radio and television broadcasting, radar, point-to-point (P2P) wireless communication, and space exploration systems. In the physical perspective, the antenna was a combination of one or more conductors, which can generate associated radiated electromagnetic field by applying alternating voltage of the alternating current. Also, it could be placed in the electromagnetic field and generated an alternating current and an alternating voltage at its terminal due to the induction field inside in the antenna.

The first type of smart antenna was the side lobe canceller developed at GE in the late 1950's [2]. As figure 1.1 shows, with the help of low gain, broad beam antennas working as side lobe cancellation, side lobe cancellers have high gain antennas for receiving the wanted resource accompanied.

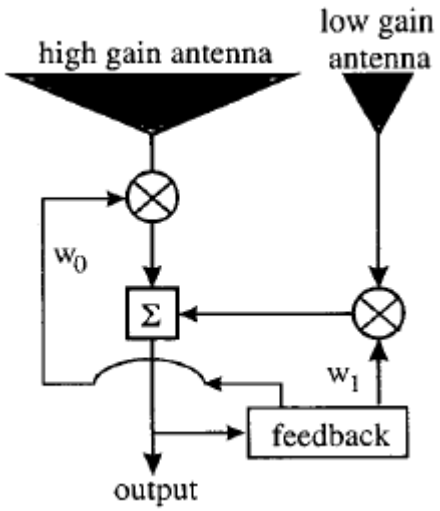

Figure 1.1 Single Howells-Applebaum loop for a sidelobe canceler [2]

Then researchers proposed the antenna array, which was a combination of antenna elements, and it was able to form beams by electronically adjusting the excitation at the antenna elements. With the combination of applications, signal processing algorithms, a correct electromagnetic model of an antenna array, the smart antenna was delivered to the electromagnetic world, and it will be the subject of this dissertation.

1.2 Smart Antenna in present age

Since the 1990s, the array processing technology came into the field of mobile communications, and soon formed a new research focus - smart antenna. Smart antennas are widely used with its unique advantages in improving the quality of system communication, easing wireless communication growing contradiction with the lack of spectrum resources, reducing the overall system cost and improving system management.

Smart antennas are devices which adapt their radiation pattern to achieve improved performance – either range or capacity or some combination of these [3].

The rapid growth in demand for mobile communications services has encouraged research into the design of wireless systems to improve spectrum efficiency, and increase link quality [4]. Using existing methods more effective by the smart antenna technology and developing its potential, we can significantly increase the wireless. With intelligent control of signal capacity and coverage, transmission and reception of the mobile network, communications applications can be greatly improved.

In the communication system, the ability to distinguish different users is essential. We can add increased spatial difference with the help of the smart antenna, which is referred to as Space Division Multiple Access (SDMA). Conventionally, employment of the most common multiple access scheme is a Code Division Multiple Access (CDMA), Time Division Multiple Access (TDMA), and frequency division multiple access (FDMA).

Potential benefits of the smart antenna show in many ways, such as anti-multipath fading, reducing the delay extended to support smart antenna holding high data rate, interference suppression, reducing the distance effect, reducing the outage probability, to improve the BER (Bit Error Rate)performance, increasing system capacity, to improve spectral efficiency, supporting flexible and efficient handoff to expand cell coverage, flexible management of the district, to extend the battery life of mobile station, as well as lower maintenance and operating costs.

1.2.1 Smart Antenna and Antenna Array

In strict definition, smart antennas are proper combination of antenna arrays and smart signal processing algorithms and software. Smart antennas are widely used in Direction of Arrival (DOA) estimation, beamforming, and communication, so there are an increasing number of researchers furthering the research of smart antenna.

As researchers' common view, the research of antenna arrays is part of smart antennas research. However, in some cases, smart antennas and antenna arrays can replace each other. For instance, in this dissertation, we discuss MUSIC, which is a DOA estimation algorithm of smart antennas, or we can say that MUSIC is a DOA estimation algorithm of antenna arrays. Therefore, the smart antenna and the antenna array may have the same usage in this dissertation.

1.2.2 Types of Antenna Array

The environment and the system's requirements decide the type of Antenna Array. There are two main types of Antenna Array. They are as follows:

Phased Array Antenna

In this type of smart antenna, there will be a number of fixed beams between which the beam will be turned on or steered to the target signal. This can be done, only in the first stage of adjustment to help. In other words, as wanted by the moving target, the beam will be the Steering [3].

Adaptive Array Antenna

Integrated with adaptive digital signal processing technology, the smart antenna uses digital signal processing algorithm to measure the signal strength of the beam, so that the antenna can dynamically change the beam which transmit power concentrated. The application of spatial processing can enhance the signal capacity, so that multiple users share a channel.

Adaptive antenna array is a closed-loop feedback control system consisting of an antenna array and real-time adaptive signal receiver processor, which uses the feedback control method for automatic alignment of the antenna array pattern. It form nulling interference signal offset in the direction of the

interference, and can strengthen a useful signal, so as to achieve the purpose of anti-jamming [4].

1.2.3 Advantages and disadvantages of Antenna array

In this section, we will introduce the characteristics of the antenna array.

Advantages

First of all, a high level of efficiency and power are provided by the smart antenna for the target signal. Smart antennas generate narrow pencil beams, when a big number of antenna elements are used in a high frequency condition. Thus, in the direction of the target signal, the efficiency is significantly high. With the help of adaptive array antennas, the same amount times the power gain will be produce, on condition that a fixed number of antenna elements are used.

Another improvement is in the amount of interference which is suppressed. Phased array antennas suppress the interference with the narrow beam and adaptive array antennas suppress by adjusting the beam pattern [3].

Disadvantages

The main disadvantage is the cost. Actually, the cost of such devices will be more than before, not only in the electronics section, but in the energy section. That is to say the device is too expensive, and it will also decrease the life of other devices. Since the use of the RF electronics and A/D converter for each antenna, the costs are increasing.

Moreover, the size of the antenna is another problem. Large base stations are needed to make this method to be efficient and it will increase the size, apart from this multiple external antennas needed on each terminal.

1.3 Comparison of Antenna Array and Ordinary Antennas

In the section, we compare the some properties (space, frequency and time) between Antenna Array and Ordinary Antennas, and demonstrate why we discuss Antenna Array in DOA (Direction of Arrival) estimation.

1.3.1 Efficiency and Power in space

As the introduction in section 1.2.2, a higher level of efficiency and power are provided by the antenna array with proper software system than ordinary antenna for the target signal. The fact is that Antenna Array can generate narrow pencil beams in the target direction. However, ordinary antennas can generate pencil beams in fixed directions or relative similar power in all directions. In the case of DOA estimation, target resources come from random directions, so both ordinary antennas generating pencil beams in fixed directions and generating similar power in all directions cannot prove as strong power and high efficiency as antenna array does in the directions of resources, on condition that a fixed number of antenna elements and same total power are used. Therefore, with higher efficiency and stronger power, antenna array is more appropriate in DOA estimation that ordinary antennas.

1.3.2 Efficiency and power in Frequency

Frequency Spectrum detection and utilization is the fundamental problem of mobile communication development. Traditionally, antennas' patterns change with frequency, which means ordinary antennas generate different power in a particular direction in various frequencies. Therefore, the DOA estimation power of ordinary antennas is excellent in some frequencies and is poor in some frequencies as well. On the contract, antenna array can adapt to various frequencies and focus the majority of its power in resources directions by software control. Thus, theoretically, antenna arrays have a higher efficiency and flexibility than ordinary antennas in different frequencies.

1.3.3 Estimation Time

Antenna Arrays can estimate recourses directions in greatly shorter time than ordinary antennas. It is common that Ordinary antennas detect DOA of resources by mechanic movement, focusing pencil beams on the directions of signals. But antenna arrays do not need to move. Antenna arrays can replace the mechanic movement of ordinary antennas by digital calculation. In most case, mechanic movement of ordinary antenna cost a long time, especially for

large antenna. Thus, antenna arrays are more efficient in time than ordinary antennas in DOA estimation.

1.3.4 Capacity and Quality of Service (QoS)

Antenna Array can improve the capacity and quality of service of DOA estimation and communication from ordinary antennas. Examples are not rare in nowadays. TD-SCDMA system is a typical example of the application of antenna array technology. TD-SCDMA system is Time Division Duplex mode, so that the upper and lower radio frequency channel can be completely symmetric. It can be addressed problems of ordinary antennas, such as antenna uplink and downlink beamforming, anti-multipath interference simultaneously. Definitely, with the help of relay switch of frequency and space, antenna array can reduce the waste of resources of the frequency channel and improve the capacity from ordinary antennas.

1.3.5 Conclusion

In general, antenna arrays have higher efficiency in space, frequency and time than ordinary antennas. Thus, increasing number of ordinary antennas are replaced by antenna arrays in practice, and researchers have transfer their focus on antenna arrays from ordinary antennas. Consequently, in this dissertation, we analyze the performance of antenna arrays, which is more widely used than ordinary antennas, in DOA estimation. In the case of antenna arrays, MUSIC, Root-MUSIC and ESPRIT algorithms are three significant algorithms in DOA estimation by antenna arrays and we will demestrate them in Chapter 4 in details.

1.4 Outline of this dissertation

In this dissertation, we have research the algorithms of Direction of arrival (DOA) estimation and array geometries. The main objective of this dissertation is to develop excellent array geometries for DOA estimation. In chapter 2, we demonstrate the problem which is concerned in this dissertation. In this chapter, we focus on the problem statement of direction of arrival (DOA) estimation and array configuration. Then the chapter 3 describes some background

knowledge of DOA estimation, where the definition of Maxwell's equations, plane wave, white noise, normal distribution and Cramer-Rao bound are demonstrate and forms a foundation for the rest of this work. In chapter 4 Some DOA estimation algorithms such as MUSIC, Root-MUSIC, Bartlett, Capon and ESPRIT are expressed, which proves a correct description of DOA estimation algorithms combining with the electromagnetic characteristics of an antenna array. We analyze various array geometries, such as ULA, UCA, LSA, YSA, RA, DLSA and DUCA, in chapter 5 by way of the time delay. The chapter 6 shows the simulation of the problem discussed in this dissertation, where the accuracy and computation performance of MUSIC, Root-MUSIC and ESPRIT algorithms are discussed. Furthermore, the directivity, accuracy and resolving ability of UCA, DUCA, LSA and DLSA are compared in two dimensions case in this chapter. We draw a short conclusion of this dissertation in chapter 7 and discuss the direction of future work. Each chapter starts with an introductory section, which outlines the arrangement of the chapter, followed by one or more sections in detail.

1.5 Reference

[1]Roald Goossens, "Direction of Arrival Estimation and Beamsteering using Realistic Antenna Arrays", PhD degree dissertation, September 2008.

[2]Haupt, R.L."The development of smart antennas", Antennas and Propagation Society International Symposium, IEEE Volume: 4, Page(s): 48 - 51 vol.4, 2001.

[3].L.C.Godara, "Application of antenna arrays to mobile communication II: Beamforming & direction of arrival considerations", Proceedings of IEEE, volume 85, issue 8, pages 1195-1245, August 1997.

[4].Dau-Chyrh Chang, "Smart Antennas for Advanced Communication Systems", Proceedings of the IEEE, Volume: PP, Issue: 99, Page(s): 1 – 17, 2012.

Chapter2 Problem Statement

The outline was shown in chapter1, and we will declare problems discussed in this dissertation. The problem of central interest in this dissertation is the estimation of the DOA of emitter signals impinging on a receiving array with a known finite data. In this chapter, we demonstrate the problem of DOA estimation, eigendecomposition algorithms and property of array geometries respectively.

2.1 Direction of Arrival (DOA) estimation

With the development of antenna array, the Direction of Arrival (DOA) estimation technique becomes a vital part of smart antenna. The antenna array, which receives several signals, collecting data at all its elements with combination of the spatial information, has the ability to optimally process this data and estimate the Directions of Arrival (DOA) of the impinging signals with high-resolution signal estimation algorithms. Therefore, the high-resolution DOA estimation algorithm is an essential part of smart antenna.

We can classify the parameter estimation techniques into two main categories, namely parametric and spectral-based approaches [1].Parametric techniques make a simultaneous search for all interesting parameters and with the expense of an increased computational complexity, these approaches often lead to more accurate outcomes. Spectral-based approaches form some spectrum-like function of the interesting parameters, and the locations of the highest peaks of the function are regarded as the DOA estimates.

DOA estimation is the forever topic of the researchers, and various algorithms were proposed, including Spectral Estimation Method first proposed by Bartlett [2] which estimates the DOA with the help of computing the spatial spectrum and deciding the local maximum then, Minimum Variance Distortionless Response (MVDR) Estimator which is spectrum estimation with Maximum-likelihood (ML) method by J. Capon [3], Maximum-likelihood Method (MLM) which estimates the DOA by maximizing the log-likelihood function from a given set of array samples [4], MUSIC which scans all the angle by the noise subspace proposed by Schmidt [5], MUSIC improves the solution ability by

Barabell [6], ESPRIT which promotes the computation efficiency by Roy [7], Weighted Subspace Fitting (WSF) Method which is a unified approach to schemes [8,9]. There is a large number of DOA algorithms developed from a signal processing point of view, but discussing all these techniques is beyond the scope of this chapter. Thus, we focus on the eigendecomposition algorithm, including MUSIC, Root-MUSIC and ESPRIT algorithms, which are kinds of subspace method, a part of Spectral-based approaches in this dissertation.

2.2 Performance of eigendecomposition algorithms

Eigendecomposition algorithms, as their names suggest, are DOA estimation methods which exploit the underlying information for DOA estimation by decomposing the variance matrix to get eigenvectors and eigenvalues. As for eigendecomposition algorithms, the problem concerned by this dissertation is the performance of three outstanding eigendecomposition algorithms, MUSIC, Root-MUSIC and ESPRIT in DOA estimation.

Eigendecomposition algorithms were the focus of the researchers in last three decades, and a great number of progresses were made, where include the discussion of maximum likelihood and Cramer-Rao Bound (CRB) of MUSIC by Stoica, P [10], promotion of MUSIC in two dimensions by Hung and Zhao [11, 12], the statistic performance of MUSIC by Kaveh[13], the resolution ability of MUSIC by Zhang[14], the development of ESPRIT in two dimensions[15]. Though MUSIC, Root-MUSIC and ESPRIT algorithms are developed for decades, where a lot detail of them have been researched, we try to compare some properties of them, which are necessary for the study of array geometries, in this dissertation.

2.3 Property of array geometry

It is not hard to accept that the array geometry represents the study of array continuation, which discuss and design the displacement of array elements. In this dissertation, what we are interested is the property of array geometry with given number of elements in DOA estimation. Definitely, different array configuration can lead to different characteristics in DOA estimation, and we try to find a optimal array geometry.

Actually, the study of array geometry became the peak topic in last years, which, of course, was based on the development of antenna array. Though there is not a long time for researchers, they have derived lots of outcomes, which are the basis of dissertation. In detail, Hua gave the CRB of array in two dimensions [16]. Gazzah, H showed the method of array geometry design based on CRB [17]. Baysal, U demonstrated the design of isotropic planar and three dimension array [18]. Goossens described the DOA estimation in complex array configuration [19]. The study of the array geometry is abstruse problem, so that we just intend to research some typical array geometries in this dissertation.

2.4 Reference

[1]Krim H., Viberg M., "Two decades of array signal processing research: the parametric approach", Signal Processing Magazine IEEE Volume: 13 Issue: 4 Page(s): 67-94, 1996.

[2] R. T. Lacoss, "Data adaptive spectral analysis method", Geophysics vol. 36 pp. 661–675, 1971.

[3] J. Capon, "High-resolution frequency-wave number spectrum analysis", Proc. IEEE vol. 57 pp. 1408–1418, 1969.

[4] M. I. Miller, D. R. Fuhrmann, "Maximum likelihood narrow-band direction finding and the EM algorithm", IEEE Trans. Acoustic. Speech Signal Processing vol. 38, pp. 1560–1577, 1990.

[5] R. O. Schmidt, "Multiple emitter location and signal parameter estimation", IEEE Trans. Antennas Propagat. vol. AP-34, pp. 276–280, 1986.

[6] A. Barabell, "Improving the resolution of eigenstructured based direction finding algorithms", in Proc. ICASSP Boston, MA, pp. 336–339, 1983.

[7] R. Roy and T. Kailath, "ESPRIT—Estimation of signal parameters via rotational invariance techniques", IEEE Trans. Acoust. Speech, Signal Processing vol. ASSP-37, pp. 984–995, 1989.

[8] M. Viberg and B. Ottersten, "Sensor array processing based on subspace fitting", IEEE Trans. Signal Processing, vol. 39, pp. 1110–1121, 1991.

[9] M. Viberg, B. Ottersten, T. Kailath, “Detection and estimation in sensor arrays using weighted subspace fitting”, IEEE Trans. Signal Processing, vol. 39, pp. 2436–2449, 1991.

[10]Stoica, P., Nehorai, A., “MUSIC, maximum likelihood and Cramer-Rao bound: further results and comparisons”, Acoustics, Speech, and Signal Processing, 1989. ICASSP-89., 1989 International Conference on Page(s): 2605 - 2608 vol.4, 1989.

[11]Hsien-Sen Hung, Shun-Hsyung Chang, Chieng-Hsing Wu, “3-D MUSIC with polynomial rooting for near-field source localization”, Acoustics, Speech, and Signal Processing, 1996. ICASSP-96. Conference Proceedings., 1996 IEEE International Conference on Volume: 6, Page(s): 3065 - 3068 vol. 6, 1996.

[12]Zhao Ping, Shi Haoshan, Shi Kui, “The 3D Location Algorithm Based on Smart Antennawith MUSIC DOA Estimates”, Computer Science and Information Engineering, 2009 WRI World Congress on Volume: 4, Page(s): 750 – 753, 2009.

[13]Kaveh M., Barabell A, “The statistical performance of the MUSIC and the minimum-norm algorithms in resolving plane waves in noise”, Acoustics, Speech and Signal Processing, IEEE Transactions on Volume: 34, Issue: 2, Page(s): 331 – 341, 1986.

[14]Zhang, Q.T., “Probability of resolution of the MUSIC algorithm”, Signal Processing, IEEE Transactions on Volume: 43 , Issue: 4 , Page(s): 978 – 987, 1995.

[15]Xiang Gu, Yunhua Zhang, “Effects of amplitude and phase errors on 2-D MUSICand 2-D ESPRIT algorithms in ISAR imaging”, Synthetic Aperture Radar, 2009. APSAR 2009. 2nd Asian-Pacific Conference on , Page(s): 634 – 638, 2009.

[16]Hua Y., Sarkar T.K., “A note on the Cramer-Rao bound for 2-D directionfinding based on 2-D array”, Signal Processing, IEEE Transactions on Volume: 39 , Issue: 5 , Page(s): 1215 – 1218, 1991.

[17]Gazzah H., Marcos S., “Cramer-Rao bounds for antenna array design”, Signal Processing, IEEE Transactions on Volume: 54 , Issue: 1 , Page(s): 336 – 345, 2006.

[18]Baysal U., Moses R.L., “On the geometry of isotropic arrays”, Signal Processing, IEEE Transactions on volume: 51 , Issue: 6 Page(s): 1469 – 1478, 2003.

[19]Roald Goossens, “Direction of Arrival Estimation and Beamsteering using Realistic Antenna Arrays”, PhD degree dissertation, September 2008.

Chapter3 Background Knowledge

In order to discuss eigendecomposition algorithms and array geometry, a thorough knowledge of the electromagnetic characteristics of an antenna array is essential. In this chapter, we will illustrate the knowledge of Maxwell's equations, plane wave, propagation, white noise, normal distribution and Cramer-Rao Bound respectively.

3.1 Maxwell's equations

Maxwell equations are four basic equation for the description of the electric and magnetic fields. Maxwell, a British physicist, established Maxwell equations in the 19th century. There are four differential forms of Maxwell's equations, which are often referred to as the Maxwell equations. Maxwell equations have become an integral base of the electric and magnetic fields. The equations system provides a rather complete overview of the basic laws of the electromagnetic field, and predicts the existence of electromagnetic waves.

The Direction of Arrival (DOA) estimation algorithm which may take various forms generally follows from the homogeneous solution of the wave equation [1]. For analytical need, we can start from the Maxwell's equations' solution. In free space the equation can be written as:

$$\nabla \cdot \vec{E}=0 \tag{3.1}$$

$$\nabla \cdot \vec{B}=0 \tag{3.2}$$

$$\nabla \times \vec{E} = -\frac{\partial \vec{B}}{\partial \mathrm{t}} \tag{3.3}$$

$$\nabla \times \vec{B} = \varepsilon_0 \mu_0 \frac{\partial \vec{E}}{\partial \mathrm{t}} \tag{3.4}$$

In equation 3.3 and 3.4, "×" and "." represent the "curl" and "divergence" respectively. Furthermore, vector $\vec{E}$ denotes the electric field and vector $\vec{B}$ denotes the magnetic field, while μ_0 and ε_0 are the permeability and permittivity respectively. From 3.1, the following curl property of 3.5, 3.6 results as:

$$\nabla \times \left(\nabla \times \vec{E}\right) = \nabla\left(\nabla \cdot \vec{E}\right) - \nabla^2 \vec{E} = -\nabla^2 \vec{E} \tag{3.5}$$

$$\nabla \times \left(\nabla \times \vec{E}\right) = -\frac{\partial}{\partial t}\left(\nabla \times \vec{B}\right) = -\varepsilon_0 \mu_0 \frac{\partial^2 \vec{E}}{\partial t^2} \qquad (3.6)$$

$$\nabla^2 \vec{E} - \frac{1}{c^2}\frac{\partial^2}{\partial t^2}\vec{E} = 0 \qquad (3.7)$$

Generally, the constant c is defined as the speed of light. In the case of free space, the speed of light follows from the derivation $c = 1 / \sqrt{\varepsilon_0 \mu_0} = 3 \times 10^8$m/s. The homogeneous wave equation 3.7 sets the base of the motivation to our supposed data model which will be demonstrated in later chapters.

3.2 Plane wave

In the physics of wave propagation, a plane wave is a constant-frequency wave whose wave fronts are infinite parallel planes of constant peak-to-peak amplitude normal to the phase velocity vector [2].

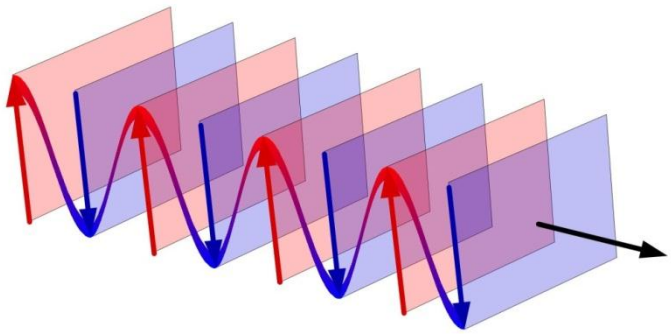

Figure 3.1 the plane wave [15]

Actually, it is impossible to get or create a rare plane wave in practice and only can a plane wave with theoretically infinite extent travel in a plane wave mode. Actually, in the localized region of space many waves are regarded as plane waves approximately, e.g., an antenna generates a field which can be regarded as a plane wave, when it is far enough from the antenna which generates the wave in its so-called far-field region. Likely, when the degree of length is greatly larger than the wave's wavelength, the wave can be regarded as plane waves.

3.2.1 Mathematical definition

We define two functions as the sine or cosine functions which meet the conditions of having constant amplitude and a constant frequency along the direction of the x axis. As the equation [2] shown below, we use the cosine function to express the case of a plane wave propagating in the positive x axis.

$$A = A_0 \cos(kx - \omega t + \varphi) \qquad (3.8)$$

The equation 3.8 defines what the magnitude and phase of the plane wave are. In the equation, A represents the magnitude of the wave at the point in space and time which are equal to x and t. k denotes the number of wave. A_0 is the amplitude of the wave and it is the peak magnitude of the oscillation. x denotes a point in the x axis. ω denotes the wave's angular frequency. t denotes a given particular point in time, and φ denotes the wave phase shift with the units of radians.

In detail, ω is also a standard of how rapid the disturbance changing in a particular length of time at a known point in space with the units as radians per unit time. It must make clear that a positive phase shift will add a shift on the wave along the negative x axis direction at a given point of time. A phase shift which equals to 2π radians means shifting it one wavelength exactly.

3.3 Propagation

Many physical phenomena are either a result of waves propagating through a medium or exhibit a wave like physical manifestation [1]. Although we only discuss one element of equation 3.7 which is a vector equation, we can define a parameter $\vec{E}$ ($\vec{r}$,t) [1] where t denotes the time and $\vec{r}$ denotes the radius vector. Assume that outputs measured by array elements are proportional to the parameter $\vec{E}$ ($\vec{r}$,t). Surely, any space of the form $\vec{E}$ ($\vec{r}$,t) = $f(t - \vec{r}^{T}\alpha)$, which will satisfy the equation 3.7, provided $|\alpha| = 1 / c$ with T representing transposition period. The function *f* depends on $t - \vec{r}^{T}\alpha$ only, but in the direction of angle α, the solution can be regard as a wave propagating with the speed $1 / |\alpha| = c$. The main idea herein is based on narrowband forcing functions. In details, in the classic book by Jordan [3] we can find the

generation of such a function. Furthermore, the paper [4] demonstrates propagation in complex notation. The waveform which is narrowband transmitted can be derived as:

$$\vec{E}(0,\mathrm{t}) = s(\mathrm{t})\mathrm{e}^{\mathrm{j}}\omega^{\mathrm{t}} \tag{3.9}$$

Here s(t) denotes the varying amplitude with time related to $\mathrm{e}^{\mathrm{j}}\omega^{\mathrm{t}}$ which is the carrier coefficient. When B represents the bandwidth of signal s(t), and $|\vec{r}| << \mathrm{c} / \mathrm{B}$, we can express as 3.10:

$$\vec{E}(\vec{r},\mathrm{t}) = s(\mathrm{t} - \vec{r}^{\mathrm{T}}\alpha)\mathrm{e}^{\mathrm{j}\omega(\mathrm{t}-\vec{r}^{\mathrm{T}}\alpha)} \cong s(\mathrm{t})\mathrm{e}^{\mathrm{j}(\omega\mathrm{t}-\vec{r}^{\mathrm{T}}\mathrm{K})} \tag{3.10}$$

In the last equation 3.10, the so-called wave vector $\vec{K}$ is used, and its magnitude $\mathrm{K} = \omega / \mathrm{c}$ is the wave number. We can also write $\mathrm{K} = 2\pi / \lambda$, where as usual, the parameter λ is the wavelength. Make sure that the direction of vector $\vec{K}$ is the same with the direction of propagation, e.g., in the x-y plane we can get:

$$\vec{K} = K(\cos\theta, \sin\theta)^{\mathrm{T}} \tag{3.11}$$

Here the parameter θ denotes the direction of propagation, which is defined as counter clockwise relative the x axis. Since an isotropic point source generates a spherical propagating wave in which the distance from the source is reciprocally proportional to the amplitude, the equation 3.9 implicitly makes an assumption of far-field conditions. The distance between the receiving antenna array and the emitters determines whether we should consider the spherical degree of the wavefront, because all points located on the surface of the sphere with radius R, which is regarded as the wavefront, share the same phase parameter. In near field reception, papers [5, 6] consider for treatments of distance. In the far field case, it implies that the radius of spherical propagation is so large that a plane wave of constant phase can be concerned. Therefore, the result and conclusion in the plane wave can be expressed in 3.9. Equation 3.9 contains both space and time information which can be used in DOA estimation or other works. We are sure that a linear space means the validity of superposition principles, and more than one propagating wave are allowed in the linear space.

3.4 White noise

White noise is defined as the noise whose power spectral density is uniformly distributed in the entire frequency domain and all frequencies have the same energy of the random noise. In another word, the white noise is a random signal with a flat power spectral density [7]. The signal contains the equal power within a particular bandwidth at the center frequency.

White noise is a power spectral density of a random signal of constant or random process. In other words, the power of the signal is the same in each frequency band. Since the white light is mixed by a variety of frequency (color) of a monochromatic light, similarly, with a flat power spectrum of this signal this nature is regarded as "white" and this signal therefore is called white noise. In opposite site, the other noise which does not have the properties mentioned above is referred to as color noise.

An ideal white noise has infinite bandwidth, and thus its energy is infinite. Actually, an infinite bandwidth white noise signal is just a theoretical construction which cannot be reached [16]. Thus, it is impossible to get an ideal white noise in the real world definitely. In practice, the bandwidth of white noise is restricted by the transmission medium, the mechanism of noise generation, and finite observation capabilities. In fact, we often regard the signal with formation of limited bandwidth as white noise, because it makes us more convenient in the mathematical analysis. If a random signal is observed with a flat spectrum in a medium's widest possible bandwidth, we will refer it as "white noise" [7]. However, the white noise is more flexible in the data treatment, so it is a powerful tool for system analysis. Usually, a noise is considered as a white noise process as long as a noise process with the spectrum width is far greater than the bandwidth of the system and the bandwidth of its spectral density are substantial constants.

Specifically, if the real and imaginary parts of noise distribution are according to a Gaussian distribution, and its power spectral density is uniformly distributed, we can define it as white Gaussian noise.

3.4.1 Mathematical definition

White random vector

A random vector $\boldsymbol{V}$ [7] is a white random vector only if its mean vector and autocorrelation matrix are corresponding to the follows:

$$\mathrm{E}[\boldsymbol{V}] = 0 \tag{3.12}$$

$$\boldsymbol{R}_{\mathrm{VV}} = \mathrm{E}[\boldsymbol{V}\boldsymbol{V}^{\boldsymbol{T}}] = \sigma^2\boldsymbol{I} \tag{3.13}$$

As above equations show, the autocorrelation matrix of white random is equal to the multiple of the identity matrix and it is a zero mean vector. We can regard it as spherical correlation, when the autocorrelation matrix is the multiple of the identity.

White random process

Only if its mean function and autocorrelation function satisfy the following equation, can a time continuous random process $\boldsymbol{V}(\mathrm{t})$ where $\mathrm{t} \in \mathrm{R}$ be regarded as a white noise signal:

$$\mathrm{E}[\boldsymbol{V}(\mathrm{t})] = 0 \tag{3.14}$$

$$\boldsymbol{R}_{\mathrm{VV}}(\mathrm{t}_1, \mathrm{t}_2) = \mathrm{E}[\boldsymbol{V}(\mathrm{t}_1)\boldsymbol{V}(\mathrm{t}_2)] = \frac{\mathrm{N}_0}{2}\delta(\mathrm{t}_1 - \mathrm{t}_2) \tag{3.15}$$

Here, when $\mathrm{t}_1 = \mathrm{t}_2$, equation 3.15 will become equation 3.13. Since its autocorrelation function is the Dirac delta function, it is clear that the process is zero mean for all time and has infinite power at zero time shift. The following power spectral density function 3.16 can be implied from the autocorrelation function 3.15.

$$S_{\mathrm{VV}}(\boldsymbol{V}) = \frac{\mathrm{N}_0}{2} \tag{3.16}$$

The Fourier transform of the delta function is equal to one. We can define it white as an analogy to the frequency spectrum of white light, because this power spectral density function 3.16 is the same with each other at all frequencies.

3.5 Normal Distribution

The normal distribution is the most important a probability distribution. The concept of normal distribution was first proposed in 1733 by the German mathematician and astronomer Moivre. However, due to the German mathematician Gauss applied it to astronomers, so the normal distribution is also called the Gaussian distribution. Gaussian impacted this work greatly on future generations, and many research outcomes attributed to the invention of the method are also base on this work.

According to the probability theory, the normal distribution is a continuous probability distribution which has a bell-shaped probability density function, known as the Gaussian function or informally as the bell curve [8].

$$p(\mathrm{x}) = \frac{1}{\sigma\sqrt{2\pi}} \mathrm{e}^{-\frac{1}{2}\left(\frac{\mathrm{x}-\mu}{\sigma}\right)^2} \tag{3.17}$$

The parameter μ is called the mean, the median or the mode of the standard distribution. The parameter σ^2 is the variance, which is a significant stand in this dissertation about DOA estimation comparison, and in any random variable case, it demonstrates the concentration degree of the distribution around its mean. Besides, the square root of σ^2 is called the standard deviation or root mean square and describes the width of the density function. The mean μ determine the centre position of the normal curve; standard deviation σ determine the normal curve steep or flat level. The standard distribution is usually denoted by N (μ, σ2) [10]. Therefore, if a random function of x is distributed normally with mean μ and variance σ^2, we can write it as 3.18:

$$\mathrm{x} \sim \mathrm{N}(\mu, \sigma^2) \tag{3.18}$$

The typical normal distribution is shown as figure 3.2:

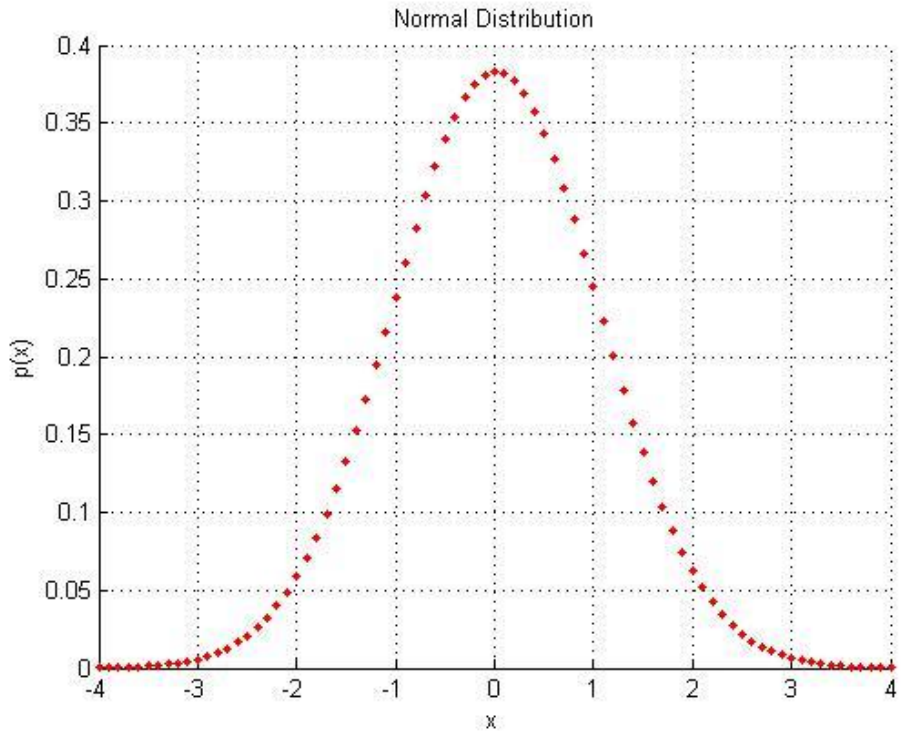

Figure 3.2 a typical normal distribution

The normal distribution is considered the most prominent probability distribution in statistics [8]. In practice, the standard distribution is commonly appeared, and is used throughout natural sciences, statistics, and even social sciences as well. As for this dissertation, the observational error in the direction of arrival estimation is usually assumed to accord to the normal distribution.

3.5.1 Standard normal distribution

Standard normal distribution is the simplest case of a standard distribution, where $\mu = 0$ and $\sigma^2 = 1$, and it can be described mathematically by the probability density function (PDF) as 3.19:

$$p(\mathrm{x}) = \frac{1}{\sqrt{2\pi}} \mathrm{e}^{-\frac{1}{2}\mathrm{x}^2} \tag{3.19}$$

Where the factor $1/\sqrt{2}$ in this equation expresses that the total area under the curve $p(\mathrm{x})$ must be equal to one, and the coefficient $1/\sqrt{2}$ in the exponent ensures the "width" of the curve also equal to one. And the probability density functions for all other distributions are always denoted with letters p [9]. The standard normal distribution is common used in statistics and we will also use it in the simulation in this dissertation.

3.6 Cramer-Rao Bound

In estimation theory and statistics field, the Cramer–Rao bound (CRB) or Cramer–Rao lower bound (CRLB), named after Harald Cramer and Calyampudi Radhakrishna Rao, were the first time to propose in[11][12]. The CRB expresses the lower bound on the variance of the estimators about a deterministic parameter. The lower bound is also referred as the Cramer–Rao inequality or the information inequality [13][14].

The Cramer-Rao Bound provides an unbeatable performance lower limit for any unbiased estimator. Therefore, it is regarded as a baseline for assessing the performance of a specific estimator and used to investigate the fundamental limits of parameter estimation problems [17]. When the exact minimum-mean-square estimation error is difficult to evaluate, the CRB is available to solve the problem.

3.6.1 Scalar unbiased Cramer–Rao bound

Assuming θ is an unknown deterministic parameter that is to be estimated by measurements data x, which are distributed according to a particular probability density function $p(\mathrm{x},\theta)$. And the variance of any unbiased estimator $\hat{\theta}$ of θ is therefore bounded by the reciprocal value of the Fisher information $Inf(\theta)$ as 3.20:

$$var\left(\hat{\theta}\right) \geq Inf(\theta)^{-1} \tag{3.20}$$

Where the Fisher information Inf(θ) can be defined by 3.21:

$$Inf(\theta) = \mathrm{E}\left[\left(\frac{\partial l(\mathrm{x},\theta)}{\partial\theta}\right)^2\right] = -\mathrm{E}\left[\frac{\partial^2 l(\mathrm{x},\theta)}{\partial\theta^2}\right] \tag{3.21}$$

Where E[] represents the expected value and:

$$l(\mathrm{x},\theta) = \ln p(\mathrm{x}) \tag{3.22}$$

The equation 3.22 expresses the natural logarithm of the likelihood function.

3.6.2 Multivariate Cramer–Rao bound

The Cramer–Rao inequality can provide a relatively simple lower bound of the variance of unbiased estimators [11]. In multi-parameter estimation can, we can express the CRB as:

$$var\left(\hat{\theta}_i\right) \geq [Inf^{-1}]_{ii} \tag{3.23}$$

Where the ijth element of the Fisher information matrix *Inf* can be expressed as:

$$Inf_{ij} = -\left[\mathrm{E}\left\{\frac{\partial^2 \ln\left[p_{\mathrm{R}/\bar{\theta}}(\mathrm{x}/\bar{\theta})\right]}{\partial\theta_i\,\partial\theta_j}\right\}\right] \tag{3.24}$$

Where $\bar{\theta}$ is the parameter vector of components θ_i and θ_j to be estimated and $p_{\mathrm{R}/\bar{\theta}}(\mathrm{x}\,/\,\bar{\theta})$ is the probability density function (PDF) of the displace vector x depending on θ.

3.7 Reference

[1]Krim H., Viberg M., "Two decades of array signal processing research: the parametric approach", Signal Processing Magazine, IEEE, Volume: 13 , Issue: 4, Page(s): 67 – 94, 1996.

[2]J. D. Jackson, Classical Electrodynamics (Wiley: New York, 1998).

[3]C. Jordan, K. G., Balman. Electromagnetic Waves and Radiating Systems. Prentice-Hall, New Jersey, second edition, 1968.

[4]S. Kay., Fundament& of Statistical Signal Processing: Estimation Theory. Prentice-Hall International Editions, Englewood Cliffs, NJ, 1993.

[5]A.B. Baggeroer, W.A. Kuperman, H. Schmidt., "Matched field processing: Source localization in correlated noise as an optimum parameter estimation problem", J. Acoust. Soc. Am., 83(2):571-587, February 1988.

[6]J.A. Cadzow., "Multiple Source Location-The Signal Subspace Approach", IEEE Trans. ASSP, A;SSP-38: 11 10-1 125, July 1990.

[7]Diebold, Frank, Elements of Forecasting (Fourth ed.), 2007.

[8] Casella George, Berger Roger L, Statistical inference (2nd ed.). Duxbury. 2001.

[9] Halperin Max, Hartley H. O., Hoel P. G., “Recommended standards for statistical symbols and notation. COPSS committee on symbols and notation”, The American Statistician 19(3): 12–14. 1965.

[10] McPherson G., Statistics in scientific investigation: its basis, application and interpretation. Springer-Verlag. 1990.

[11]Cramér Harald., Mathematical Methods of Statistics. Princeton, NJ: Princeton Univ. Press. 1946.

[12]Rao Calyampudi Radakrishna, “Information and the accuracy attainable in the estimation of statistical parameters”, Bulletin of the Calcutta Mathematical Society **37**: 81–89, 1945.

[13]Rao, Calyampudi Radakrishna. S. Das Gupta. ed. Selected Papers of C. R. Rao. New York: Wiley. 1994.

[14]Bobrovsky, Mayer-Wolf, Zakai, "Some classes of global Cramer-Rao bounds", Ann. Stats., 15(4):1421-38, 1987.

[15]http://upload.wikimedia.org/wikipedia/commons/5/59/Plane_Wave_Oblique_View.jpg

[16]Matt Donadio. "How to Generate White Gaussian Noise", Retrieved 2012.

[17]Bell, K.L. Steinberg, Y. Ephraim, Y. Van Trees, H.L. "Extended Ziv-Zakai lower bound for vector parameter estimation" Information Theory, IEEE Transactions on Volume: 43 , Issue: 2 Page(s): 624 – 637, Mar 1997.

Chapter4 Direction of Arrival estimation algorithm

In previous chapters, the problems of Direction of Arrival (DOA) are introduced and the background knowledge of implementation on DOA estimation is demonstrated. In this chapter, the algorithms of DOA will be discussed. We exploit algorithms developed for ULA to estimate DOA as the simplest case. Moreover, we will make a comparison between MUSIC, Root-MUSIC and ESPRIT algorithm in the aspect of theory and simulation.

4.1Music Algorithm

MUSIC is an acronym which stands for Multiple Signal classification [1]. MUSIC algorithm is a relatively simple and efficient spectral estimation method, based on the space of matrix eigenvalue decomposition method [2, 3]. In the geometric field, the signal processing of the observation space can be decomposed into signal subspace and noise subspace, and it has been proved in [1] that these two spaces are orthogonal. The eigenvectors of signal corresponding to the received signal subspace from the array data covariance matrix which composed of the noise subspace is the smallest eigenvalue from the covariance matrix of eigenvector. MUSIC algorithm uses the orthogonal between these two complementary spaces to estimate the orientation of the signal in space. Noise subspace of all vectors is used to construct the spectrum, in which the peak position corresponding to wave azimuth and elevation signal in the spectrum of all spatial orientation. MUSIC algorithm greatly improves the resolution direction finding, while adapting to the antenna array of arbitrary shape. But the prototype of the MUSIC algorithm requirements wave signal is irrelevant.

4.1.1 The Data Formulation

In order to demonstrate the algorithm, a few feasible assumptions must be proposed. First of all the transmission space in MUSIC algorithm is assumed to be isotropic and non-dispersed that means the radiation propagating straight and the signals are considered to be in the far-field of the smart antenna, so that

the radiation received by the array elements is in the form of a linear sum of plane waves.

Mathematically, assume that the linear combinations of the D incident signals as well as noise are received by the smart antenna with M array elements and D ≤ M. The received complex matrix ***X*** of the smart antenna in the multiple signal classification algorithms can be formulated as:

$$\begin{bmatrix} x_1 \\ x_2 \\ x_3 \\ . \\ . \\ . \\ x_m \end{bmatrix} = [a(\theta_1)a(\theta_2)a(\theta_3) \dots a(\theta_m)] \begin{bmatrix} F_1 \\ F_2 \\ F_3 \\ . \\ . \\ . \\ F_m \end{bmatrix} + \begin{bmatrix} w_1 \\ w_2 \\ w_3 \\ . \\ . \\ . \\ w_m \end{bmatrix} \quad (4.1)$$

or

$$\boldsymbol{X}=\boldsymbol{AFi}+\boldsymbol{W} \quad (4.2)$$

The incident signals are denoted in phase and amplitude at some arbitrary reference point by the complex parameters F_1 **,** F_2,… F_D, and appear as the complex vector ***Fi.*** The noises appear as the complex vector ***W***. The vector ***A***, which represents the relation among array elements, is also complex. a_{ij} are the elements of ***A***, and a_{ij} depend on the relationship between the array element locations and signal arrival angles. Besides, the basic assumption of MUSIC algorithm is that the incident signals and the noise are uncorrelated and the noise is white noise.

4.1.2 The Covariance Matrix

MUSIC is an Eigen structure algorithm and it means that eigenvalue decomposition of the estimated covariance matrix ***R*** is the first step of this algorithm. Here, ***R*** can be implied by equation 4.2

$$\boldsymbol{R}=\mathrm{E}[\boldsymbol{XX^T}]=\mathrm{E}[\boldsymbol{AFiFi^TA^T}+\boldsymbol{WW^T}] \quad (4.3)$$

Here E[] denotes the expectation value. We can regard the noise as white noise which means the elements of vector ***W*** are mean zero, and variance σ^2. The factor that the incident signals and the noise are uncorrelated is the basic

assumption, so that we can analyze the eigenvalues of the covariance matrix and get:

$$\boldsymbol{R}=\boldsymbol{A}\mathrm{E}[\boldsymbol{FiFi^T}]\boldsymbol{A^T}+\lambda_e\boldsymbol{R_0} \qquad (4.4)$$

Where λ_e is the eigenvalue actually and this will be proved in 4.5. The incident signals represented by the complex vector $\boldsymbol{Fi}$ may be uncorrelated or may contain completely correlated pairs. Then, $\mathrm{E}[\boldsymbol{FiFi^T}]$ reflects the degrees of arbitrary in pair-wise correlations occurring among the incident signals and it will be positive definite.

As assumed in section 4.1.1, the number of incident wave fronts D is less than the number of array elements M, so the matrix $\boldsymbol{A}\mathrm{E}[\boldsymbol{FiFi^T}]\boldsymbol{A^T}$ is singular, and it has a rank less than M. Therefore, the determinant of $\boldsymbol{A}\mathrm{E}[\boldsymbol{FiFi^T}]\boldsymbol{A^T}$ is zero as equation 4.5:

$$\left|\boldsymbol{A}\mathrm{E}[\boldsymbol{FiFi^T}]\boldsymbol{A^T}\right|=|\boldsymbol{R}-\lambda_e\boldsymbol{R_0}|=0 \qquad (4.5)$$

Only when λ_e equal to one of the eigenvalues of $\boldsymbol{R}$, this equation 4.5 is satisfied. Thus, λ_e is the eigenvalues of $\boldsymbol{R}$. Definitely, $\boldsymbol{A}\mathrm{E}[\boldsymbol{FiFi^T}]\boldsymbol{A^T}$ must be nonnegative. And since $\boldsymbol{A}$ is full rank and $\mathrm{E}[\boldsymbol{FiFi^T}]$ is positive, λ_e must be the minimum eigenvalue denoted as $\lambda_{\min}$. Then, any measured covariance matrix $\boldsymbol{R}=\mathrm{E}[\boldsymbol{XX^T}]$ matrix can be written as:

$$\boldsymbol{R}=\boldsymbol{A}\mathrm{E}[\boldsymbol{FiFi^T}]\boldsymbol{A^T}+\lambda_{\min}\boldsymbol{R_0} \qquad \lambda_{\min}\geq 0 \qquad (4.6)$$

Where $\lambda_{\min}$ is the smallest solution to $|\boldsymbol{R}-\lambda_e\boldsymbol{R_0}|=0$. Based on the special case that the mean of the elements of the noise vector $\boldsymbol{W}$ is zero, and that variance of them is σ^2, it implies that:

$$\lambda_{\min}\boldsymbol{R_0}=\sigma^2\boldsymbol{I} \qquad (4.7)$$

4.1.3 Eigenvalue and Eigen Matrix

Eigenvalue and Eigen structure are the key points of MUSIC. After decomposition we can get eigenvalues of $\boldsymbol{R}$ which directly determine the rank of $\boldsymbol{A}\mathrm{E}[\boldsymbol{FiFi^T}]\boldsymbol{A^T}$ (it is D). Because of the complete set of eigenvalues of $\boldsymbol{R}$, $\lambda_{\min}$ is not always simple. Actually, in all cases, the eigenvalues of $\boldsymbol{R}$ and those of $|\boldsymbol{A}\mathrm{E}[\boldsymbol{FiFi^T}]\boldsymbol{A^T}|=|\boldsymbol{R}-\lambda_e\boldsymbol{R_0}|$ differ by λ_e, so $\lambda_{\min}$ occurs repeated N

= M - D times. λ_{min} must occur repeated N times, since the minimum eigenvalue of $\boldsymbol{A}\mathrm{E}[\boldsymbol{FiFi^T}]\boldsymbol{A^T}$ is zero because of being singular. Thus, the number of incident signals sources satisfy 4.8:

$$D = M - N \tag{4.8}$$

Where N is the multiplicity of λ_{min} ($\boldsymbol{R}$, $\boldsymbol{R_0}$), which means "λ_{min} of $\boldsymbol{R}$ in the metric of $\boldsymbol{R_0}$."

4.1.4 Signal and Noise Subspace

It is important to know that the eigenvalues of $\boldsymbol{R}$ can be subdivided into two parts when the data consist of uncorrelated desired signals corrupted by uncorrelated white noise. The eigenvectors associated with λ_{min} ($\boldsymbol{R}$, $\boldsymbol{R_0}$) are perpendicular to the space which is spanned by the columns of the incident signal mode vectors $\boldsymbol{A}$, so it is acceptable that for each of λ_i which is equal to λ_{min} (there are N), we have $\boldsymbol{A}\mathrm{E}[\boldsymbol{FiFi^T}]\boldsymbol{A^T}*e_i = 0$ or $\boldsymbol{A}*e_i = 0$.

Therefore, we can define the N×M dimensional noise subspace which is spanned by the N noise eigenvectors and the D dimensional signal subspace which is spanned by the D incident signal eigenvectors. These two subspaces are orthogonal.

4.1.5 Direction of Arrival Scanning

Then we can turn to solve for the incident signal vectors, the search for directions is made by scanning steering vectors that are as perpendicular to the noise subspace as possible, once the noise subspace has been estimated. If $\boldsymbol{E_N}$ is defined to be the M × N dimensional noise subspace whose columns are the N noise eigenvectors, and we use the ordinary Euclidean distance from a vector $\vec{a}(\theta)$ which is a continuum function of azimuth θ ,to the signal subspace for the judgment standard:

$$d^2 = \vec{a}(\theta)^T \boldsymbol{E_N}\boldsymbol{E_N^T}\vec{a}(\theta) \tag{4.9}$$

For the convenient of distinction, we use the graph of $1/d^2$ rather than d^2, and define $P_{MU}(\theta)$ that is:

$$P_{MU}(\theta) = \frac{1}{\vec{a}(\theta)^T \boldsymbol{E_N} \boldsymbol{E_N^T} \vec{a}(\theta)} \quad (4.10)$$

Where $\vec{a}(\theta)$ does not depend on the data. In this case, we get the DOA by searching for peaks in the $P_{MU}(\theta)$ spectrum. Clearly, $\boldsymbol{R}$ is asymptotically perfectly measured so $\boldsymbol{E_N}$ is asymptotically perfectly measured. Then, it is acceptable that even for multiple incident signals MUSIC is asymptotically unbiased. The $\boldsymbol{A}$ matrix becomes available to compute other parameters of the incident signals, after finding the directions of arrival (DOA) of the D incident signals

4.1.6 Conclusion

MUSIC algorithm is an experimental and theoretical techniques involved in estimating the parameters of multiple signals received by a smart antenna [1]. MUSIC approach solve the problem of DOA by scanning peaks according to the spectrum which is decided by an M × N dimensional noise subspace with its N columns of the eigenvectors refer to the array correlation matrix $\boldsymbol{R}$'s smallest eigenvalues.

The steps of the MUSIC algorithm in practice can be shown in summary as:

Step 0: Collect data, form correlation matrix $\boldsymbol{R}$;

Step 1: Calculate Eigen structure of $\boldsymbol{R}$ in metric of $\boldsymbol{R_0}$;

Step 2: Decide number of signals D;

Step 3: Choose N columns to form the noise subspace $\boldsymbol{E_N}$;

Step 4: Evaluate $P_{MU}(\theta)$ versus θ;

Step 5: Pick D peaks of $P_{MU}(\theta)$.

In conclusion, the MUSIC algorithm is significant because it can be implemented as a basic algorithm to provide asymptotically unbiased estimates of directions of arrival (DOA), number of signals, and then we can calculate strengths and cross correlations among the directional signals, directivity, and strength of noise interference.

4.2 Root-MUSIC Algorithm

The Root-MUSIC method [4], as the name shown, is a polynomial-rooting promotion of the original MUSIC method. In the case of Uniform Linear Array (ULA), the scanning for DOA can be transformed into solving the roots of a corresponding polynomial. Root-MUSIC solves the rooting problem of a polynomial rather then finding the spectral peaks in the MUSIC algorithm. After lots of research and simulation, it is proved that Root-MUSIC has a better property than spectral MUSIC in some cases [5], such as resolution ability. The pre-process of Root-MUSIC is the same with MUSIC and the only difference between Root-MUSIC and MUSIC is the Direction Finding method.

4.2.1 Direction of Arrival Scan

From MUSIC algorithm, we can get:

$$P_{MU}(\theta) = \frac{1}{\vec{a}(\theta)^T \boldsymbol{E_N E_N^T} \vec{a}(\theta)} \tag{4.10}$$

Which is used to scan by degree. However, for the moment, if we restrict our attention to uniform linear arrays with inter element spacing Δ, so that the ith element of $a(\theta)$ may be written as:

$$a_i(\theta) = \mathrm{e}^{\mathrm{j}2\pi i(\Delta/\lambda)\sin\theta} \qquad i = 1,2,\ldots,\mathrm{M} \tag{4.11}$$

Let us restrict our attention to the denominator$P_{MU}^{-1}(\theta)$, it may be written as:

$$P_{MU}^{-1}(\theta) = \vec{a}(\theta)^T \boldsymbol{E_N E_N^T} \vec{a}(\theta) =$$
$$\sum_{i=1}^{\mathrm{M}} \sum_{k=1}^{\mathrm{M}} \mathrm{e}^{-\mathrm{j}2\pi i(\Delta/\lambda)\sin\theta} \boldsymbol{E_N E_N^T} \mathrm{e}^{\mathrm{j}2\pi k(\Delta/\lambda)\sin\theta} =$$
$$\sum_{l=-\mathrm{M}+1}^{\mathrm{M}-1} \mathrm{E_l} \mathrm{e}^{-\mathrm{j}2\pi l(\Delta/\lambda)\sin\theta} \tag{4.12}$$

Where $\mathrm{E_l}$ is the sum of entries of $\boldsymbol{E_N E_N^T}$ along the *i*th diagonal:

$$\mathrm{E_l} = \sum_{i-k=l} \boldsymbol{E_N E_N^T} \tag{4.13}$$

If we define the polynomial $P(z)$ as:

$$P(z) = \sum_{\mathrm{l}=-\mathrm{M}+1}^{\mathrm{M}+1} \mathrm{E_l} \mathrm{z}^{-\mathrm{l}} \tag{4.14}$$

On the unit circle, evaluating the spectrum $P_{MU}(\theta)$ is equivalent to evaluating the polynomial $P(z)$. We can use the roots of $P(z)$ for direction of arrival estimation rather than scanning for peaks in $P_{MU}(\theta)$ [4]. Definitely, peaks in $P_{MU}(\theta)$are due to roots of $P(z)$lying close to the unit circle. Take the pole of $P(z)$ at z_1 for example:

$$z_1 = |z_1|\mathrm{e}^{\mathrm{j}\arg(\mathrm{z}_1)} \tag{4.15}$$

It will result in a peak in $P_{MU}(\theta)$ at:

$$\sin(\theta) = (\lambda / 2\pi\Delta)\arg(\mathrm{z}_1) \tag{4.16}$$

Therefore, after solving the polynomial $P(z)$, we can get D roots which locate near the unit circle mostly. Then, based on the relationship between z and θ, direction of arrival can be found.

4.2.2 Conclusion

Root-MUSIC algorithm is used to calculate the direction of arrival by the underlying information of noise subspace and distinguish some nearby signal sources. The steps of the MUSIC algorithm in practice can be shown in summary as:

Step 0: Collect data, form correlation matrix $\boldsymbol{R}$;

Step 1: Calculate eigenstructure of $\boldsymbol{R}$ in metric of $\boldsymbol{R_0}$;

Step 2: Decide number of signals D;

Step 3: Choose N columns to form the noise subspace $\boldsymbol{E_N}$;

Step 4: Transform$P_{MU}(\theta)\ to\ get\ \ P(z)$;

Step 5: Find roots of $P(z)$and choose D roots which are nearest to the unit circle;

Step 6: Calculate the direction by D roots.

It has been shown in [6, 7] that Root-MUSIC has identical asymptotic properties, though in a small number of date Root-MUSIC has empirically been found to perform greatly better. Comparing with MUSIC approach, Root-

MUSIC has an especially better performance when dealing with some nearby signal sources.

4.3 Bartlett Algorithm

The Bartlett algorithm is a Fourier spectrum analysis method [16]. The main idea of Bartlett algorithm is to exclude the noise signal by the covariance matrix and find a set of weights that maximize the power of received signals. The received signals usually contain both information of direct path and multipath signals, which are most likely from different directions of arrival angles [17]. Actually, Bartlett algorithm is base of MUSIC algorithm, and the beginning steps of Bartlett Algorithm is the same with MUISC algorithm. So it is no hard to imply Bartlett algorithm from MUSIC algorithm as follows.

4.3.1 Direction of Arrival Scan

From MUSIC algorithm, we can get:

$$P_{MU}(\theta) = \frac{1}{\vec{a}(\theta)^T \boldsymbol{E_N E_N^T} \vec{a}(\theta)} \tag{4.10}$$

which is used to scan maximum value by degree. However, for the moment, we replace $\boldsymbol{E_N E_N^T}$ by $\boldsymbol{R}$, where R is the covariance matrix of data matrix $\boldsymbol{X}$, and we can get the output power spectrum of Bartlett method as:

$$P_B(\theta) = \frac{1}{\vec{a}(\theta)^T \boldsymbol{R} \vec{a}(\theta)} \tag{4.17}$$

4.3.2 Conclusion

Bartlett approach solves the problem of DOA by scanning peaks according to the spectrum which is decided by the array correlation matrix $\boldsymbol{R}$.

The steps of the Bartlett algorithm in practice can be shown in summary as:

Step 0: Collect data, form correlation matrix $\boldsymbol{R}$;

Step 1: Decide number of signals D;

Step 2: Evaluate $P_B(\theta)$ versus incident angle θ;

Step 3: Pick D peaks of $P_B(\theta)$.

Bartlett algorithm is a significant approach in the development of DOA estimation, though the accuracy of Bartlett Algorithm is not as good as modern algorithms. MUSIC algorithm further Bartlett algorithm in the case of output power spectrum function and makes a better performance in DOA estimation.

4.4 Capon Algorithm

Capon algorithm employs a wavenumber window whose shape changes and it is a function of the wavenumber at which an estimate is obtained [18]. The key idea of Capon Algorithm is using a better factor as the inverse covariance matrix $\boldsymbol{R^{-1}}$ to replace the factor $\boldsymbol{R}$ in the output power spectrum function of Bartlett algorithm. Actually, Capon algorithm is based on Bartlett algorithm, so it is easy to develop Capon algorithm from Bartlett algorithm.

4.4.1 Direction of Arrival Scan

From Bartlett algorithm, we can get:

$$P_B(\theta) = \frac{1}{\vec{a}(\theta)^T \boldsymbol{R} \vec{a}(\theta)} \tag{4.10}$$

which is used to scan peak values by degree. However, for the moment, we replace $\boldsymbol{R}$ by $\boldsymbol{R^{-1}}$ and we can get the output power spectrum function of Capon algorithm as:

$$P_C(\theta) = \frac{1}{\vec{a}(\theta)^T \boldsymbol{R^{-1}} \vec{a}(\theta)} \tag{4.18}$$

4.4.2 Conclusion

Capon approach solves the problem of DOA by scanning peaks according to the spectrum which is decided by the array correlation inverse matrix $\boldsymbol{R^{-1}}$.

The steps of the Capon algorithm in practice can be summarized as:

Step 0: Collect data, form correlation matrix $\boldsymbol{R}$;

Step 1: Calculate the inverse matrix of $\boldsymbol{R}$ as $\boldsymbol{R^{-1}}$;

Step 2: Decide number of signals D;

Step 3: Evaluate $P_C(\theta)$ versus incident angle θ;

Step 4: Pick D peaks of $P_C(\theta)$.

Capon algorithm is a significant algorithm in the development of DOA estimation and it was widely implemented before the proposal of MUSIC algorithm. Application of this algorithm is given to seismic data obtained from the large aperture seismic array located in eastern Montana [18]. MUSIC algorithm further Capon algorithm in the output power spectrum function and replaces $\boldsymbol{R^{-1}}$ by the noise subspace matrix $\boldsymbol{E_N E_N^T}$, improving the performance of DOA estimation.

4.5 ESPRIT Algorithm

ESPRIT stands for Estimation of Signal Parameters via Rotational Invariance Techniques [8]. The idea of ESPRIT is that the sensor array is decomposed into two identical sub-arrays. In the sub-arrays, two elements which are corresponding to each have the same pan. That is to say, the array has translational invariance. Every two shifts match the same array element pairs. Fortunately, in practice many of the arrays satisfy this condition, such as uniform linear array. It also has some improved algorithms, such as least squares ESPRIT, total least squares ESPRIT.

ESPRIT algorithm has the following advantages: Firstly, it is different from MUSIC algorithm which scans all steering vector directly by the ordinary Euclidean distance; it greatly reduces the computation of the MUSIC algorithm. Secondly, it does not need to know precisely the array manifold vector, and not require the strict array calibration. However, both ESPRIT algorithm and MUSIC algorithm cannot deal with coherent signals.

4.5.1 Array Geometry

ESPRIT algorithm [9] is a robust and computationally efficient algorithm of DOA finding. The main idea of ESPRIT is using two identical arrays whose elements need to form doublets with an identical location vector, and the second element of each doublet should be located at the same distance and direction relative to the first element.

In detail, assume an array of arbitrary geometry composed of M sensor doublets. The elements in each doublet have identical sensitivity array elements and are separated by a known constant displacement matrix $\boldsymbol{\Delta}$. ESPRIT algorithm has a lot of advantages. Firstly, the nonzero sensitivity in all directions of arrival, the gain, phase of each sensor are not required. Secondly, there is no requirement that any of the doublets is the same sensitivity patterns though [8]. Lastly, the directivity sensitivity of the array elements in the doublets is arbitrary located.

4.5.2 The Data Mode

The ESPRIT algorithm is based on assumption that the underlying 2M-dimensional signal subspace contain the entire given array output. Also, we should assume that signals received by the smart antenna with M array elements are linear combinations of the D narrow-band source signals as well as noise and D ≤ M. The sources are located sufficiently far from the array so that the wave fronts impinging on the array elements are planar in homogeneous isotropic transmission space. The received vector $\boldsymbol{X}$ of the ESPRIT algorithm can be formulated as:

$$\begin{bmatrix} x_1 \\ x_2 \\ x_3 \\ \cdot \\ \cdot \\ \cdot \\ x_m \end{bmatrix} = [a(\theta_1)a(\theta_2)a(\theta_3)\dots a(\theta_m)] \begin{bmatrix} F_1 \\ F_2 \\ F_3 \\ \cdot \\ \cdot \\ \cdot \\ F_m \end{bmatrix} + \begin{bmatrix} w_1 \\ w_2 \\ w_3 \\ \cdot \\ \cdot \\ \cdot \\ w_m \end{bmatrix} \quad (4.19)$$

or

$$\boldsymbol{X}=\boldsymbol{A_0 Fi}+\boldsymbol{W} \quad (4.20)$$

The incident signals, which appear as the complex vector $\boldsymbol{Fi}$, are represented in amplitude and phase at some arbitrary reference point by the complex parameters F_1 , F_2,… F_D. The noise appears as the complex vector $\boldsymbol{W}$. As other researchers do, the sources in this model can be assumed to be deterministic signals or stationary zero mean random signals. Additive white noise which is assumed to be a stationary zero mean random signal with a spatial

covariance σ^2, is present at all 2M array elements. The elements of $\boldsymbol{X}$ and $\boldsymbol{A_0}$ are also complex in general. a_{ij} are the elements of $\boldsymbol{A_0}$, and a_{ij} depend on the relationship between signal arrival angles and the array element locations.

In order to make a mathematical demonstration of the theory of the translational invariance of the array, we can regard the array as being consist of two subarrays, $\boldsymbol{X_a}$ and $\boldsymbol{X_b}$. They are identical in all elements and geometrically located from each other by a given displacement matrix $\boldsymbol{\Delta}$ with magnitude Δ. The combination signals impinged on each subarray can then be expressed as:

$$\boldsymbol{X_a} = \boldsymbol{AFi} + \boldsymbol{W} \tag{4.21}$$

$$\boldsymbol{X_b} = \boldsymbol{A\Delta Fi} + \boldsymbol{W} \tag{4.22}$$

ESPRIT algorithm does not require the knowledge of the sensitivities, gain and phase patterns, so that the subarray location matrix $\boldsymbol{\Delta}$ contents not only the information of scale for the problem, but also the reference of the direction. It is acceptable that the DOA finding outcomes are direction-of-arrival related to the direction of the location matrix $\boldsymbol{\Delta}$. Consequently, this fact supports the necessity for a corresponding location vector for each dimension with desired parameters. The subarray outputs $\boldsymbol{X_a}$ and $\boldsymbol{X_b}$ can be combined as 4.23:

$$\boldsymbol{X} = \begin{bmatrix} \boldsymbol{X_a} \\ \boldsymbol{X_b} \end{bmatrix} \tag{4.23}$$

Defining the combination of $\boldsymbol{A}$ *and* $\boldsymbol{A\Delta}$:

$$\overline{\boldsymbol{A}} = \begin{bmatrix} \boldsymbol{A} \\ \boldsymbol{A\Delta} \end{bmatrix} \tag{4.24}$$

4.5.3 Covariance matrix

The main idea of ESPRIT is to develop the rotational invariance of the underlying information of signal subspace induced by the translational invariance of the sensor arrays [9]. The related signal subspace is $\boldsymbol{X}$ which contains the outputs from the two subarrays, $\boldsymbol{X_a}$and $\boldsymbol{X_b}$. The combination of the output of the arrays leads to two sets of eigenvectors, $\boldsymbol{E_a}$ and $\boldsymbol{E_b}$, corresponding to $\boldsymbol{X_a}$and $\boldsymbol{X_b}$ respectively.

After filtering the noise, the signal subspace can be obtained by collecting sufficient measurement data and finding any set of D linearly independent measurement vectors. These vectors can span the D-dimensional subspace [19]. Consequently, it is significant to filter the noise by covariance matrix. We can imply the signal subspace from knowledge of the covariance of the original data as 4.25:

$$\boldsymbol{R}_{\mathrm{XX}}=\mathrm{E}[\boldsymbol{XX^T}]=\bar{\boldsymbol{A}}\mathrm{E}[\boldsymbol{F_i F_i^T}]\bar{\boldsymbol{A}}^{\boldsymbol{T}}+\lambda\sigma^2 \tag{4.25}$$

4.5.4 Eigen matrix

ESPRIT is an eigenstructure algorithm and it means that this algorithm relies on the eigenvalue decomposition of the estimated covariance matrix $\boldsymbol{R_{XX}}$. Because the rank of $\boldsymbol{E_s}$, which is the eigen matrix of $\boldsymbol{R_{XX}}$, is the same with $\bar{\boldsymbol{A}}$, there must exist a unique nonsingular matrix $\boldsymbol{T}$ to transform $\bar{\boldsymbol{A}}$ *to* $\boldsymbol{E_s}$.

$$\boldsymbol{E_s}=\bar{\boldsymbol{A}}\boldsymbol{T} \tag{4.26}$$

Where $\boldsymbol{E_s}$ *can be decomposed in to* $\boldsymbol{E_a}$ *and* $\boldsymbol{E_b}$**.**

$$\boldsymbol{E_s}=\begin{bmatrix}\boldsymbol{E_a}\\ \boldsymbol{E_b}\end{bmatrix}=\begin{bmatrix}\boldsymbol{AT}\\ \boldsymbol{A\Delta T}\end{bmatrix} \tag{4.27}$$

4.5.5 Direction of Arrival finding

Make an assumption that:

$$\boldsymbol{E_{ab}}=[\boldsymbol{E_a}|\boldsymbol{E_b}] \tag{4.28}$$

The rank of $\boldsymbol{E_{ab}}$ is D, and D ≤ M. It implies that there exists and only exist one matrix denoted as $\boldsymbol{F}$ with rank D to make:

$$\boldsymbol{E_{ab}F}=[\boldsymbol{E_a}|\boldsymbol{E_b}]\begin{bmatrix}\boldsymbol{F_a}\\ \boldsymbol{F_b}\end{bmatrix}=\boldsymbol{E_aF_a}+\boldsymbol{F_bF_b}=\boldsymbol{ATF_a}+\boldsymbol{A\Delta TF_b}=0 \tag{4.29}$$

Where matrix $\boldsymbol{F}$ can span a null-space (the orthogonal space) of $[\boldsymbol{E_a}|\boldsymbol{E_b}]$. Then we use the two subspace of $\boldsymbol{F}$ and define $\boldsymbol{\Psi}$:

$$\boldsymbol{\Psi}=-\boldsymbol{F_aF_b^{-1}} \tag{4.30}$$

From the equation $\boldsymbol{ATF_a + A\Delta TF_b}$=0, we can get:

$$\boldsymbol{T\Psi T^{-1}=\Delta} \tag{4.31}$$

In consequence, based on the theory of relevant matrix, the eigenvalues of $\boldsymbol{\Psi}$ are equal to the corresponded diagonal elements of $\boldsymbol{\Delta}$, and all the columns of matrix $\boldsymbol{T}$ are the eigenvectors of $\boldsymbol{\Psi}$. The above outcomes are the key relations of ESPRIT algorithm. Parameters of the signal are gain as non-linear functions of the eigenvalues of $\boldsymbol{\Psi}$ .These eigenvalues can be regard as rotating a series of vectors $\boldsymbol{E_a}$which span the M-dimensional signal subspace into another vectors $\boldsymbol{E_b}$.

Once we obtained $\boldsymbol{\Delta}$, we can calculate the direction directly by the configuration of the antenna arrays and the relationship among elements, which are represented in vector $\boldsymbol{A}$.

4.5.6 Conclusion

ESPRIT is an eigenstructure algorithm which means that this algorithm is based on the covariance model and the computation step of ESPRIT algorithm can be summarized as follows:

Step 0: From two identical subarrays, we get measurements and subarrays are displaced by $\boldsymbol{X_b}$ $\boldsymbol{and}$ $\boldsymbol{X_b}$. Then calculate the covariance matrixes $\boldsymbol{R}_{\mathrm{XX}}$ of two arrays;

Step 1: Find their eigenvalues λ_e and eigenvectors $\boldsymbol{E_s}$ from the measurements;

Step 2: Decide the number of directional sources;

Step 3: Decompose $\boldsymbol{E_s}$to obtain $\boldsymbol{E_a}$ and $\boldsymbol{E_b}$where

$$\boldsymbol{E_s} = \begin{bmatrix} \boldsymbol{E_a} \\ \boldsymbol{E_b} \end{bmatrix} \tag{4.32}$$

Step 4: Compute the eigendecomposition. Form an eigenmatrix and derive its eigenvectors, which are columns of a matrix $\boldsymbol{E_e}$

$$\boldsymbol{E_{ab}^T E_{ab}}=\begin{bmatrix} \boldsymbol{E_a^T} \\ \boldsymbol{E_b^T} \end{bmatrix} [\boldsymbol{E_a}|\boldsymbol{E_b}]=\boldsymbol{E_e}\Lambda\boldsymbol{E_e^T} \tag{4.33}$$

Step 5: Divide the matrix $\boldsymbol{E_e}$ into four D × D parts

$$\boldsymbol{E_e} = \begin{bmatrix} \boldsymbol{E_{11}} & \boldsymbol{E_{12}} \\ \boldsymbol{E_{21}} & \boldsymbol{E_{22}} \end{bmatrix} \tag{4.34}$$

Step 6: Calculate the eigenvalues of the matrix

$$\boldsymbol{\Psi} = -\boldsymbol{E_{12}}\boldsymbol{E_{22}^{-1}} \tag{4.35}$$

Step 7: Estimate the angle of arrival using the eigenvalues of $\boldsymbol{\Psi}$.

In practice, ESPRIT algorithm is generally developed and implemented to a wide range of areas. ESPRIT maintains most of the essential advantages of the arbitrary displacement of array elements, and makes a definite reduction in computational complexity from MUSIC algorithm by adding a subspace constraint to the structure of the smart antenna.

4.6 Summary and Conclusion of algorithms

In this section, we will make a summary of above mentioned algorithm and review some performance of these algorithm researched by other researchers. The properties of these three algorithms can be summarized as table 4.1:

Table 4.1

Algorithm	Consistency	Coherent Signal	Accuracy	Resolution	Computation efficiency
MUSIC	Yes	No	Exact	Good	Good
Root-MUSIC	Yes	Yes	Good	Exact	Good
ESPRIT	Yes	Yes	Good	Exact	Efficient

4.4.1 Consistency

From the method described in section 4.1, 4.2 and 4.5, it is not difficult to figure out that all these three algorithms can deal with consistent insert angle as table 4.1 shows. Definitely, the MUSIC algorithm estimate DOA by scan incident angle one by one, and the step of scanning decide the estimation

accuracy. However, ESPRIT and Root-MUSIC algorithm can compute the incident angle directly by subspaces and polynomial respectively for all consistent DOA.

4.4.2 Addressing Coherent signals

Coherent signals are referred to signals which are greatly correlated with each other. When the coefficient of correlation [15] is equal to 1, we define signals as coherent signals. It is well accepted that MUSIC algorithm is the first significant and classical DOA estimation algorithm [14]. But one of its most serious problems is solving coherent signals. As developed algorithms base on MUSIC, ESPRIT and Root-MUSIC have overcome this problem.

4.4.3 Accuracy

The accuracy is the most effective evidence to judge am algorithm. According to above researches [11, 12], it is fair to say these three methods have great accuracy. In detail, some past simulation results of MUSIC, Root-MUSIC and ESPRIT algorithms show that their performance improves with more elements number of the array elements, with larger signal noise ratio (SNR), with larger snapshots of signals and greater angular separation between the signals. These improvements can be seen in form of the sharper peaks in the MUSIC simulation and smaller errors in angle detection in the ESPRIT and Root-MUSIC simulation.

However, it is said that there are more errors in DOA estimation by using ESPRIT algorithm compared to the MUSIC algorithm [13], which means that MUSIC is slightly more accurate than ESPRIT. In this dissertation, we will also simulate the accuracy of these three algorithms and prove the outcomes of above researches. The simulation and comparison about accuracy are demonstrated in chapter 6.

4.4.4 Resolution ability

The resolution is defined as the ability to distinguish two or more sources with the same of similar incident angle in this dissertation. As for MUSIC algorithm, the resolution ability is another weakness. It is not hard to understand that we

cannot decide the exact number of signal from one peak in the graph of MUSIC algorithm. A small step of scanning can improve the resolution ability but cannot solve this problem totally. However, ESPRIT and Root-MUSIC have excellent resolution, based on their idea of DOA estimation.

4.4.5 Computation efficiency

The computation efficiency is defined as the amount of calculation in a particular DOA estimation work. Definitely, the greatest improvement of ESPRIT is in the area of computation efficiency. A large number of researches prove that ESPRIT has better computation efficiency than MUSIC. The computation efficiency of Root-MUSIC is the worst in these three algorithms. In chapter 6, we will compare the computation efficiency by simulation.

4.4.6 Implementation in Multiple dimensions array

Multiple dimension DOA estimation is an interesting area of DOA in the long run. Some past researches proved that MUSIC and ESPRIT algorithms are convenient and efficient in two dimensions DOA. However, the Root-MUSIC is seldom used in two or more dimensions DOA, though it can be implemented in two or three dimensional arrays theoretically. According to the simulation results of [10], MUSIC algorithm shows slightly better performance than ESPRIT algorithm in two dimensions case, and for both algorithms, the Root Mean Square Error (RMSE) of azimuth are smaller than those of elevation. In section 6.2, we will discuss this in detail.

4.7 Reference

[1]R. O. Schmidt, “Multiple emitter location and signal parameter estimation,” IEEE Trans. Antennas Propagat., vol. AP-34, pp. 276–280, 1986.

[2].Stoica P., “Statistical analysis of MUSIC and ESPRIT estimates of sinusoidal frequencies”, Acoustics, Speech, and Signal Processing, 1991. ICASSP-91., 1991 International Conference on, On Page(s): 3273 - 3276 vol.5

[3].Franz A. de Leon, “Application of MUSIC, ESPRIT and SAGE Algorithms for Narrowband Signal Detection and Localization”, TENCON 2006. IEEE Region 10 Conference, On Page(s): 1 – 4, 2006.

[4] A. Barabell, “Improving the resolution of eigenstructured based direction finding algorithms”, in Proc. ICASSP, Boston, MA, pp. 336–339, 1983.

[5]Krim H., Viberg M., “Two decades of array signal processing research: the parametric approach”, Signal Processing Magazine, IEEE, Volume: 13 , Issue: 4, Page(s): 67 – 94, 1996.

[6] Y. Iiguni, H. Sakai, and H. Tokumaru, “Convergence properties of simplified gradient adaptive lattice algorithms”, IEEE Trans. Acoust., Speech, Signal Processing, vol. ASSP-33, pp. 1427–1434, 1985.

[7] G. R. L. Sohie, L. H. Sibul, “Stochastic convergence properties of the adaptive gradient lattice”, IEEE Trans. Acoust., Speech, Signal Processing, vol. ASSP-32, pp. 102–107, 1984.

[8].L.C.Godara, “Application of antenna arrays to mobile communication II: Beamforming & direction of arrival considerations”, Proceedings of IEEE, volume 85, issue 8, pages 1195-1245 , August 1997.

[9] R. Roy, T. Kailath, “ESPRIT—Estimation of signal parameters via rotational invariance techniques”, IEEE Trans. Acoust., Speech, Signal Processing, vol. ASSP-37, pp. 984–995, 1989.

[10]Xiang Gu, Yunhua Zhang, “Effects of amplitude and phase errors on 2-D MUSIC and 2-D ESPRIT algorithms in ISAR imaging”, Synthetic Aperture Radar, 2009. APSAR 2009. 2nd Asian-Pacific Conference on Digital Object , Page(s): 634 – 638, 2009.

[11]Jeong-Geun Hong, Chan-Sik Park, Bo-Seok Seo,
“Comparison of MUSIC and ESPRIT for direction ofarrival estimation of jam ming signal”, Instrumentation and Measurement Technology Conference (I2MTC), 2012 IEEE International Digital Object, Page(s): 1741 – 1744, 2012.

[12]Kangas A., Stoica P., Soderstrom,T.,
“Finite sample and modelling error effects on ESPRIT

and MUSIC direction estimators" Radar, Sonar and Navigation, IEEE Proceedings - Volume: 141 , Issue: 5 , Page(s): 249 – 255, 1994.

[13]Ottersten B., Viberg M., Kailath, T.,
"Performance analysis of the total least squares ESPRIT algorithm", Signal Processing, IEEE Transactions on Volume: 39, Issue: 5 , Page(s): 1122 – 1135, 1991.

[14]Porat B., Friedlander B.,
"Analysis of the asymptotic relative efficiency of the MUSIC algorithm", Acoustics, Speech and Signal Processing, IEEE Transactions on Volume: 36, Issue: 4, Page(s): 532 – 544, 1988.

[15]J. S. Bendat, A. G. Piersol, Random Data, Wiley-Interscience, 1986

[16]M. S. Bartlett, "Periodogram analysis and continuous spectra," Biometrica, vol. 37, no. 1/2, pp. 1-16, Jun. 1950.

[17]Abusultan, M. Harkness, S. LaMeres, B.J. Yikun Huang "FPGA implementation of a Bartlett direction of arrival algorithm for a 5.8ghz circular antenna array" Aerospace Conference, 2010 IEEE Page(s): 1 – 10, March 2010

[18]J. Capon, "High-Resolution Frequency Wavenumber Spectrum Analysis", Proc. IEEE, vol. 57, pp. 1408-1418, Aug. 1969.

[19] Glisic, S. "Antenna Array Signal Processing", Advanced Wireless Communications, 2005.

Chapter 5 Array Geometry

Scientists never stop searching for smart antennas with a higher performance. Besides the promotion in algorithms which permit optimal use of existing array configurations, we can research and figure out array geometries with more excellent properties.

Here, we will introduce some kinds of array geometries, which are also known as array configurations. Different kinds of array geometry with ten elements and inter-element spacing equal to 0.5m, which is half wavelength of the signal, are taken into account, and we try to analysis the characteristic of each array geometry based on the time delay between elements. The analyzing is the preparation of array geometry simulation and compare in later chapters.

In this chapter, on one hand, we will demonstrate the configuration of elements. On the other hand, it will imply the delay, which is the key point effecting the DOA performance, among elements decided by the elements configuration. Definitely, the array geometry considerably decides the performance of DOA by way of different combination of elements delays.

5.1 Data Model

Before demonstration, it is necessary to make the assumption that a plane wave propagating through an isotropic space is received by the antenna array [1]. Then, the signal derived by any sensor can be represented as a time delayed version to the signal impinging on the reference sensor.

First of all we should define the coordinate and incident angle. In this chapter, we consider the geometry in the rectangular coordinate system, defining the azimuth as φ and the elevation as θ . As shown in Figure, D narrow-band signals transmitted from far-field sources travel through a homogeneous isotropic medium and impinge on an array of M identical isotropic elements or sensors located at $\vec{l}_m$ for m ∈ [1, M]. Let us note the DOA of the dth source by $[\varphi_d,\theta_d]$, where elevation angle $\theta_d \in [0, \pi]$ and azimuth angle $\varphi_d \in [-\pi,\pi]$.

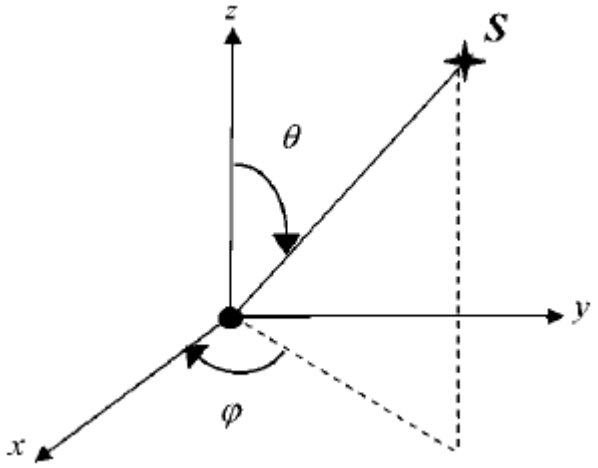

Figure 5.1 3D system showing a signal arriving from azimuth φ and elevation θ [1]

The received signal of the antenna array is modeled as:

$$\boldsymbol{x}(\mathrm{t}) = \boldsymbol{A}(\varphi, \theta)\boldsymbol{s}(\mathrm{t}) + \boldsymbol{n}(\mathrm{t}) \tag{5.1}$$

where $\boldsymbol{x}(\mathrm{t})$ is the M ×1 snapshot vector of the signals received simultaneously on all the sensors, $\boldsymbol{s}(\mathrm{t})$ is the D×1 vector of the source signals, $\boldsymbol{n}(\mathrm{t})$ is the M ×1 noise vector that is assumed to be white, Gaussian and uncorrelated with the source signals. The M×D steering matrix $\boldsymbol{A}(\varphi, \theta)=[\vec{a}(\varphi_1, \theta_1), \ldots, \vec{a}(\varphi_d, \theta_d)]$ defines the array manifold and consists of the steering vectors $\vec{a}(\varphi_d, \theta_d)$ whose components are:

$$\vec{a}_m(\varphi_d, \theta_d) = \mathrm{e}^{\mathrm{j}2\pi f \Delta_{\mathrm{m}}(\varphi_{\mathrm{d}}, \theta_{\mathrm{d}})} \tag{5.2}$$

where

$$\Delta_{\mathrm{m}}(\varphi_d, \theta_d) = \vec{V}_d^T(\varphi_d, \theta_d) \cdot \vec{l}_m \,/\, \mathrm{c} \tag{5.3}$$

$\Delta_{\mathrm{m}}(\varphi_d, \theta_d)$ is the propagation delay of source signal d received sensor m, c is the speed of light and $\vec{V}_d(\varphi_d, \theta_d)$ is the unit vector pointing towards the dth source. It is acceptable to regard the array steering vector as a unique function of the angle of arrival.

In order to compare the performance of different geometry, firstly, we should consider the different delay of sources received by sensors.

5.2 One Dimension

One dimension is the most easy and feasible case. In this case, since $\theta_d \in [0, \pi]$, the unit vector pointing towards the dth source $\vec{V}_d(\varphi_d, \theta_d)$ can be shown as:

$$\vec{V}(\theta)=[\cos(\theta)] \quad (5.4)$$

Definitely, there is only one kind of array geometry in one dimension case.

5.2.1 Uniform Linear Array (ULA)

Uniform linear array (ULA) composed of M (in this dissertation, M=10) elements placed on the x axes with inter-element spacing equal to p ($p=\frac{\lambda}{2}=0.5$m) is presented. The element placed at the origin is common for referencing purposes.

Uniform linear array (ULA) is a classical kind of array geometry and it is the base configuration of the antenna arrays. Therefore, it is necessary to discuss the performance of DOA estimation by Uniform Linear Array. It is widely used because of its simple structure. Currently, a lot of DOA estimation algorithms are based on the uniform linear array, but the biggest drawback of the uniform linear array is that it can only estimate in the range of 0 °to 180 °, and can only receive one-dimensional angular information, e.g. θ. The displacement of sensors of Uniform linear array (ULA) discussed in this dissertation is shown as 5.2 and 5.3. In this chapter, the unit of position description is meter.

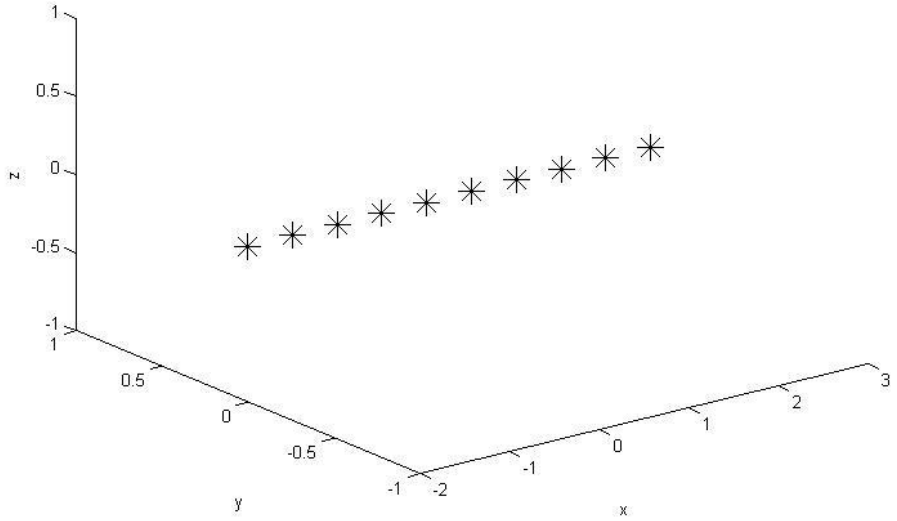

Figure5.2 3D view of Uniform linear array (ULA)

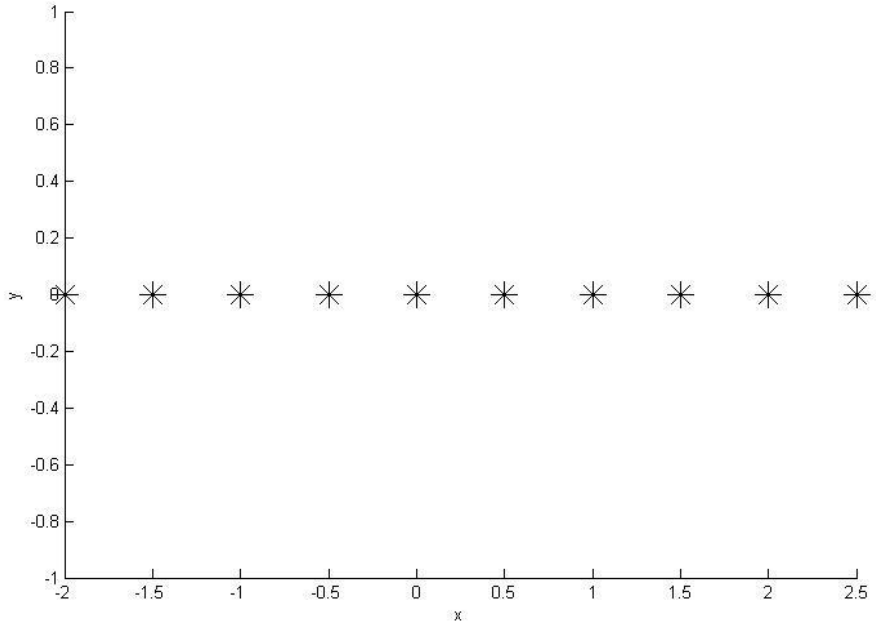

Figure 5.3 x-y plane view of Uniform linear array (ULA)

From figure 5.2 and figure 5.3, we are cleared that the array elements are located in the x axis. Then, we will attempt to express the received signal in each of the element in terms of the signal received in the first element or the reference element. In the figure, the Uniform linear array (ULA) receives the

signal from a direction of angle $\boldsymbol{\theta}$ relative to the array broadside. Besides, the location of elements can be represented as:

$$\vec{l}_m = [\mathrm{x_m}] \tag{5.5}$$

Where, $\mathrm{x_m}$ denotes the displacement of mth sensor. Then we can get the time delay based on propagation manifests in a phase shift in the received signal at the reference element. Now we can use θ to express the time delay $\Delta_{\mathrm{m}}(\theta_d)$. The delays of elements are representing as:

$$\Delta_{\mathrm{m}}(\theta_{\mathrm{d}})=\frac{\mathrm{x_m}\sin(\theta_{\mathrm{d}})}{\mathrm{c}} \tag{5.6}$$

The equation 5.6 relates the incident signal with the time delay which can exploit from the data received by the array sensors.

Uniform linear array (ULA) is the simplest configuration of array antenna, and thus it is commonly used in theoretic analysis. In this dissertation, we analyse the performance of MUSIC, Root-MUSIC and ESPRIT algorithms with Uniform linear array (ULA) as well. In practice, however, we always need a 2D DOA estimation in the 3D space, so that we usually form plane antenna arrays with the same number of sensors.

5.3 Two Dimensions

Two dimensions is the most common case, which has been researched by scientist for decades. In this case, the unit vector pointing towards the dth source $\vec{V}_d(\varphi_d, \theta_d)$ can be shown as:

$$\vec{V}(\varphi,\theta)=[\cos(\varphi)\sin(\theta), \sin(\varphi)\sin(\theta), \cos(\theta)] \tag{5.7}$$

There are various kinds of array geometry in two dimension case. In this chapter, we focus on some classical array configuration as Uniform Circle Array, L Shaped Array, Y Shaped Array and Rectangular Array.

5.3.1 Uniform Circular Array (UCA)

Uniform Circular Array (UCA) composed of M (in this dissertation, M=10) elements placed on the x- y plane with inter-element spacing equal to p

(p= $\frac{\lambda}{2}$ =0.5m) is presented. Uniform Circle Array (UCA) is a significant kind of array geometry.

Uniform Circular Array (UCA) is a classical kind of array geometry and it is the base configuration of the antenna arrays, so it is necessary to analyze the performance of DOA estimation by Uniform Circular Array. It is widely used because of its wonderful performance in two dimensions case with such a simple structure. Uniform Circular Array can provide constant DOA estimation within the range of 0 °to 360 °and resolute two-dimensional angular source of information, but its resolution is low and its CRB is relatively large. Given Uniform Circular Array more number of array elements to improve performance, the amount of calculation will be larger, and structures will become more complex.

As Figure 5.4 shows, a UCA with 10 elements locate at x-y plane. Figure 5.4 shows the 3D perspective and figure 5.5 shows the x-y plane perspective.

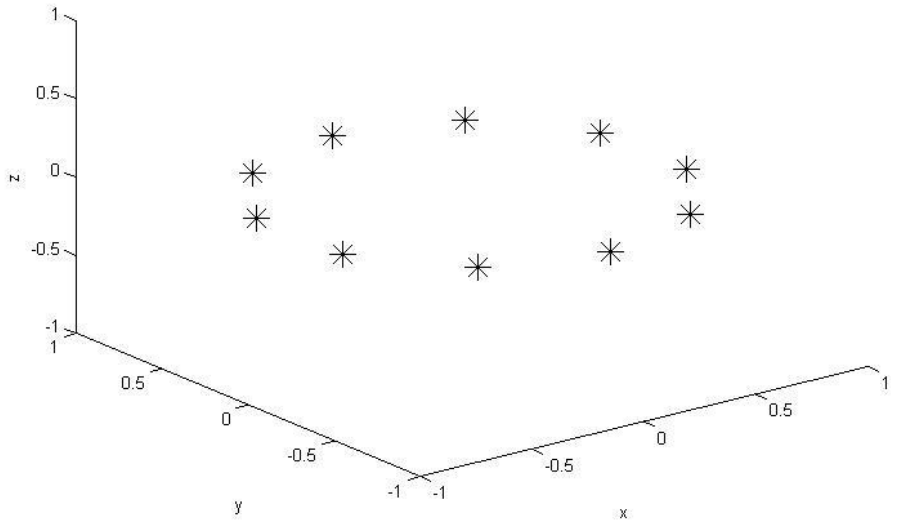

Figure 5.4 3D view of UCA

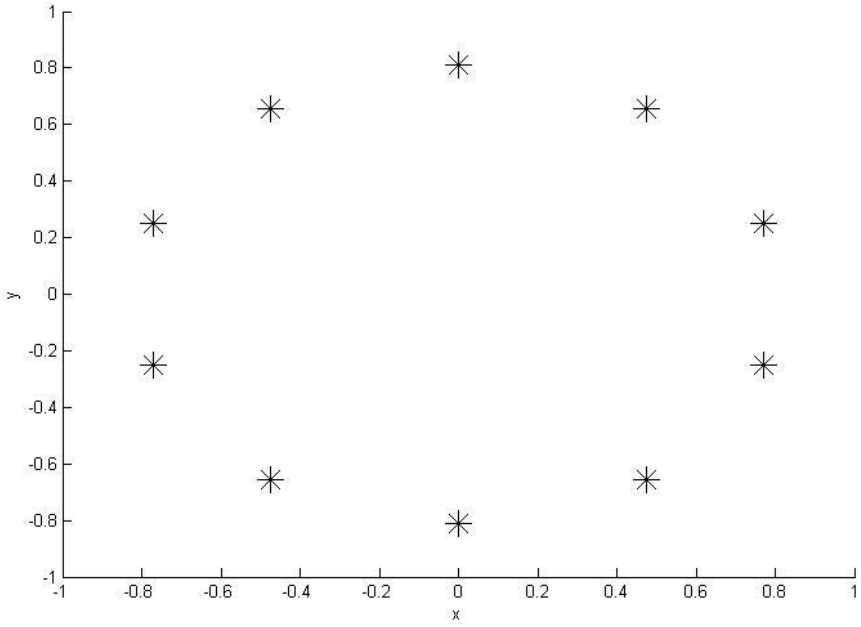

Figure 5.5 x-y plane view of UCA

Definitely, UCA is isotropic along the z-axis. Based on this characteristic, UCA has good performance in mutable incident angles estimation. In this dissertation, we consider the UCA with radius ρ, allowing that the elements are spaced by half a wavelength. The position vector can be shown as:

$$\vec{l}_m = [\rho \cos \varphi_m, \rho \sin \varphi_m, 0] \tag{5.8}$$

Where φ_m denotes the azimuth of mth array sensor. Then we can get the time delay based on propagation manifests in a phase shift in the received signal at the reference element as mentioned above. Here, we use θ to express the time delay $\Delta_m(\theta_d)$. The delays of elements are representing as:

$$\Delta_{cm}(\varphi_d, \theta_d) = \frac{\rho \sin(\theta_d) \cos(\varphi_d - \varphi_m)}{c} \tag{5.9}$$

There is no denying that UCA is one of the most common array geometries in research, based on its unique characters. First of all, UCA is isotropic along the z axis according to the displacement in this dissertation, which means the azimuth will not affect the performance of DOA estimation. Also, UCA is not a concentrated displacement, so that there are some spaces for configuration development from it. e.g., adding two sensors above and below the centre of the circle, we can get a spherical array.

5.3.2 L Shaped Array (LSA)

L Shaped Array (LSA) composed of two uniform linear sub-arrays placed on the x and y axes, with inter-element spacing equal to p ($p=\frac{\lambda}{2}=0.5$m) is presented. The element placed at the origin is common for referencing purposes.

L-shaped array has characteristics of Uniform Linear Array and the planar array, such as simple structure, and the research outcomes of the ULA can be applied on the L-shaped array as well. The Cramer-Rao bounds (CRB) of the estimated wave directions based on the L-shaped array are about 37% smaller than those for the cross array [5]. Since the space is not full used by this configuration, this type of array geometry has not been researched much. Thus, it is innovative for this section to analyze the performance of L Shaped Array.

Here, we choose ten elements in this case, where six elements placed on x axes and five elements placed on y axes in this dissertation.

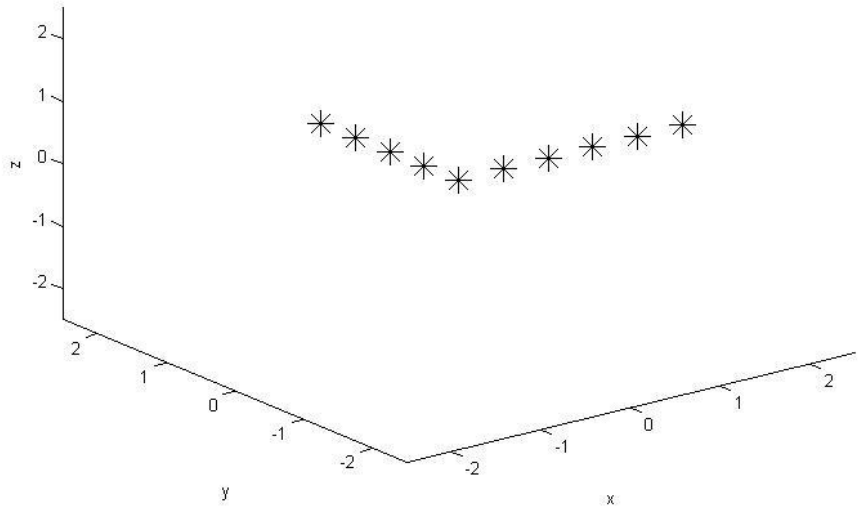

Figure 5.6 3D view of LSA

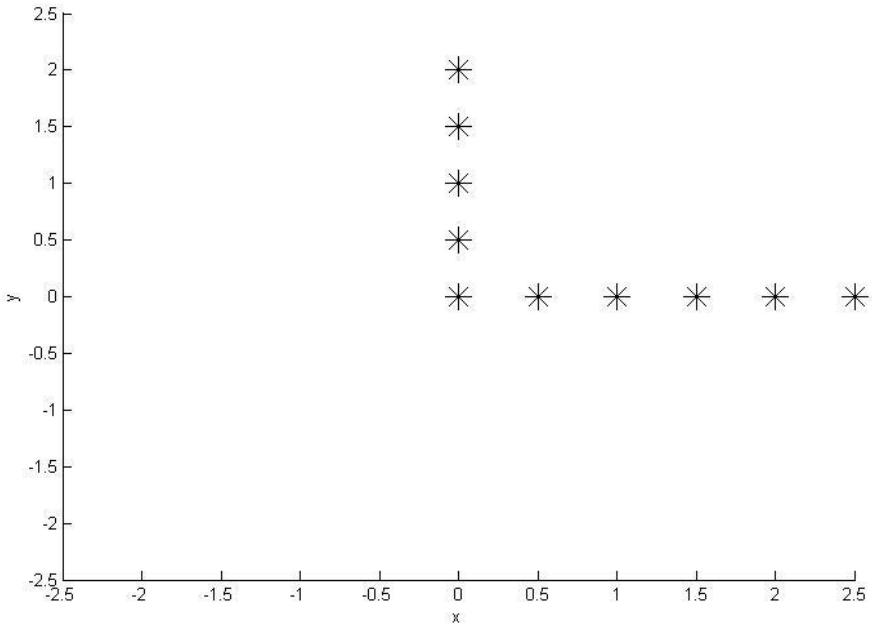

Figure 5.7 x-y plane view of LSA

L Shape Array (LSA) is a array geometry which is always used to compare the performance of DOA estimation with other geometry. It is not hard to make sense that LSA is no isotropic. The location of elements can be represented as:

$$\vec{l}_m = [\mathrm{x_m}, \mathrm{y_m}, 0] \tag{5.10}$$

And the delay of every element can be expressed as:

$$\Delta_{lm}(\varphi_d, \theta_d)=\frac{\sin(\theta_d)[x_m \cos(\varphi_d)+y_m \sin(\varphi_d)]}{c} \qquad (5.11)$$

LSA is not hard to image that it has a similar character with ULA in data processing, since it is a combination of two ULAs. However LSA improves ULA to 2D DOA estimation. From figure 5.6, it is not hard to find out that there are various kinds of L shaped configuration with the same number of elements, e.g. one element in x axis and nine elements in y axis, and two elements in x axis and eight elements in y axis etc. The properties of different LSA configurations are various. With the limitation of time, we just discuss the configuration with ten elements, where six elements placed on x axes and five elements placed on y axes in this dissertation.

5.3.3 Y Shaped Array (YSA)

Y Shaped Array (YSA) composed of three uniform linear sub-arrays placed on the x axes, 2/3 degree and -2/3 degree, with inter-element spacing equal to p ($p=\frac{\lambda}{2}=0.5$m) is presented. We take ten sensors in to account in this case, where there are four elements in every uniform linear sub array. The element placed at the origin is common for referencing purposes.

The performance of Y shaped array is the best among ULA L Shaped Array and Y Shaped Array and that the proposed self-calibration algorithm can achieve the high resolution under the condition of unknown coupling [6]. However, this kind of array has not been research much even it is not difficult to image the array geometry. It is not clear about some features of Y Shaped Array and we try to gain some data of it in this dissertation. We try to analyze the performance of YSA in DOA estimation in this chapter.

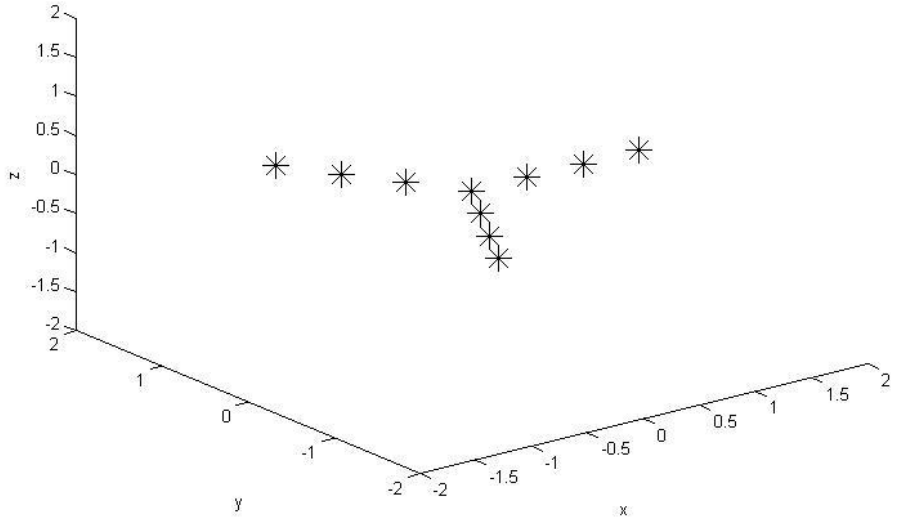

Figure 5.8 3D view of YSA

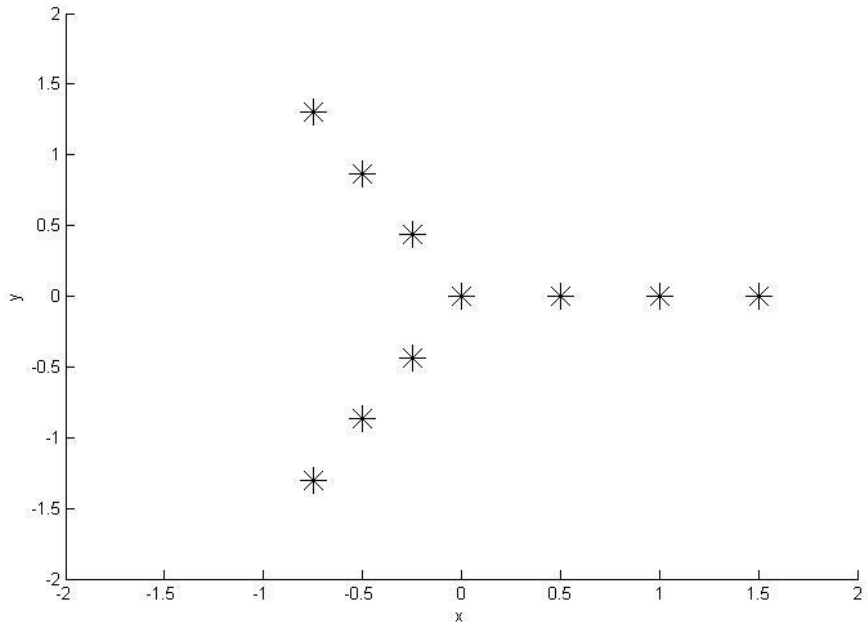

Figure 5.9 x-y plane view of YSA

Y Shape Array (YSA) is a particular array geometry which has been proved has good performance. The location of element can be represented as:

$$\vec{l}_m = [\rho_m \cos \Psi_m, \rho_m \sin \Psi_m, 0] \qquad (5.12)$$

The delay of elements can be shown as:

$$\Delta_{ym}(\varphi_d, \theta_d)=\frac{\rho_m \sin(\theta_d)\cos(\varphi_d-\Psi_m)}{c} \qquad (5.13)$$

The YSA is symmetry along the axis of each sub arrays and the x-y plane, and this property can lead to some special performance is DOA estimation. Wu has performance analysis of DOA algorithm for Y-shaped array [2]. However, there were not many further research outcomes of YSA in last years.

5.3.4 Rectangular Array (RA)

The Rectangular Array composed of two uniform linear sub-arrays placed near the x axes in the x-y plane, and the axis of two ULA is (y=0.25m, z=0m) and (y=-0.25m, z=0m) in this case. The inter-element spacing equal to d (p= $\frac{\lambda}{2}$ =0.5m) is presented. The element placed at (0, 0.25, 0)m is common for referencing purposes.

The configuration of rectangular array is common when the number of elements is large, but in this case, the number of elements is not large enough. Here, we just try to compare the performance of DOA estimation of RA with other array geometries.

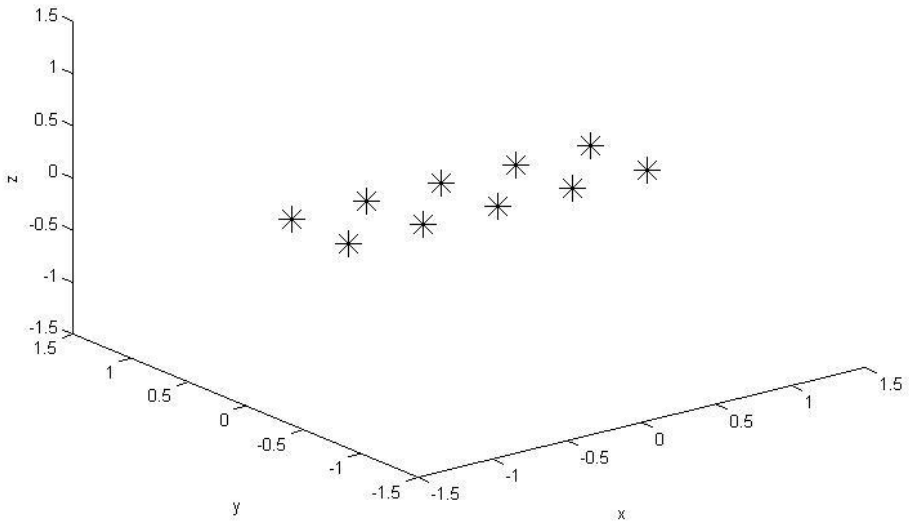

Figure 5.10 3D view of RA

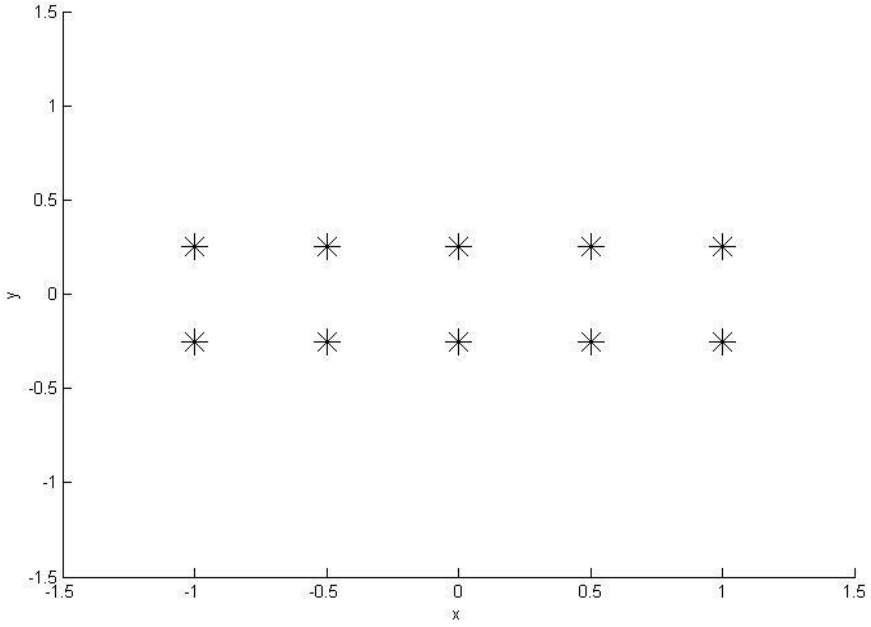

Figure 5.11 x-y plane view of RA

The antenna array in Figure has a rectangular configuration composed by two ULAs placed in parallel on the x–y plane. The inter-sensor distance p is taken to be half a wavelength of the signal waves. Then the position vector can be expressed as:

$$\vec{l}_m = [\mathrm{x_m}, \mathrm{y_m}, 0] \tag{5.14}$$

The propagation delay for the dth source on the mth sensor is derived as:

$$\Delta_{\mathrm{rm}}(\varphi_{\mathrm{d}}, \theta_{\mathrm{d}}) = \frac{\sin(\theta_{\mathrm{d}})[\mathrm{x_m}\cos(\varphi_{\mathrm{d}}) + \mathrm{y_m}\sin(\varphi_{\mathrm{m}})]}{\mathrm{c}} \tag{5.15}$$

RA is a widely implemented array geometry, because it is a kind of concentrated displacement, which means that a maximum number of array elements can be displace in a given plane space. In this way, we can improve the performance of smart antenna in a limited space by way of increasing the number of elements.

5.4 Three Dimension

The three dimension case is a new area in array geometry. There is no much research has been made in this case. In the 3D case, the position vector of sensors can be expressed as:

$$\vec{V}(\varphi,\theta)=[\cos(\varphi)\sin(\theta),\sin(\varphi)\sin(\theta),\cos(\theta)] \qquad (5.16)$$

Definitely, the performance depends on the geometry of the antenna array. There are various kinds of array geometry in three dimension case. In this chapter, we focus on some classical array configuration as Double Uniform Circle Array and Double L Shaped Array.

5.4.1 Double L Shaped Array (DLSA)

The 3D Double L shaped array with M (in this dissertation, M=10) elements composed of three uniform linear sub-arrays placed on the x, y and z axes (four elements in each axes in this dissertation) with inter-element spacing equal to p (p= $\frac{\lambda}{2}$ =0.5m) is presented. The element placed at the origin is common for referencing purposes.

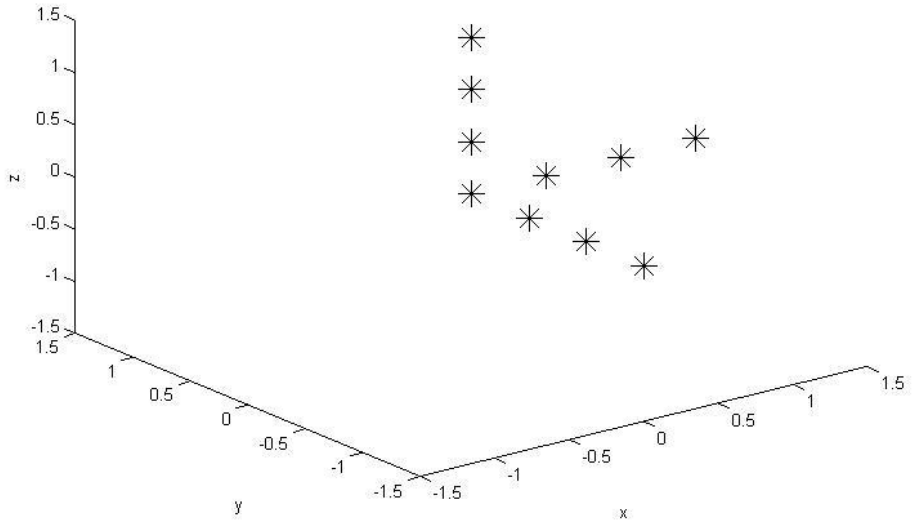

Figure 5.12 3D view of DLSA

This antenna array configuration has already been proposed in [3] for the estimation of the 2D directions of arrival. DLSA consist of three ULAs and it is not difficult to find out that we can get a new DLSA by changing the scale of each ULA. e.g., we can remove one element from the z axis to x axis. In this dissertation, we study this particular configuration of DLSA shown as figure 5.12 because it is the most symmetric one and thus it can be expected to give

the most isotropic accuracy and resolutions characteristics. Here, the position vector of the mth element is expressed as:

$$\vec{l}_m = [x_m, y_m, z_m] \tag{5.17}$$

Then the propagation delay for the dth source on the mth sensor is derived as

$$\Delta_{2lm}(\varphi_d, \theta_d) = \frac{[x_m \cos(\varphi_d)\sin(\theta_d) + y_m \sin(\varphi_m)\sin(\theta_d) + z_m \cos(\theta_d)]}{c} \tag{5.18}$$

DLSA is the simplest 3D displacement antenna array. With the 3D located sensors, we can easily guess that it has a better performance in 3D space, at least in some aspects. Not matter what the incident angle is, there are two sub arrays receiving the impinging signal at least, which means that DLAS does not have black spot in DOA estimation.

5.4.2 Double Uniform Circular Array (DUCA)

The Double Uniform Circular Array (DUCA) composed of two uniform circle sub-arrays (five elements in each sub-array) placed on the plane z=p/2 and z=-p/2, with inter-element spacing equal to p (p= $\frac{\lambda}{2}$ =0.5m) is presented.

Double Uniform Circular Array is seldom referred by papers, so we cannot learn its characteristics from previous researchers. We try to analyze Double Uniform Circular Array in the same way with other array geometries. In this dissertation, we take ten sensors in to account, so the configuration is derived as.

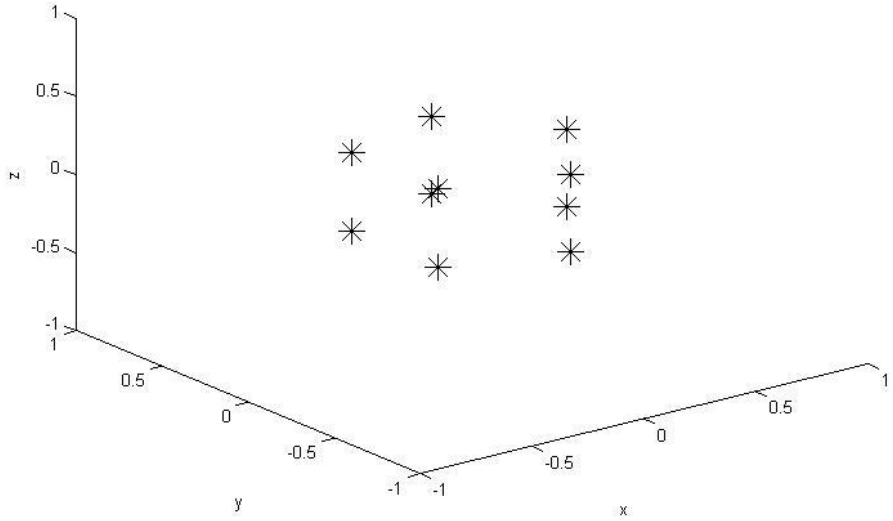

Figure 5.13 3D view of DUCA

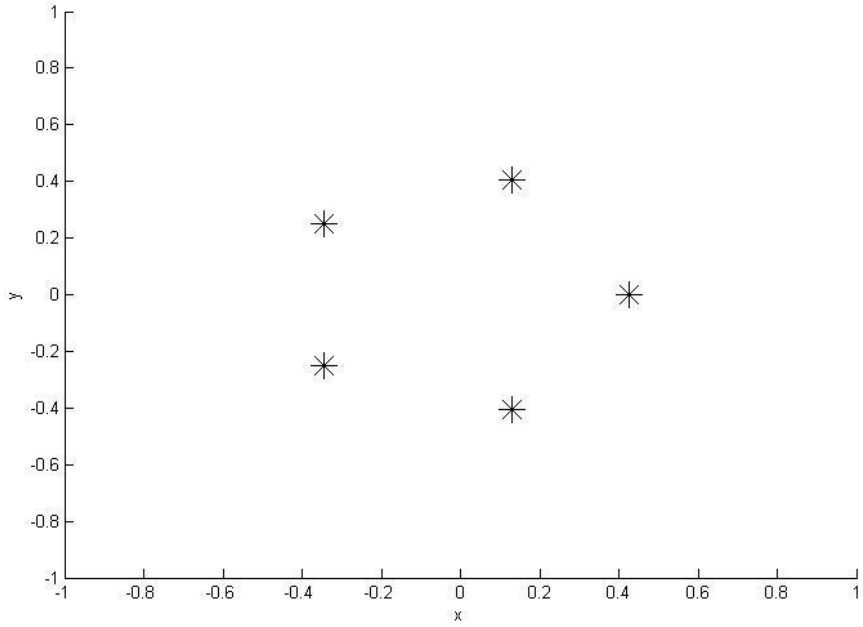

Figure 5.14 x-y plane view of DUCA

As figure 5.13 and 5.14 shows, each circle has five elements, and locates at z=0.25m and z=-0.25m plane respectively. Assume that the radius of the subarrays circle denotes as $\boldsymbol{\rho}$. The displacement vector of the mth element can be expressed as:

$$\vec{l}_m = [\rho \cos \Psi_m, \rho \sin \Psi_m, z_m] \qquad (5.19)$$

Then the propagation delay for the dth source on the mth sensor is derived as:

$$\Delta_{2cm}(\varphi_d, \theta_d)=\frac{\rho \sin(\theta_d) \cos(\varphi_d-\Psi_m)+z_m \cos(\theta_d)}{c} \qquad (5.20)$$

In practice, DUCA is commonly implemented because we combine two UCA which can just receive signal in one surface to have the ability of DOA estimation in all space. However, if the sensor can receive signal from all space, the performance of DUCA will be particular. Hence, we try to discuss this kind of DUCA in this dissertation.

5.5 General view of DOA estimation simulation by MUSIC

In this dissertation, the main topic is the performance of array geometries in DOA estimation. Therefore, in order to simplify the computation, we ignore the mutual coupling of resources, which is not the most important factor of judgment of array geometries' performance in DOA estimation. The simulation deals with one dimensional array, two dimensional array and three dimensional array respectively.

5.5.1 Simulation of one dimensional case

In this dissertation, we analyzed the performance of DOA estimation with various array geometries, where MUSIC algorithm was implemented. As demonstrated in section 4.1, the last step of MUSIC is scanning all the angles by equation 4.10. Then we can get a graph of $P_{MU}(\varphi, \theta)$. In this section, we tried to show the peak graph of array geometries mentioned above, and gained a general view of the graph which will be used in further data analysis.

In 1D DOA estimation, the DOA peak graph of ULA is shown as figure 5.15, where the incident angles are 10, 80 and 130 degree.

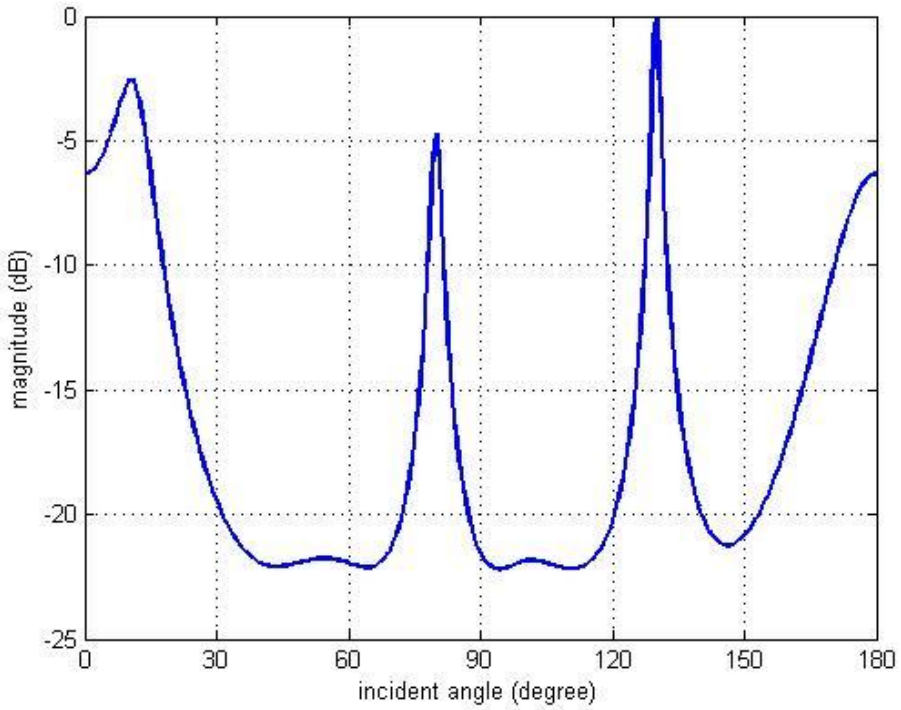

Figure 5.15 ULA

From figure 5.15, we can find out three peaks in the graph, whose incident angles are around 10, 80 and 130 degree respectively. The angles 80 and 130 degree are distinguished easily because peaks are -5dB to lower than -20dB. However, the angle 10 degree is not easy to distinguish from the curve because the values of nearby angles are relative close to the peak. Therefore, it is reliable to predict that the incident angle will affect the ability of signal detection. When the incident angle comes close to 0 degree or 180 degree, which means that the incident signal is paralleled to the ULA, the ability of detection of the Uniform Linear Array will decrease greatly.

5.5.2 Simulation of two dimensional case

In 2D DOA estimation, the peak graph of two dimension and three dimension array geometries are shown as follows, where the incident angles (φ, θ) are $(10°, 10°)$, $(80°, 60°)$, $(130°, 20°)$. Here, the SNR=10 and snapshot is 50.

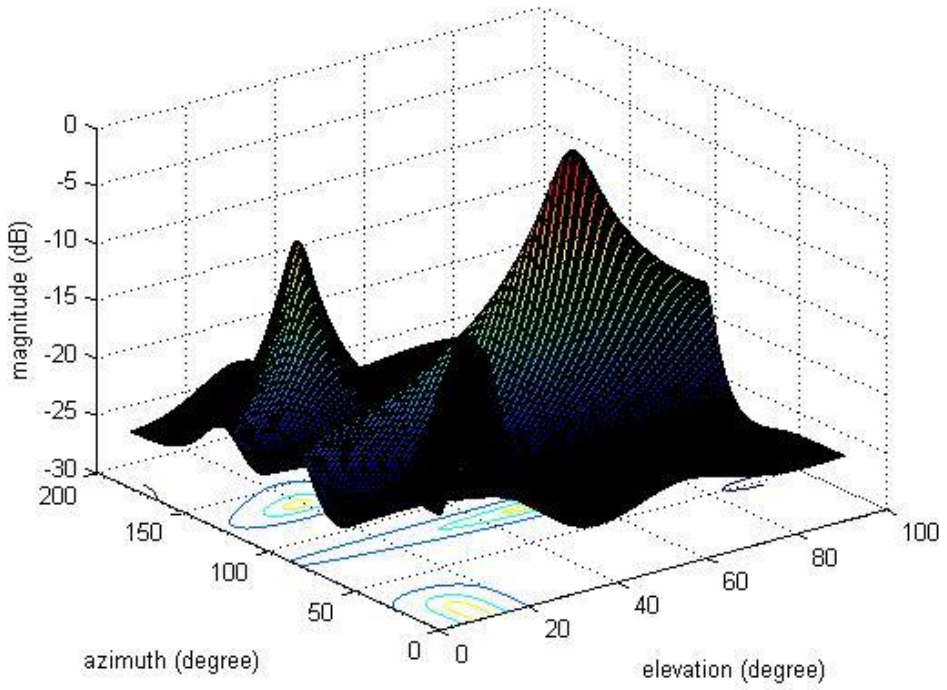

Figure 5.16 $P_{MU}(\varphi, \theta)$ graph with UCA

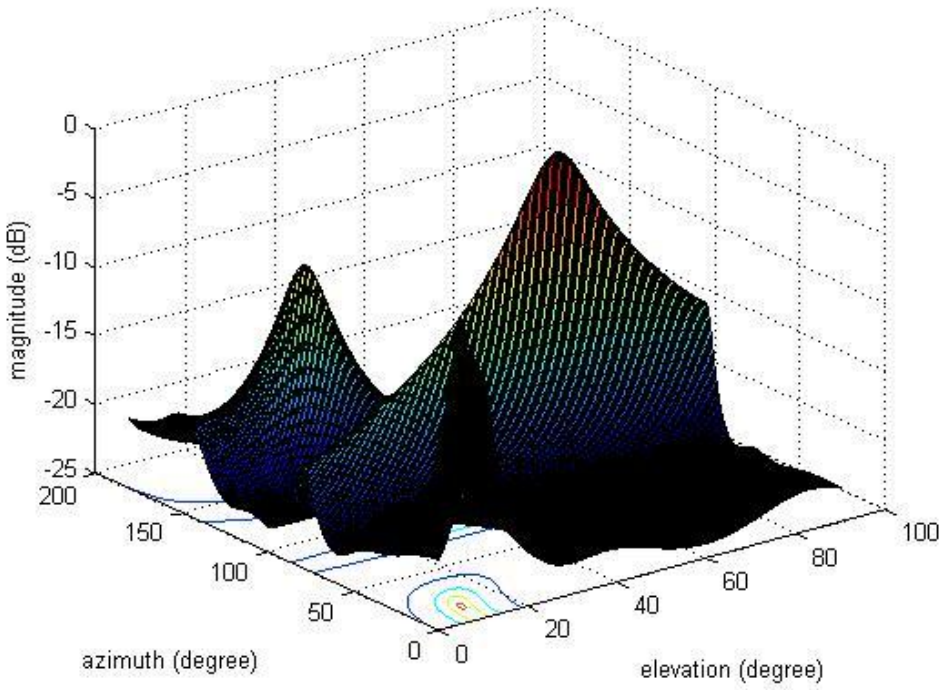

Figure 5.17 $P_{MU}(\varphi, \theta)$ graph with LSA

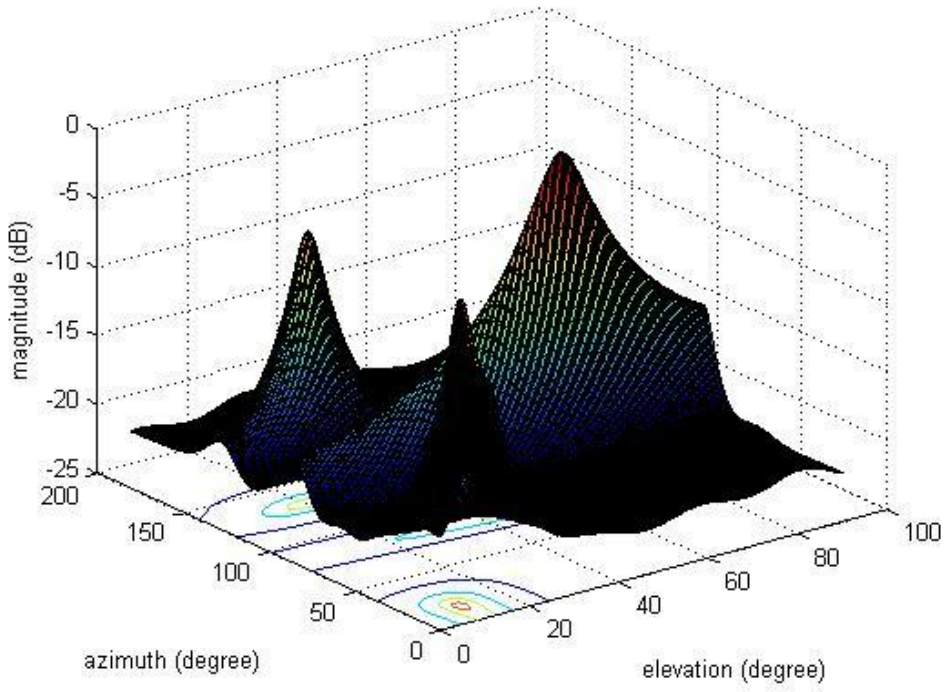

Figure 5.18 $P_{MU}(\varphi, \theta)$ graph with YSA

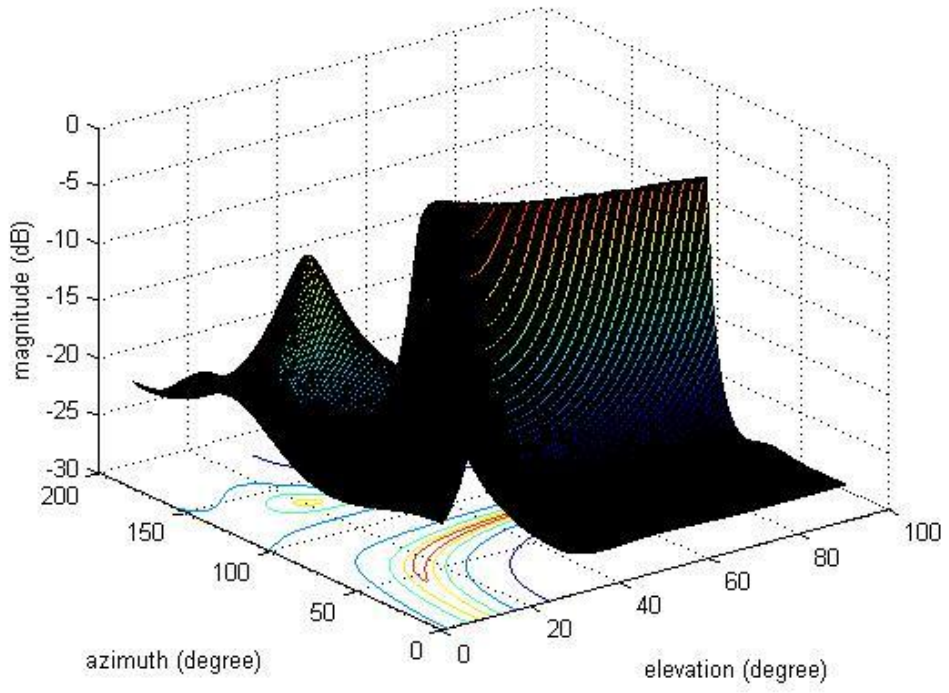

Figure 5.19 $P_{MU}(\varphi, \theta)$ graph with RA

From figure 5.16, 5.17 and 5.18 we can discover three peaks without trouble. Relatively, the incident angle $(80°, 60°)$ is not easy to find from the graph of

Rectangular Array (RA), so Rectangular Array is not as good as other three geometries to some degree. We will further comparison by data analysis in chapter 6.

5.5.3 Simulation of three dimensional case

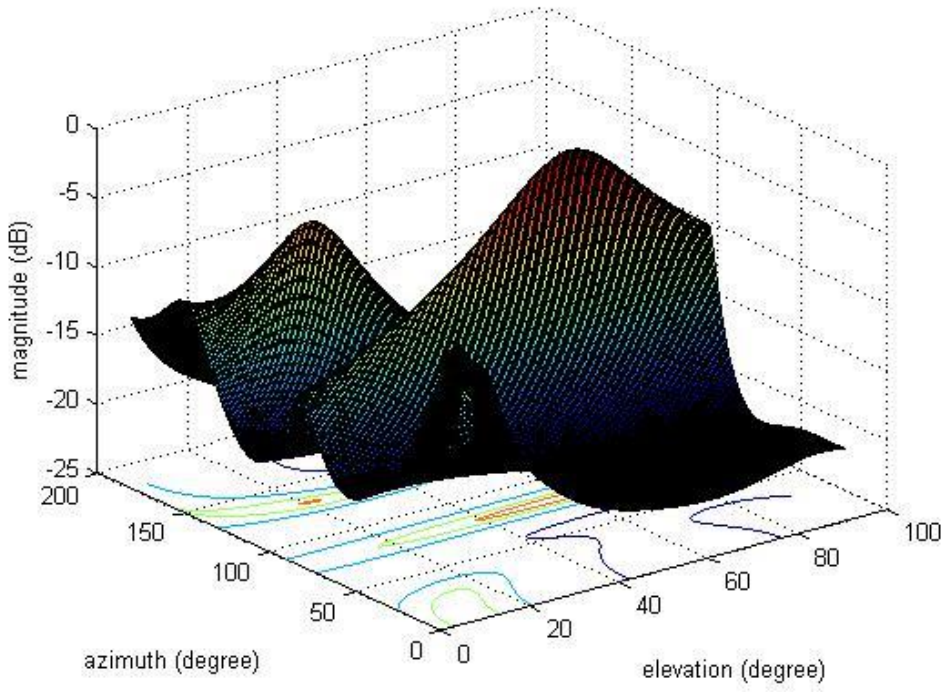

Figure 5.20 $P_{MU}(\varphi, \theta)$ graph with DLSA

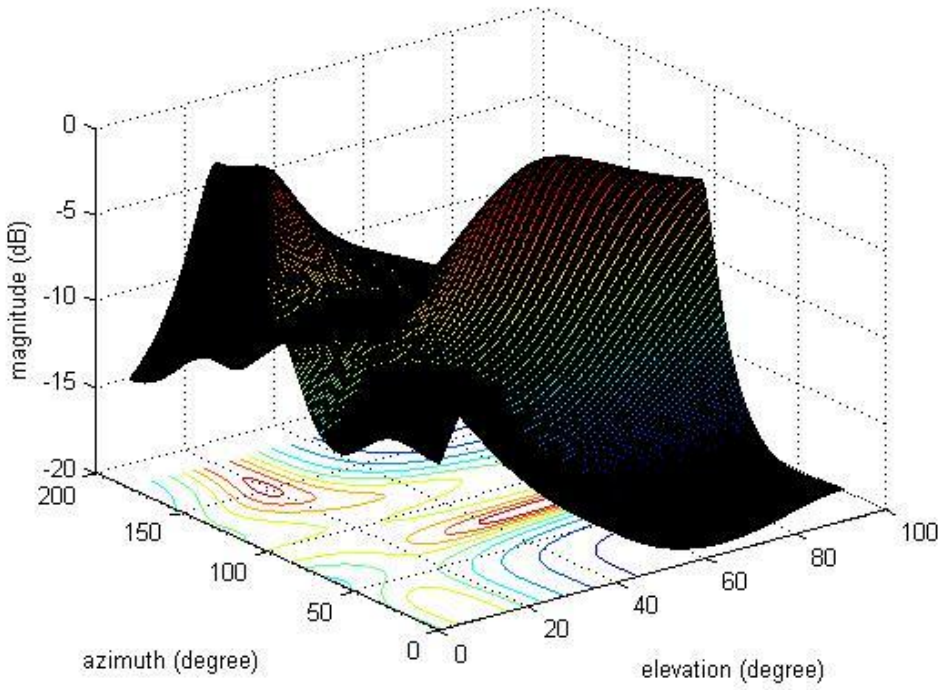

Figure 5.21 $P_{MU}(\varphi, \theta)$ graph with DUCA

From figure 5.20 and figure 5.21, the condition of DOA estimation simulation is not poor, which means the Signal Noise Ratio (SNR) and snapshot is not low. However, peaks are not definite in graphs of Double Uniform Circular Array (DUCA), implying that it is difficult to detect peaks and errors are generated with limited number of array elements. We will validate this in section 6.2.

5.6 Cramer-Rao Bound of array geometries

In this section, we focus on the Cramer-Rao Bound (CRB) for different array geometries which has been introduced in this chapter. Here we try to formulate the problem of one signal with elevation and azimuth. From [4] we can get method to calculate the CRB for one source.

$$CRB(\varphi, \theta) = [G(\boldsymbol{B} \quad \varphi \quad \theta) \cdot \mathrm{T}]^{-1} \tag{5.23}$$

where φ is the azimuth and θ is the elevation as demonstrated in section 5.1. T and $G(\boldsymbol{B} \quad \varphi \quad \theta)$ can be expressed as 5.24 and 5.25 repectively:

$$\mathrm{T} = \frac{2\mathrm{n}(2\pi\mathrm{M}/\lambda)^2 \cdot \mathrm{SNR}^2}{1+\mathrm{SNR} \cdot \mathrm{M}} \tag{5.24}$$

$$G(\boldsymbol{B},\quad \varphi,\quad \theta) = \boldsymbol{U^T B U} \tag{5.25}$$

Where **U** is the incident angle matrix and **B** is the array configuration matrix as 5.26 and 5.27:

$$\boldsymbol{U} = \begin{bmatrix} \sin\theta\sin\varphi & -\cos\theta\cos\varphi \\ \sin\theta\cos\varphi & \cos\theta\sin\varphi \\ 0 & \sin\theta \end{bmatrix} \tag{5.26}$$

$$\boldsymbol{B} = \frac{1}{\mathrm{M}}\sum_{m=1}^{M}\left(\vec{l}_m - \vec{l}_c\right)\left(\vec{l}_m - \vec{l}_c\right)^T \tag{5.27}$$

Where M denotes the number of array elements. $\vec{l}_m$ which is demonstrated above is the displace vector of the mth element. $\vec{l}_c$ denotes the geometric centre of the array and can de expressed as:

$$\vec{l}_c = \frac{1}{\mathrm{M}}\sum_{\mathrm{m}=1}^{\mathrm{M}}\vec{r}_m \tag{5.28}$$

From 5.23, it is clear that CRB consist of two parts ($G(\boldsymbol{B}\quad\varphi\quad\theta)$ and T).We can find out that T depends on the SNR, the number of snapshot n, the wavelength λ and the number of elements M from 5.24. $G(\boldsymbol{B}\quad\varphi\quad\theta)$ is decided by array geometry through matrix $\boldsymbol{B}$ and the the incident angle (φ, θ) through $\boldsymbol{U}$ based on equation 5.25.

5.7 Conclusion

In this chapter, we introduced different kinds of array geometries, and explained some parameters of them. Then we made a simulation of DOA estimation for three signal resources with these arrays by MUSIC algorithm and gained a general view of their performance. At the end of the chapter, we implied the CRB of array geometries, which will be taken in to simulation in chapter 6, from other papers.

5.8 Reference

[1]Harabi F., Gharsallah A., Marcos S., "Three dimensional antennas array for the estimationof direction of arrival", Microwaves, Antennas & Propagation, IET Volume: 3 , Issue: 5 , Page(s): 843 – 849, 2009.

[2]Wu Biao, Chen Hui, "Performance analysis of self-calibration algorithm for Y-shaped array in the presence of mutual coupling", Microwave, Antenna, Propagation and EMC Technologies for Wireless Communications, 2009 3rd IEEE International Symposium on, Page(s): 97 – 102, 2009.

[3] Maohui X., 'New method of effective array for 2-D direction of arrival estimation', Int. J. Innov. Comput. Inf. Control, 2, pp. 1391–1397, 2006.

[4] ULKU B., RANDOLPH L.M., 'On the geometry of isotropic arrays', IEEE Trans. Signal Process, 51, (6), pp. 1469–1478, 2003.

[5] Hua, Y. Sarkar, T.K. Weiner, D.D. 'An L-shaped array for estimating 2-D directions of wave arrival', Antennas and Propagation, IEEE Transactions on Volume: 39 , Issue: 2 Page(s): 143 - 146 1991.

[6] Wu Biao, Chen Hui 'DOA Estimation and Self-Calibration Algorithm for Y-Shaped Array in the Presence of Mutual Coupling' Image and Signal Processing, 2009. CISP '09. 2nd International Congress on, **Page(s):** 1 - 5 Oct. 2009.

Chapter6 Simulation and Comparison

In this chapter, the simulation of questions mentioned in above chapters was made. The simulation consisted of two major parts that performance research of MUSIC, Root-MUSIC and ESPRIT algorithms and the property analyse of different array geometries. We used the Matlab 2012b to simulate the problems discussed in this dissertation.

6.1 One dimension simulation of MUSIC, Root-MUSIC and ESPRIT algorithm

In this section, we tried to compare the accuracy and computation efficiency of these three algorithms by simulation. Let's defined the incident angle $\theta \in [0, \pi]$ measured anticlockwise relatively to the x-axis.

6.1.1 Accuracy of algorithms

As for the simulation of accuracy comparison, we set one source impinging on the Uniform Linear Array (ULA) with 10 elements placed on the x axes with inter-element spacing equal to p ($p=\frac{\lambda}{2}=0.5$m). It was a common method to change only one parameter in the comparison, so that we changed SNR, snapshot and incident angle respectively in this section.

RMSE versus SNR

We regarded the Root Mean Square Error (RMSE) as a measurement of accuracy. RMSE could be expressed as:

$$\mathbf{RMSE(x)} = \sqrt{\frac{\sum_{i=1}^{n} \left(x_i - E(x)\right)^2}{n}} \qquad (6.1)$$

As demonstrated in section 4.4.4, the parameter of SNR was an important element which will affect the accuracy deeply. Therefore, in the first place, we set the same condition but vary the SNR in the simulation. Here, we set the snapshot n=50, the incident angle θ =80 degree, the times of trial was 100. The parameter SNR increased from 1dB to 30 dB. Besides, the step of MUSIC

algorithm in this case was 0.1 degree. We could get the graph of RMSE of three algorithms as figure 6.1 shows:

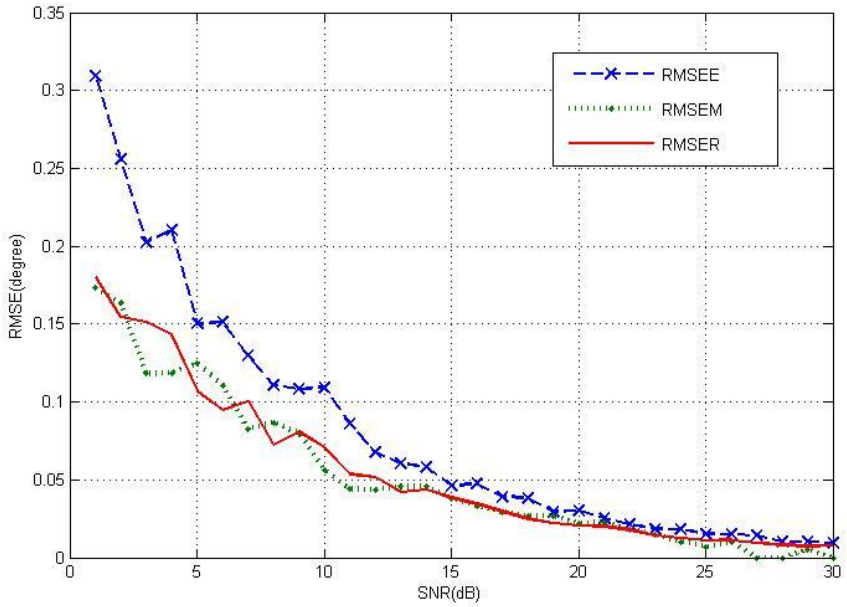

Figure 6.1 RMSE by SNR

In the figure 6.1 RMSEE, RMSEM and RMSER represent the RMSE of ESPRIT, MUSIC and Root-MUSIC respectively. Definitely, the RMSE of ESPRIT is bigger than MUSIC and Root-MUSIC, which means the accuracy of MUSIC and Root-MUSIC is better than ESPRIT. The simulation has proved previous conclusions of other researchers. As for the comparison between the MUSIC and Root-MUSIC, the performances of these two algorithms are similar.

RMSE versus snapshot

As demonstrated in section 4.4.4, the parameter of snapshot was another significant element which will affect the accuracy deeply. Therefore, we set the same condition but snapshot in the simulation. Here, we set the SNR=10 dB, the incident angle θ =80 degree, the times of trial was 100. The parameter snapshot increased from 1 to 50. Besides, the step of MUSIC algorithm in this case was 0.1 degree. We got the graph of RMSE of three algorithms as figure 6.2 shows:

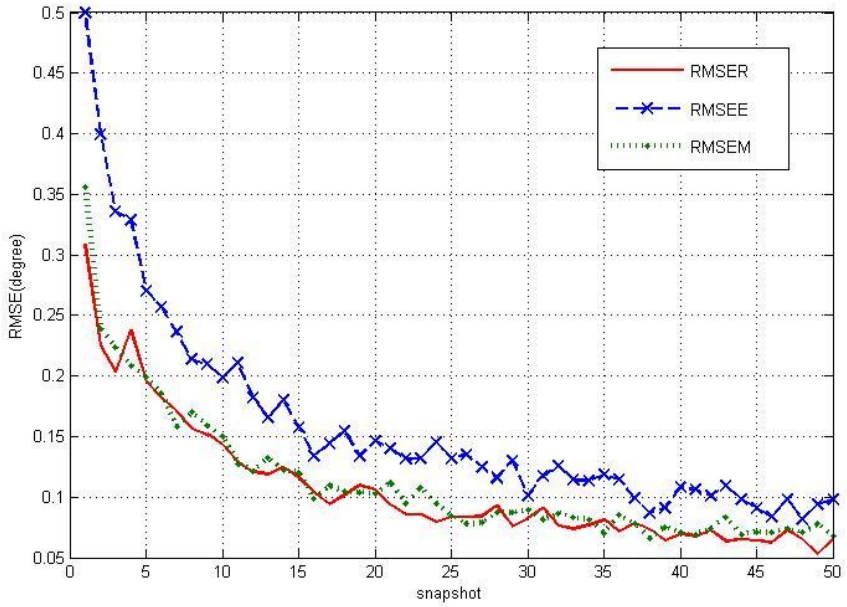

Figure 6.2 RMSE by snapshot

In the figure 6.2 RMSEE, RMSEM and RMSER represent the RMSE of ESPRIT, MUSIC and Root-MUSIC respectively. Obviously, the RMSE of ESPRIT is bigger than MUSIC and Root-MUSIC, which means the accuracy of MUSIC and Root-MUSIC is better than ESPRIT, and it is the same with figure 6.1. The simulation has proved previous researches of other researchers again. As for the comparison between the MUSIC and Root-MUSIC, the performances of these two algorithms are similar, from which we cannot tell a better one.

RMSE versus incident angle

We considered that the incident angle may affect the accuracy, so that we made a simulation of different incident angle. Here we set the same condition but incident angle in the simulation. As above, the SNR=10 dB, the snapshot n=50, the times of trial was 100. The parameter θ increased from 0 to 180 degree. Besides, the step of MUSIC algorithm in this case wass 1 degree. We got the graph of RMSE of three algorithms as figure 6.3 and figure 6.4 and the DOA estimation of three algorithms was shown at figure 6.5.

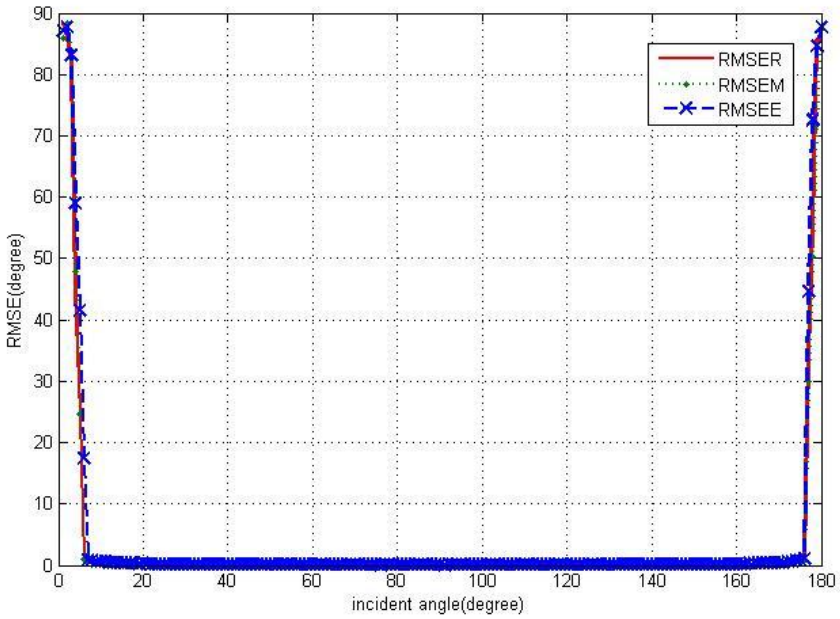

Figure 6.3 the RMSE by incident angle (0 to 180 degree)

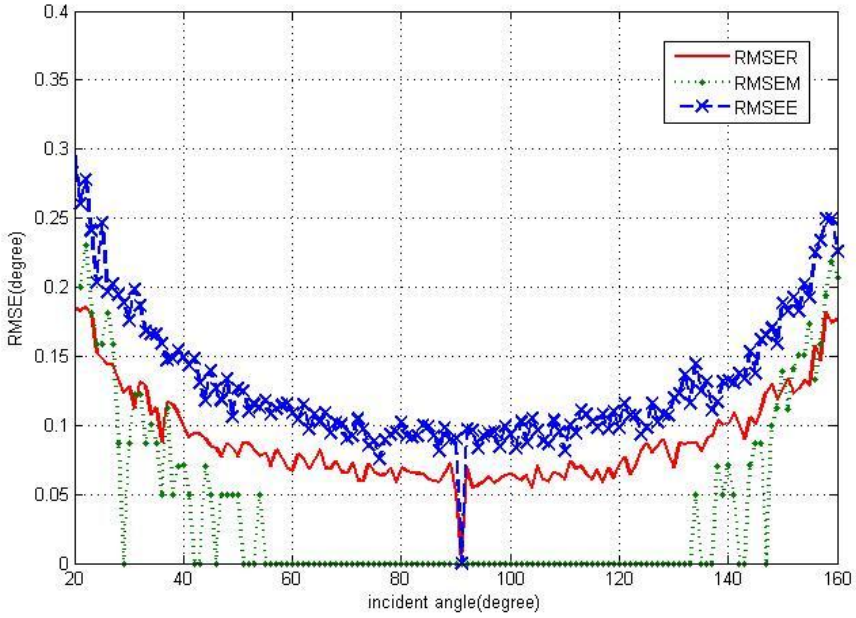

Figure 6.4 the RMSE by incident angle (20 to 160 degree)

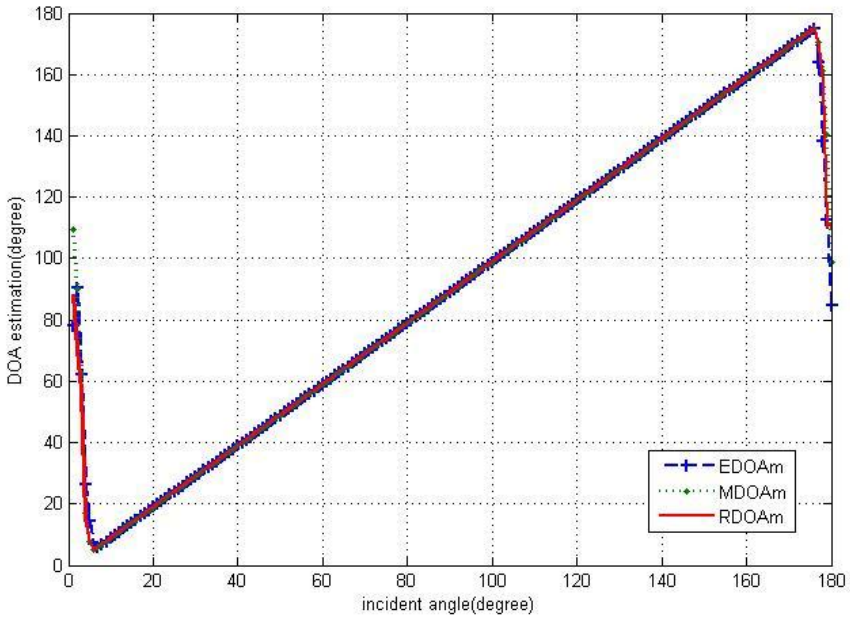

Figure 6.5 the DOA estimation by incident angle (0 to 180 degree)

In the figure 6.3 and 6.4, RMSEE, RMSEM and RMSER represent the RMSE of ESPRIT, MUSIC and Root-MUSIC respectively and in figure 6.5 EDOAm, MDOAm, RDOAm represent the DOA estimation with ESPRIT, MUSIC and Root-MUSIC algorithm respectively. From figure 6.3 and figure 6.5, it is not hard to find out an unexpected outcome that both RMSE and DOA are seriously wrong in these entire three algorithms when the incident angle ranges from around 0 to 5 degree 175 to 180 degree. Definitely, it is the weakness of the configuration of ULA that lead to the problem. Here, the incident angle in the range which was surfed from mistakes means the signal is almost paralleled to the array. In this case, the ULA may have trouble in estimation and a little scale of noise can make big difference.

From figure 6.4, which is a close view of RMSE with incident angle ranging from 20 degree to 160 degree, we can also find out that the accuracy of ESPRIT is not as good as Root-MUSIC. From 40 degree to 140 degree, the RMSE of MUSIC is smallest of three. Thus, it is fair to say that the MUSIC has better accuracy performance in the “face” case. Here, the scanning step of MUSIC is 1 degree, which means it may have better performance than this case with a smaller scanning step.

6.1.2 Computation efficiency of algorithms

The computation efficiency is a vital property of an algorithm, which decides the calculation time and energy cost. Therefore, an algorithm with good computation efficiency performance is what we wanted. In this section, we regarded the computation time in Matlab (tic/toc) as a standard of computation efficiency. The simulation progress is 6.1.1. The outcome of calculation time could be represented as table 6.1.

Table 6.1 Computation Time

	SNR(1 to 30dB)	Snapshot (1 to 50)	Incident angle (0 to 180 degree)
ESPRIT	9.859488 seconds	10.345005 seconds.	35.738154 seconds
MUSIC	41.787838 seconds	71.628077 seconds	261.868409 seconds
Root-MUSIC	390.086829 seconds	661.938485 seconds	2400.736639 seconds

In the simulation the number of trial was 100. In these three cases, ESPRIT was the most efficient algorithm, and MUSIC was the middle one. Though Root-MUSIC was good at estimating signal with the same incident angle, the computation efficiency was not good. Definitely, ESPRIT had an efficient calculation speed because it calculated the incident angle by subspace rather than scan angle by angle. As for Root-MUSIC, the progress to form and solve the polynomial took a long time, so that the efficiency of Root-MUSIC was not good.

6.1.3 Conclusion

According to the above analysis and simulation, we could draw a conclusion about the comparison of these three Eigen decomposing algorithms that ESPRIT was the most efficient algorithm in these three algorithms, where it

used around one fourth calculation time of MUSIC, and that MUSIC was the best in accuracy in these three algorithms.

In detail, the ESPRIT was proposed in order to promote the computation efficiency from MUSIC, sacrificing a part of accuracy. Errors would be amplified in computational calculation with increasing steps in ESPRIT, which did not have feedback or calibration, so that the accuracy of ESPRIT was not as good as MUSIC, whose step of $P_{MU}(\varphi, \theta)$ scanning works as calibration.

MUSIC algorithm, which was the most common used in practice, would got a balance between accuracy and efficiency with a proper step length. From section 4.1, it was clear that the only step of calculation was the computation of covariance and eigendecomposition, and few computational errors were added to the data. In this way, the excellent accuracy was proved. However, we could never ignore weakness of MUSIC, the ability of resolution. Therefore, previous researchers had proposed Root-MUSIC to improve the ability of resolution, increasing the computation amount meanwhile.

6.2 Array geometry simulation

Although above section deals with a comparison of classical DOA estimation algorithms from a signal impinging on ULA, the final target is to apply these algorithms in antenna arrays.

In this section, we have tried to compare the performances of various array geometries with the some number of elements (10). Let us note the DOA of the dth source by (φ_d,θ_d), where elevation angle $\theta_d \in [0, \pi]$ and azimuth angle $\varphi_d \in [-\pi,\pi]$ as figure 6.6 shows.

This section will demonstrate and simulate the directivity, accuracy and detection ability of these array geometries in two dimensions case, including Uniform Circle Array (UCA), L Shaped Array (LSA), Double L Shaped Array (DLSA) and Double Uniform Circle Array (DUCA). As discussed in 6.1, we take MUSIC as the estimator in this section in order to have good accuracy outcomes.

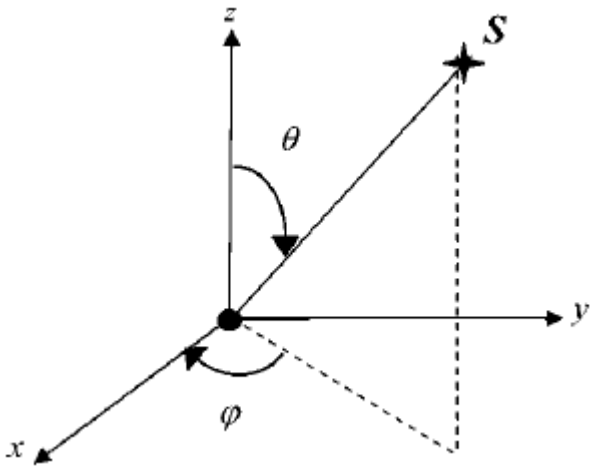

Figure 6.6 the coordinate and incident angle (φ, θ) [1]

6.2.1 Directivity of array geometry in DOA estimation

The array geometries mentioned in Chapter 5 are not isotropic in geometrical case, so it is easy to imply that they do not have isotropic performance in DOA estimation. Thus, it is interested to research to directivity of these array geometries.

According to section 5.5 (figure 5.15 to 5.21), the magnitude of estimation outcomes by array geometries are different with various incident angle. Then, in section 5.6, equation 5.23, 5.25 and 5.26 which are rewritten as follow shows that CRB of array geometry depends on the incident angle. Therefore, we can demonstrate the directivity of array geometries in DOA estimation by their CRB of estimation which are calculated from constant various incident angles. Then we can discuss the relationship between symmetry and incident angle in different geometries by CRB.

$$CRB(\varphi, \theta) = [G(\boldsymbol{B} \quad \varphi \quad \theta) \cdot \mathrm{T}]^{-1} \tag{5.23}$$

$$G(\boldsymbol{B}, \quad \varphi, \quad \theta) = \boldsymbol{U^T B U} \tag{5.25}$$

$$\boldsymbol{U} = \begin{bmatrix} \sin\theta \sin\varphi & -\cos\theta \cos\varphi \\ \sin\theta \cos\varphi & \cos\theta \sin\varphi \\ 0 & \sin\theta \end{bmatrix} \tag{5.26}$$

In order to describe the directivity of array geometries by CRB, It is significant to ensure other parameters of array geometries and incident resources in the

same value, the so-called some condition. In the simulation progress, we set the power of incident resources SNR=10dB, the number of array elements M=10, the wavelength of incident resources λ=1m and snapshot of data as 50. Here define the elevation angle $\theta \in [0, \pi/2]$ and azimuth angle $\varphi \in [-\pi,\pi]$, and denote the incident angle as (φ, θ).

The CRB of Uniform Circular Array (UCA), L Shaped Array (LSA), Double L Shaped Array (DLSA) and Double Uniform Circular Array (DUCA) will be simulated and analyzed in this section, and we try to demonstrate directivity of these array geometries by CRB of DOA estimation.

Uniform Circular Array (UCA)

In this section, we tried to demonstrate the directivity of UCA in DOA estimation by their CRB of estimation which is calculated from constant various incident angles. The configuration of UCA was demonstrated in section 5.3.1. Geometrically, UCA was isotropic in the x-y plane. Therefore, the variety of azimuth would not affect the performance of DOA estimation. Here, the simulation would get the CRB of azimuth and elevation in DOA estimation respectively.

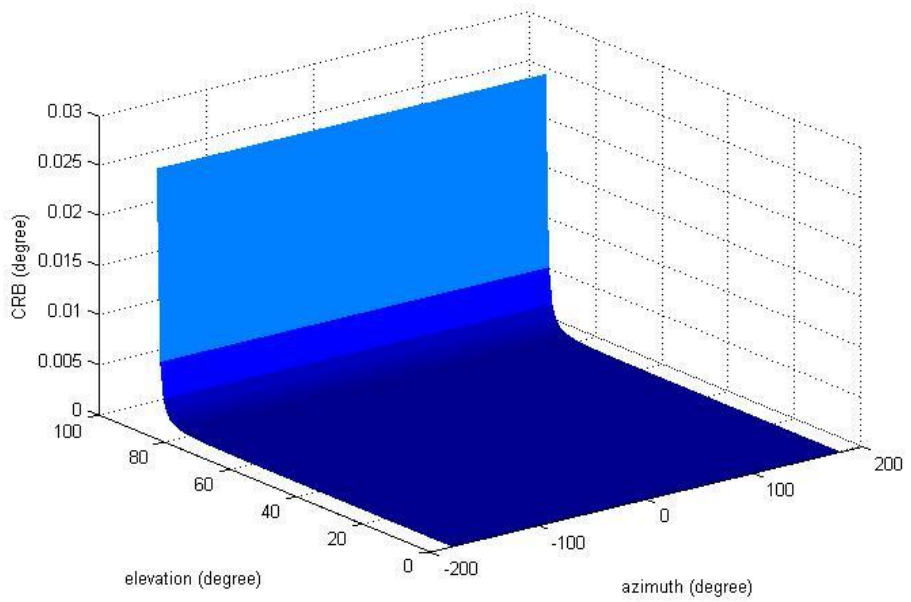

Figure 6.7 CRB (θ) of UCA in DOA estimation

Figure 6.7 describes the relationship between CRB of estimation of elevation θ and various incident angles in UCA. As figure 6.7 shows, the maximum magnitude of CRB is around 0.03 degree, which is much larger than CRB in other incident angles, when the elevation is near 90 degree. Thus, it is reliable to imply that the UCA has relatively poor performance in estimating elevation θ when the elevation is around 90 degree, which means the incident signals are parallel to the UCA plane. Besides, figure 6.7 shows the general tendency of CRB of estimation of elevation θ that with the increasing of elevation (0 to 85 degree), the CRB of estimation of elevation θ increases as well.

Based on CRB of estimation of elevation θ analysis, the directivity of UCA in the estimation of elevation θ was that the performance of elevation estimation decreased with the increasing incident elevation and was not affected by incident azimuth. This inference was identical with the geometric configuration of UCA as well.

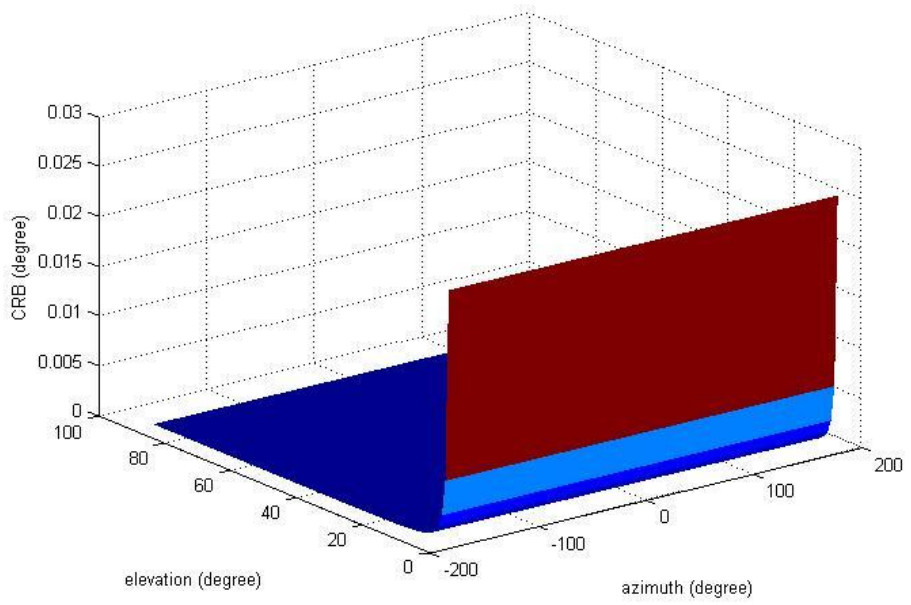

Figure 6.8 CRB (φ) of UCA in DOA estimation

Figure 6.8 describes the relationship between CRB of estimation of azimuth φ and various incident angles in UCA. According to the figure, the maximum magnitude of CRB of estimation of azimuth φ is around 0.3 degree when the elevation is close to 0 degree. Thus, it is acceptable to imply that the UCA is not good at estimating azimuth φ when the elevation locates around 0 degree.

This case describes the incident signals are perpendicular to the UCA in the x-y plane. Besides, figure 6.8 shows the general tendency of CRB of estimation of azimuth φ that with the increasing of elevation (5 to 90 degree), the CRB of estimation of azimuth φ decreases.

According to the CRB of estimation of azimuth φ analysis, the directivity of UCA in the estimation of azimuth φ was that the performance of azimuth estimation increased with the increasing incident elevation and was not affected by incident azimuth. This inference was identical with the geometric configuration of UCA as well.

L Shaped Array (LSA)

In this section, we tried to demonstrate the directivity of LSA in DOA estimation by their CRB of estimation which was calculated from constant various incident angles. The configuration of LSA was demonstrated in section 5.3.2. In order to make the simulation succinct and typical, we assumed elements of LSA displace on the positive axis of x and y axis, where six elements on x axis and five elements on y axis. According to geometrical configuration, it was not hart to understand that LSA was not isotropic or symmetrical along any axis or plane. Here, the simulation would gain the CRB of estimating azimuth and elevation respectively.

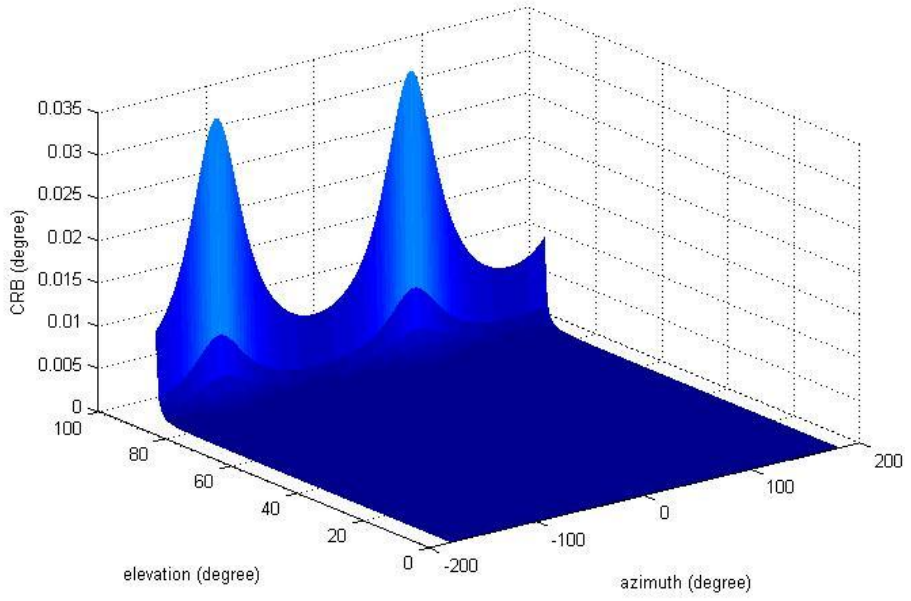

Figure 6.9 CRB (θ) of LSA in DOA estimation

Figure 6.9 describes the relationship between CRB of estimation of elevation θ and various incident angles in LSA. As shown in figure 6.9, the maximum magnitude of CRB of estimation of elevation θ is around 0.035 degree, when the elevation comes close to 90 degree. In a general view, figure 6.9 shows the tendency of CRB of estimation of elevation θ that with the increasing of elevation (0 to 85 degree), the CRB of estimation of elevation θ increases. Because of the large CRB value, LSA can have poor performance in estimating elevation θ when elevation is around 90 degree.

It is clear in figure 6.9 that the CRB of estimation of elevation θ depends on azimuth φ as there are peaks when azimuth are -125 and 55 degree. Thus, it is acceptable to imply the directivity of LSA that LSA is anisotropic and the relative weakness of elevation estimation is the case when the elevation is near 90 degree and the azimuth is near -125 or 55 degree.

From the CRB of estimation of elevation θ analysis, the directivity of LSA in the estimation of elevation θ was that the performance of elevation estimation decreased with the increasing incident elevation and is period with constant change of incident azimuth. Given an incident elevation, it would be worst performance in estimating elevation θ when the incident azimuth was near -125 or 55 degree. This inference was identical with the geometric configuration of LSA as well.

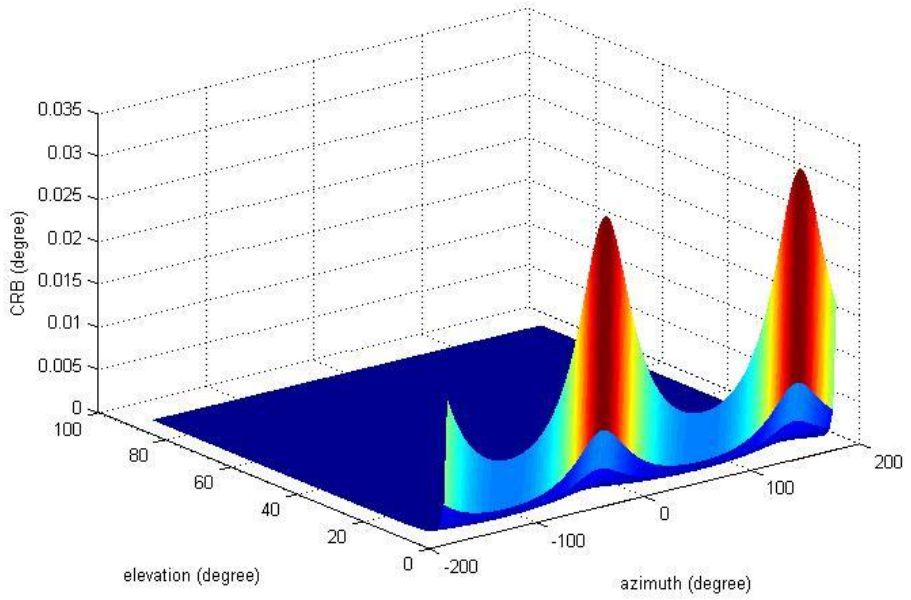

Figure 6.10 CRB (φ) of LSA in DOA estimation

Figure 6.10 describes the relationship between CRB of estimation of azimuth φ and various incident angles in LSA. As shown in figure 6.10, the maximum magnitude of CRB of estimation of azimuth φ is around 0.035 degree, when the elevation comes close to 0 degree. In a general view, figure 6.10 shows the tendency of CRB of estimation of azimuth φ that with the increasing of elevation (5 to 90 degree), the CRB of estimation of azimuth φ decreases. Theoretically, the LSA can have relatively poor performance in estimating azimuth when elevation is around 0 degree, which means the incident direction is perpendicular to x-y plane.

It is definite in figure 6.10 that the CRB of estimation of azimuth φ depends on azimuth as there are peaks when azimuths are -35 and 145 degree. Thus, it is acceptable to draw the conclusion in these cases that LSA is anisotropic and the relative weakness of azimuth estimation is the case when elevation is near 0 degree and azimuth is near -35 or 145 degree.

Based on CRB of estimation of azimuth φ analysis, the directivity of LSA in the estimation of azimuth φ was that the performance of azimuth estimation increased with the increasing incident elevation and was period with constant change of incident azimuth. Given an incident elevation, it would be worst performance in estimating azimuth φ when the incident azimuth was near -35

or 145 degree. This inference was identical with the geometric configuration of LSA as well.

Double L Shaped Array (DLSA)

In this section, we tried to demonstrate the directivity of DLSA in DOA estimation by their CRB of estimation which was calculated from constant various incident angles. In section 5.4.1, the configuration of DLSA was demonstrated. Here, in order to make simulation typical and simple, we assumed elements of DLSA displace on the positive axis of x, y and z axis, where four elements in each axis. Geometrically, it was not difficult to accept that DLSA is symmetric along axis $(45^0, 45^0)$. The simulation would get the CRB of estimating azimuth and elevation respectively.

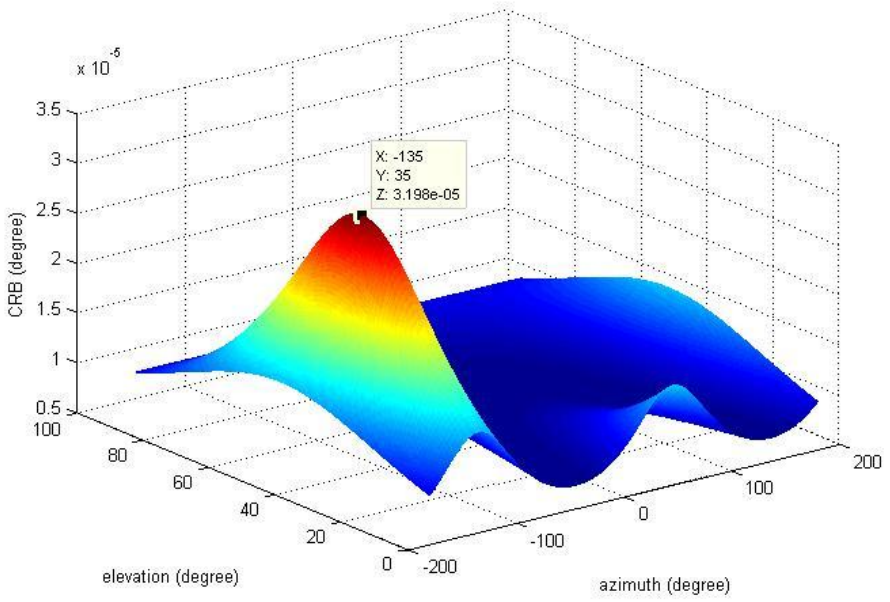

Figure 6.11 CRB (θ) of DLSA in DOA estimation

Figure 6.11 describes the relationship between CRB of estimation of elevation θ and various incident angles in DLSA. As figure 6.11 shows, the maximum magnitude of CRB is around 3.5×10^{-5}degree when the incident angle is around$(-135^0, 35^0)$. It is reliable to imply that the DLSA has relative worse performance in estimating elevation θ when φ is around -135 degree and

elevation is around 35 degree based on the peak of CRB of estimation of elevation θ shown in the figure 6.11.

According to this graph, it is fair to predict that DLAS is able to exactly estimate elevation of all incident angles, though a relative worse performance with incident angle $(-135^0, 35^0)$. Besides, the accuracy of estimation of elevation can displace coarsely isotropic along the axis$(-135^0, 35^0)$.

From the CRB of estimation of elevation θ analysis, the directivity of DLSA in the estimation of elevation θ was that the performance of elevation estimation decreased when then the incident angle comes to $(-135^0, 35^0)$ and the performance can be similar with other incident angles. This inference was different from the geometric configuration of DLSA that the symmetric axis was $(45^0, 45^0)$.

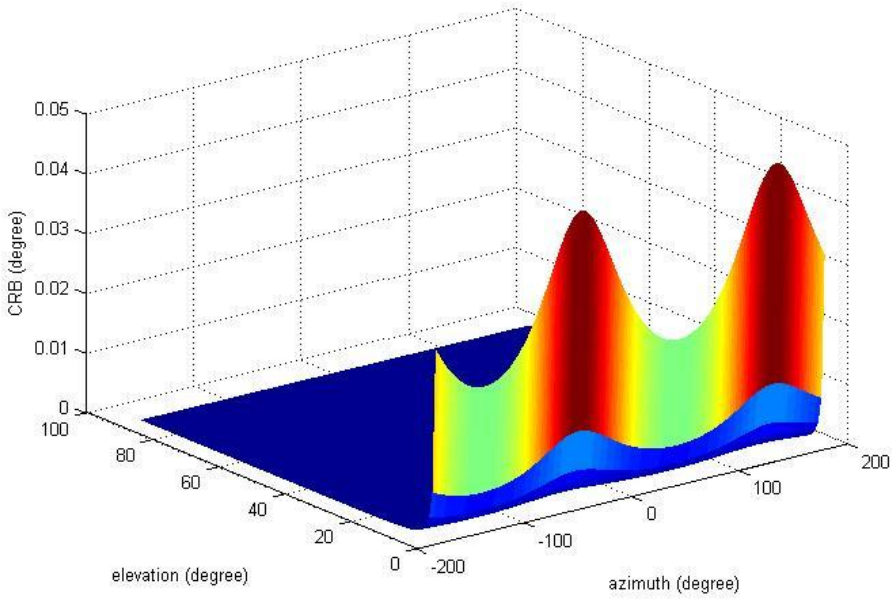

Figure 6.12 CRB (φ) of DLSA in DOA estimation

Figure 6.12 describes the relationship between CRB of estimation of azimuth φ and various incident angles in DLSA. As figure 6.12 shows, the maximum magnitude of CRB of estimation of azimuth φ is around 0.05 degree when the elevation is near 0 degree. In a general view, figure 6.12 shows the tendency of CRB of estimation of azimuth φ that with the increasing of elevation (5 to 90 degree), the CRB of estimation of azimuth φ decreases. Theoretically, the

DLSA can have relatively poor performance in estimating azimuth when elevation is around 0 degree, which means the incident direction is perpendicular to x-y plane.

The incident azimuth affects the performance, according to the graph. The CRB of estimation of azimuth φ depends on azimuth as there are peaks when azimuths are -45 and 135 degree. Thus, it is acceptable to draw the conclusion in this case that DLSA is anisotropic and the weak point of azimuth estimation is the case when elevation is near 0 degree and azimuth is near -45 or 135 degree.

According to the CRB of estimation of azimuth φ analysis, the directivity of DLSA in the estimation of azimuth φ was that the performance of azimuth estimation increased with the increasing incident elevation and was period with constant change of incident azimuth. Given an incident elevation, it would be worst performance in estimating azimuth φ when the incident azimuth was near -45 or 135 degree. This inference was identical with the geometric configuration of DLSA in some extent.

Double Uniform Circular Array (DUCA)

In this section, we tried to demonstrate the directivity of DUCA in DOA estimation by their CRB of estimation which was calculated from constant various incident angles. In section 5.4.2, the configuration of DUCA was demonstrated. Here, in order to make simulation typical and simple, we assumed elements of DUCA displace on the planes which were paralleled to x-y plane and z=0.25m and -0.25m respectively, where five elements located in each plane. Geometrically, it was not difficult to accept that DUCA was isotropic along z axis. The simulation could gain the CRB of estimating azimuth and elevation respectively.

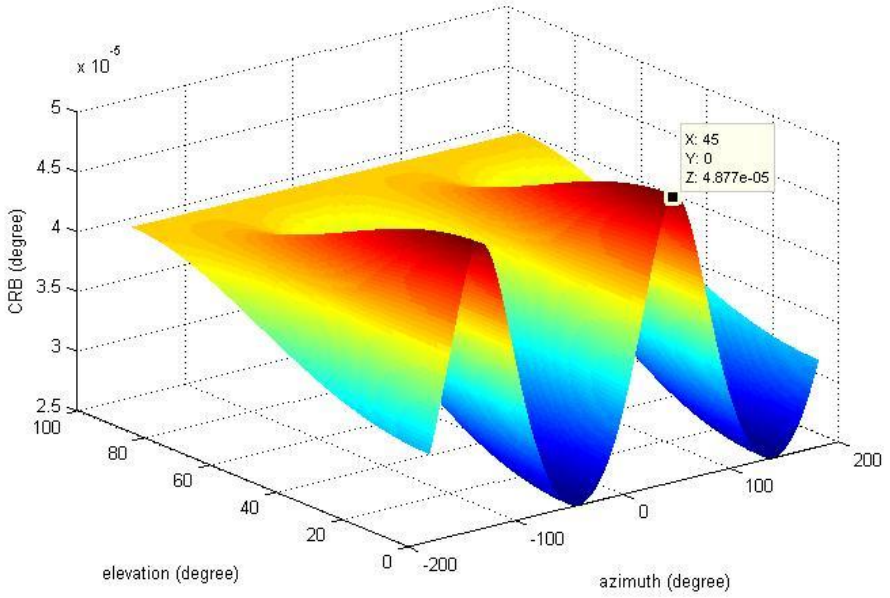

Figure 6.13 CRB (θ) of DUCA in DOA estimation

Figure 6.13 describes the relationship between CRB of estimation of elevation θ and various incident angles in DUCA. As figure 6.13 shows, the maximum magnitude of CRB is around 5×10^{-5}degree, when the incident azimuth is -135 or 45 degree and the incident elevation is around 0 degree. As we can figure out two peaks from the graph, these mean largest CRB of estimation of elevation θ values. Besides, the CRB of estimation of elevation θ trend to be the same with increasing elevation, not matter how azimuth changes.

According to figure 6.13, it was reliable to say that the DUCA had relative worse performance in estimating θ when azimuth φ was around -135 or 45 degree and elevation θ was around 0 degree. But, anyway, the DUCA was able to exactly estimate elevation of all incident angles, though the performance could be various with different incident angles.

As the simulation outcome of estimation of elevation θ in UCA showed, UCA was isotropic along the z axis in elevation estimation. Similarly, the DUCA should be isotropic along the z axis as well, which meant that the azimuth did not affect CRB of estimation of elevation θ. However, the simulation outcome that the performance of estimation of elevation θ depended on incident azimuth φ was conflict with the well accepted view and this was proved by the information shown in figure 6.13.

Reasons of the CRB of estimation depending on the azimuth could be the limitation of array elements or the inaccuracy of the equation 5.23, which did not consider all the conditions of configuration. In detail, there were only five elements in each circle plane in this case, and this number of array elements was not large enough to make the array isotropic along z axis in total. In contrast, the DUCA would have the isotropic along z axis property, if the number of elements was large enough.

Based on CRB of estimation of elevation θ analysis, the directivity of DUCA in the estimation of elevation θ was that the performance of difference in elevation estimation decreased with the increasing incident elevation and was period with constant change of incident azimuth. Given an incident elevation, it would be worst performance in estimating elevation θ when the incident azimuth was near -135 or 45 degree. This inference was different from the geometric configuration of DUCA.

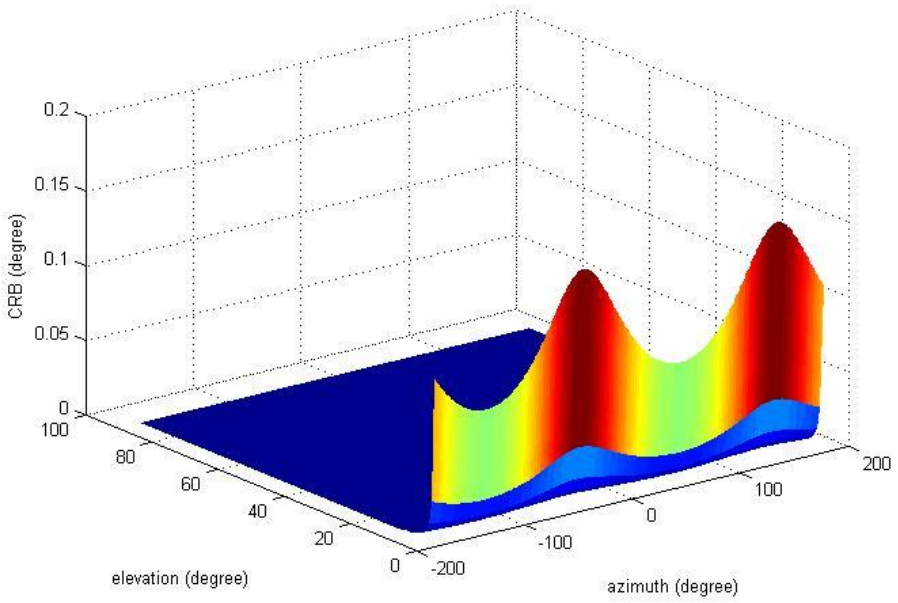

Figure 6.14 CRB (φ) of DUCA

Figure 6.14 describes the relationship between CRB of estimation of azimuth φ and various incident angles in UCA. As figure 6.14 shows, the maximum magnitude of CRB of estimation of azimuth φ is around 0.2 degree, when the elevation is near 0 degree. In a general view, figure 6.14 shows the tendency of CRB of estimation of azimuth φ that with the increasing of elevation (5 to 90

degree), the CRB of estimation of azimuth φ decreases. Theoretically, the DUCA can have relatively poor performance in estimating azimuth when elevation is around 0 degree, which means the incident direction is perpendicular to x-y plane.

The incident azimuth affects the performance, according to the graph. The CRB of estimation of azimuth φ depends on the azimuth as there are peaks when azimuths are -45 and 135 degree. Thus, it is acceptable to draw the conclusion in this case that DUCA is anisotropic and the weak point of azimuth estimation is the case when elevation is near 0 degree and azimuth is near -45 or 135 degree.

From the CRB of estimation of azimuth φ analysis, the directivity of DUCA in the estimation of azimuth φ was that the performance of azimuth estimation increased with the increasing incident elevation and was period with constant change of the incident azimuth. Given an incident elevation, it would be worst performance in estimating azimuth φ when the incident azimuth was near -45 or 135 degree. This inference was different from the geometric configuration of DUCA.

Conclusion

Generally, the directivity of estimation of above array geometries was identical with their geometric directivity. However, the directivity of estimation was different from geometric directivity in some cases, such as DUCA. From figure 6.13, where there are two periods rather than five periods in the diversion of azimuth according to the geometry, we can imply that equation 5.23 cannot demonstrate the CRB of array configurations exactly.

Also, according to the simulation and analysis mentioned above, we should make sure that the performance of estimation could be terrible when the elevation was near 0 degree or 90 degree. Therefore, we should try to prevent estimating signal with these incident angle not only in simulation but also in practice. When the elevation ranged from 10 to 80 degree, CRB value of estimation of various geometries located at a relative similar range and this range was called isotropic range by some researchers [2]. In this range, it was feasible to make further researches and comparisons of array geometries. It was

clear that we need take more differential geometries to analyze the directivity of the array geometry in further research.

6.2.2 Accuracy of array geometry

In this section, we tried to simulate the case that one signal with a particular incident angle impinges on various kind of array geometries and to research the accuracy by CRB and RMSE in this section. In order to set the same condition for all geometries, we should set all the conditions the same. We implemented MUSIC in all simulations is this section. Besides, the incident angle (φ, θ) denoted the azimuth and the elevation respectively.

CRB versus SNR

Here, the incident angle(φ, θ) is $(140°, 160°)$. The number of snapshot was 50, λ=1m and M=10. The CRB of UCA, LSA, DLSA and DUCA were shown in figure 6.15 and 6.16.

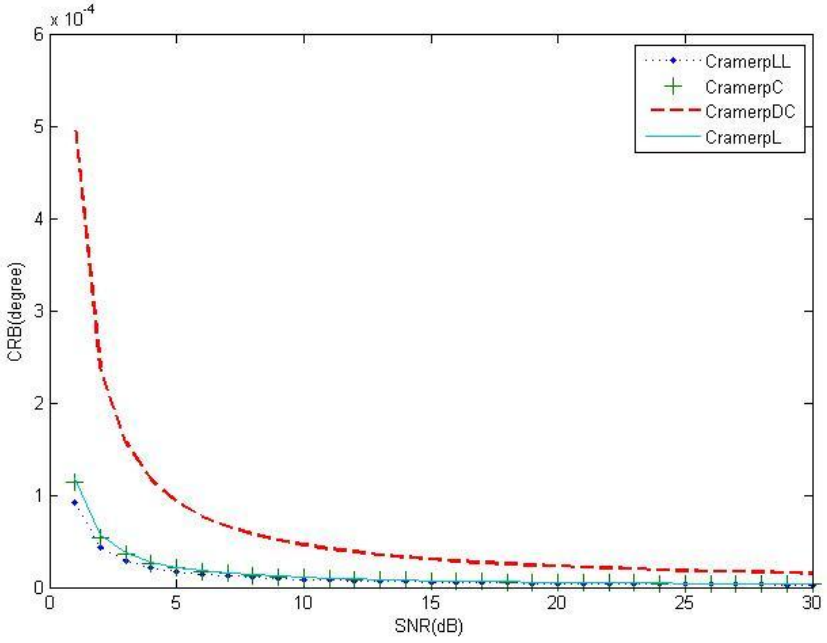

Figure 6.15 CRB (θ) of different array geometries versus SNR

Figure 6.15 demonstrates the relationship between the accuracy of elevation estimation and SNR. Here, CramerpLL, CramerpL, CramerpDC and CramerpC represent the Cramer-Rao Bound of elevation estimation of Double L Shaped Array, L Shaped Array, Double Uniform Circular Array and Uniform Circular

Array respectively. With this particular incident angle, we can find out the CRB of elevation estimation decreases with the incensement of SNR. In detail, performances of LSA, DLSA and UCA are better than DUCA's.

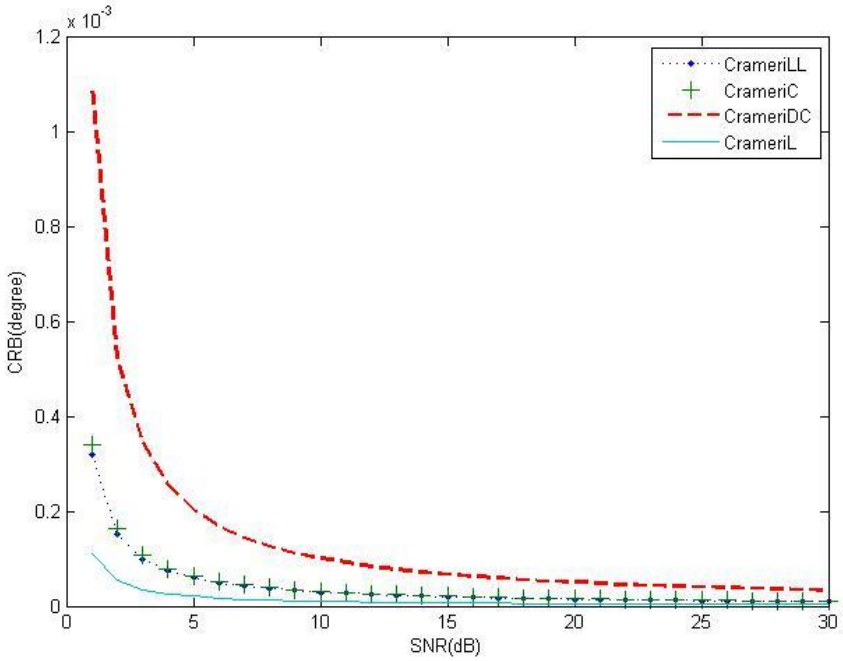

Figure 6.16 CRB (φ) of different array geometries versus SNR

Figure 6.16 demonstrates the relationship between the accuracy of azimuth estimation and SNR. Here, CrameriLL, CrameriL, CrameriDC and CrameriC represent the Cramer-Rao Bound of azimuth estimation of Double L Shaped Array, L Shaped Array, Double Uniform Circular Array and Uniform Circular Array respectively. With the particular incident angle, we can find out the CRB of azimuth estimation decreases with the incensement of SNR. Relatively, performances of LSA, DLSA and UCA are better than DUCA's, where the LSA has the best performance.

CRB versus snapshot

Similarly, the incident angle(φ, θ) was $(140°, 160°)$. SNR is 10dB, λ=1m and M=10. The CRB of UCA, LSA, DLSA and DUCA were shown in figure 6.17 and 6.18.

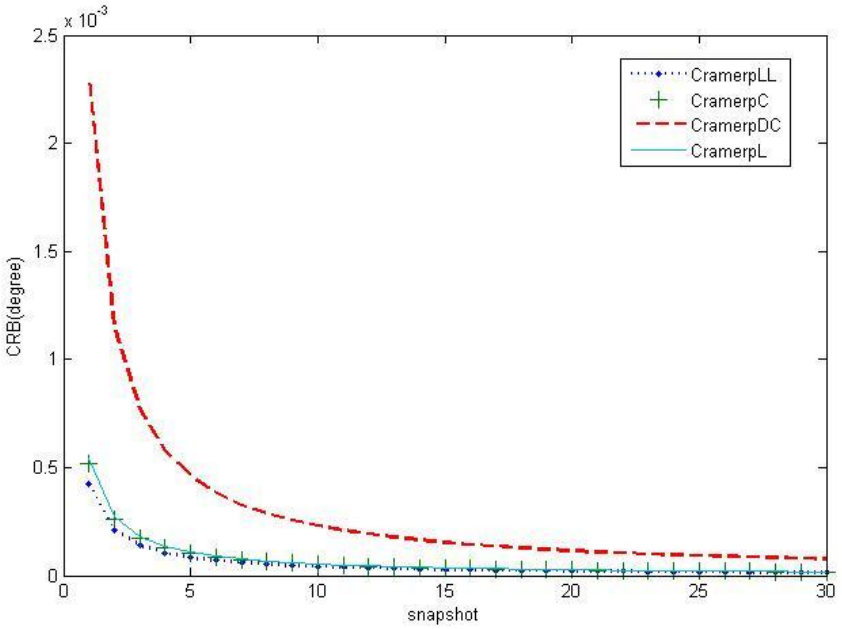

Figure 6.17 CRB (θ) of different array geometries versus snapshot

Figure 6.17 describes the relationship between the accuracy of elevation estimation and snapshot. Here, CramerpLL, CramerpL, CramerpDC and CramerpC represent the Cramer-Rao Bound of elevation estimation of Double L Shaped Array, L Shaped Array, Double Uniform Circular Array and Uniform Circular Array respectively. With this particular incident angle, we can find out the CRB of elevation estimation decreases with the incensement of snapshot. In detail, performances of LSA, DLSA and UCA are similar, but better than DUCA's.

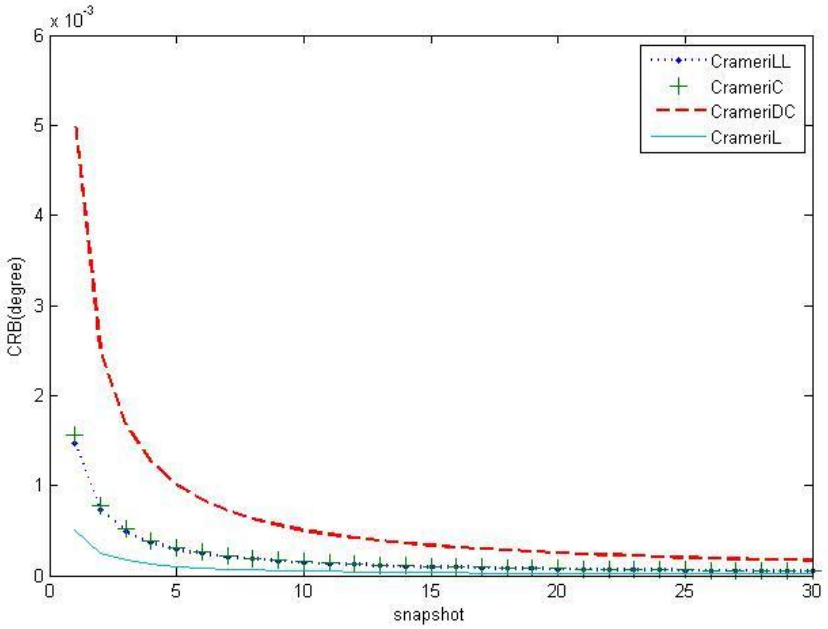

Figure 6.18 CRB (φ) of different array geometries versus SNR

Figure 6.18 explains the relationship between the accuracy of azimuth estimation and snapshot. Here, CrameriLL, CrameriL, CrameriDC and CrameriC represent the Cramer-Rao Bound of azimuth estimation of Double L Shaped Array, L Shaped Array, Double Uniform Circular Array and Uniform Circular Array respectively. With the particular incident angle, we can find out the CRB of azimuth estimation decreases with the incensement of snapshot. Relatively, performances of LSA, DLSA and UCA are better than DUCA's, where the LSA has the best accuracy theoretically.

Consequently, we could predict by the CRB performance that LSA, UCA and DLSA would have a good accuracy in simulation trials.

RMSE versus SNR

It was common to take RMSE as a measurement of accuracy as we did in this section. Here, the incident angle(φ, θ) was $(140°, 160°)$. The number of snapshot was 50 when SNR was a parameter, and SNR=10dB when snapshot was a parameter. The number of array elements was 10. The number of trials was an important factor, and definitely the more trials were the better outcome which was close to the true will be derived. In this simulation, we chose the number of trials as 500.

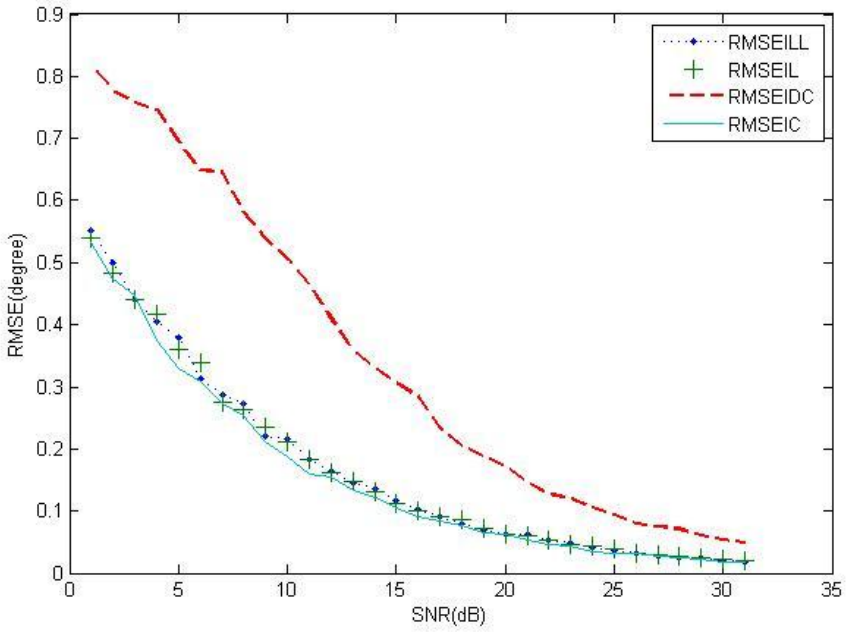

Figure 6.19 RMSE of elevation estimation of different array geometries versus SNR

Figure 6.19 demonstrates the relationship between the RMSE of elevation estimation and SNR. Here, RMSEILL, RMSEIL, RMSEIDC and RMSEIC represent the Root Mean Square Error of elevation estimation of Double L Shaped Array, L Shaped Array, Double Uniform Circular Array and Uniform Circular Array respectively. With this particular incident angle, we can find out the RMSE of elevation estimation decreases with the incensement of SNR, and it is the same with CRB. As for all SNR value, RMSEs of LSA, DLSA and UCA are smaller than DUCA's, and RMSEs of LSA, DLSA and UCA are similar meanwhile.

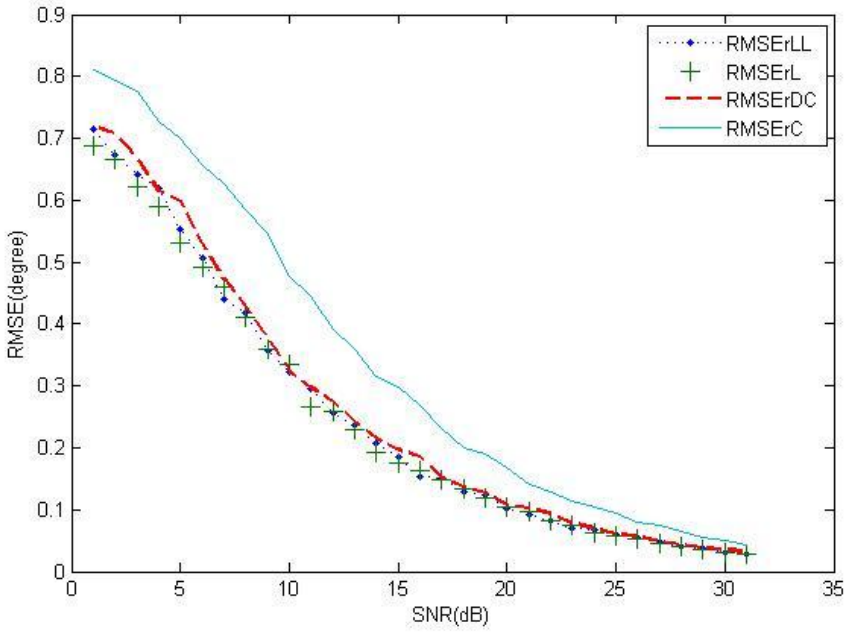

Figure 6.20 RMSE of azimuth estimation of different array geometries versus SNR

Figure 6.20 shows the relationship between the RMSE of azimuth estimation and SNR. Here, RMSErLL, RMSErL, RMSErDC and RMSErC represent the Root Mean Square Error of azimuth estimation of Double L Shaped Array, L Shaped Array, Double Uniform Circular Array and Uniform Circular Array respectively. With this particular incident angle, we can see that the RMSE of azimuth estimation decreases with the incensement of SNR, and it is the same with CRB. For all SNR value, RMSEs of LSA, DLSA and DUCA are smaller than UCA's, and RMSEs of LSA, DLSA and DUCA are similar, which is not the same with CRB shown in 6.16.

RMSE versus snapshot

Here, the incident angle(φ, θ) was $(140°, 160°)$. SNR=10dB and the number of array elements was 10. The number of trials was 500 as well.

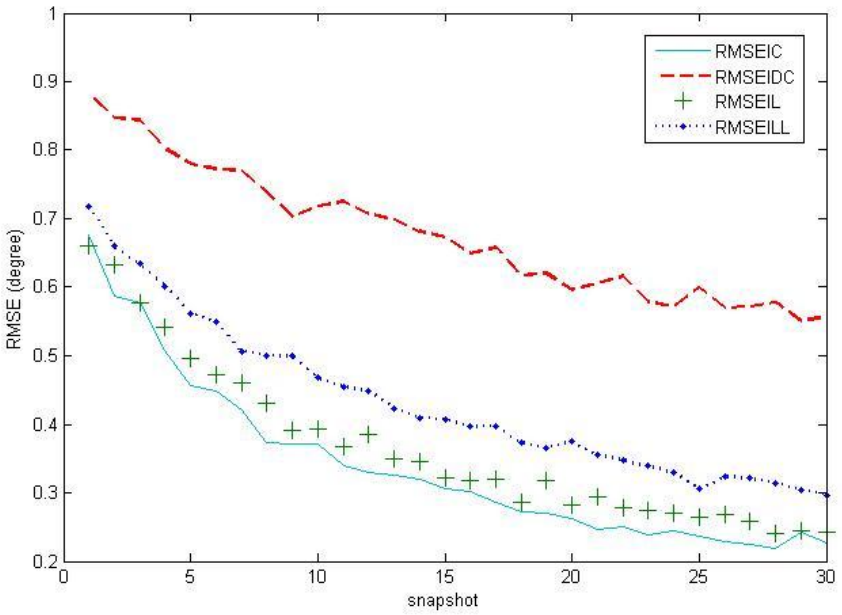

Figure 6.21 RMSE of elevation estimation of different array geometries versus snapshot

Figure 6.21 demonstrates the relationship between the RMSE of elevation estimation and snapshot. Here, RMSEILL, RMSEIL, RMSEIDC and RMSEIC represent the Root Mean Square Error of elevation estimation of Double L Shaped Array, L Shaped Array, Double Uniform Circular Array and Uniform Circular Array respectively. With this particular incident angle, we can find out the RMSE of elevation estimation decreases with the incensement of snapshot, and it is the same with CRB. As for all SNR value, RMSEs of LSA, DLSA and UCA are smaller than DUCA's, and UCA has the best RMSE performance.

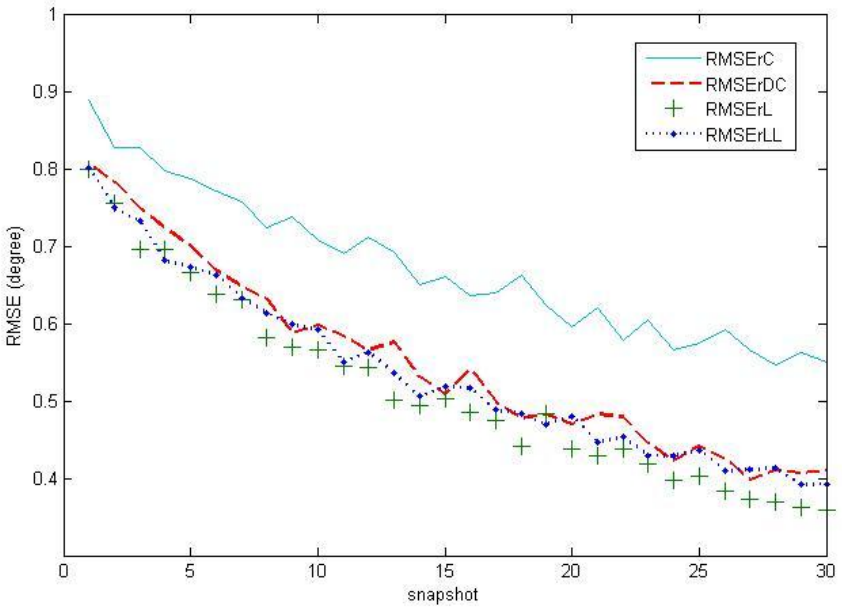

Figure 6.22 RMSE of azimuth estimation of different array geometries versus snapshot

Figure 6.22 demonstrates the relationship between the accuracy of azimuth estimation and snapshot. Here, RMSErLL, RMSErL, RMSErDC and RMSErC represent the Root Mean Square Error of azimuth estimation of Double L Shaped Array, L Shaped Array, Double Uniform Circular Array and Uniform Circular Array respectively. With this particular incident angle, we can see that the RMSE of azimuth estimation decreases with the incensement of snapshot, and it is the same with CRB. For all SNR value, RMSEs of LSA, DLSA and DUCA are smaller than UCA's, and RMSEs of LSA, DLSA and DUCA are similar, which is not the same with CRB shown in 6.18.

Conclusion

In general, as for this particular incident angle, accuracy performances of LSA and DLSA were better than the other two array geometries, because they were excellently adapted to both elevation and azimuth estimation. It was not hard to accept their adaptable performance, because DLSA had at least two sub arrays (one for LSA) to receive signals with whatever incident angles.

Though UCA was isotropic to azimuth, the accuracy of azimuth estimation was worst in simulation. The particular incident angle could be a possible reason of the good performance in elevation estimation but poor performance in azimuth

estimation. The further feasible analysis needed the help of differential geometry.

In this dissertation, we implemented DUCA in simulation and proved its poor accuracy. In a more general word, we could predict that array geometries, whose elements maybe prevented the signal from other elements, would not perform as good as those whose elements did not. e.g., the element of a cube shaped array would disturb other elements with 45 degree elevation and a particular azimuth.

6.2.3 Resolving ability

In this section we tried to research the detection ability of array geometries. Here, we defined the detection ability as the ability to generate the exact peak in the $P_{MU}(\theta)$ graph, which was demonstrated in 4.2. In the simulation, if the estimation angle was near the incident angle within 3 degree (both azimuth and elevation), and the peak value was more than three times of the mean of $P_{MU}(\theta)$, we would regard the detection as successful. The incident angle(φ, θ) was $(140°, 160°)$ in this case.

Resolving ability versus SNR

In the simulation, the snapshot number was 1, and the elements number was 10. SNR ranged from 1 to 20 dB. We made 50 trials in each SNR.

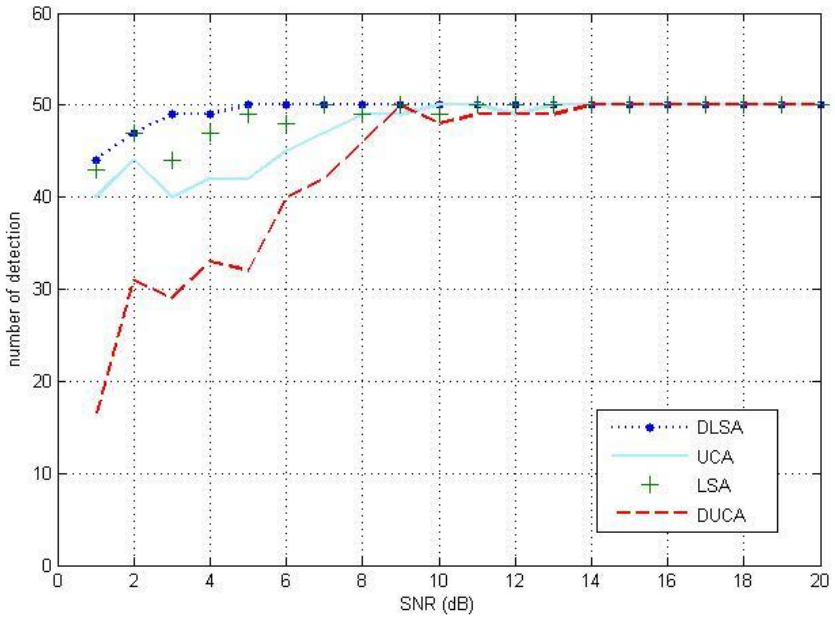

Figure 6.23 the number of detection versus SNR

From the figure 6.23, we can figure out that DLSA has the best ability to resolve the signal, regardless of the accuracy. The resolving ability of LSA and UCA is acceptable even in poor condition, which means low SNR and low snapshots number. The DUCA is not good at the DOA estimation in low SNR case.

Resolving ability versus snapshot

In the simulation, the SNR was 0 dB, and the elements number was 10. The number of snapshots ranged from 1 to 20. We made 50 trials in each SNR.

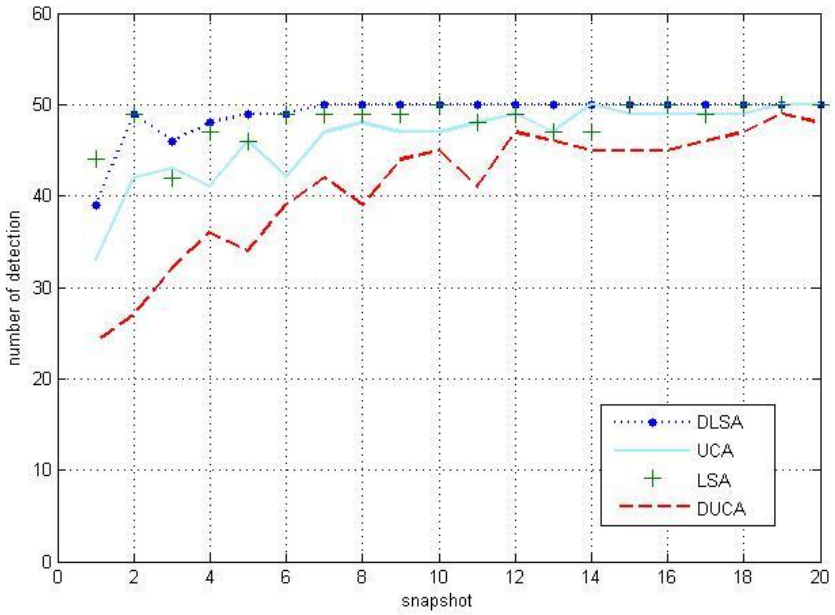

Figure 6.24 the number of detection versus snapshot

From the figure 6.24, we can figure out that DLSA has the best ability to resolve the signal, in the low snapshots number condition. The resolving ability of LSA and UCA is acceptable even in poor condition, which means low SNR and low snapshots number. The DUCA is not good at the DOA estimation in low SNR case.

Conclusion

According to the simulation is this section, it was fair to say that DLSA had a good performance in signal resolving. Here, the snapshot number decided the reaction time. e.g., the estimation could be made as once, if the number of snapshot was. As we known, SNR meant the ratio of signal power to noise power, and good resolving ability in low SNR represented the big chance to detect the signal in a noisy condition.

6.3 Conclusion and comparison

In this section, we simulated MUSIC, Root-MUSIC and ESPRIT with ULA of one dimension in 6.1 and various array geometries with MUSIC of two dimensions in 6.2.

From the simulation of these three algorithms, we could get the conclusion that MUSIC a good accuracy, which was better than ESPRIT and Root-MUSIC, and ESPRIT, had the best computation efficiency.

From the analysis of array geometry, in general, we could declare that DLSA had good performance in the aspects of both accuracy and detection ability. Furthermore, the LSA and UCA were acceptable in the accuracy and detection ability test, and it meant that these two kinds of array geometries were able to be used in other researches. We must note that DUCA has relative poor property in almost all simulation in this section.

6.4 Reference

[1]Harabi F., Gharsallah A., Marcos S., "Three-dimensional antennas array for the estimationof direction of arrival", Microwaves, Antennas & Propagation, IET Volume: 3, Issue: 5, Page(s): 843 – 849, 2009.

[2]Baysal U., Moses R.L., "On the geometry of isotropic arrays", Signal Processing, IEEE Transactions on volume: 51 , Issue: 6 Page(s): 1469 – 1478, 2003.

Chapter7 Conclusion and Future work

Previous chapters have analyzed eigendecomposition algorithms and array geometries. In this chapter, we will draw a conclusion of the whole dissertation and make a plan for the further research.

7.1 Conclusion

In this dissertation, we researched the algorithms of Direction of arrival estimation and array geometries. In chapter 2, we demonstrated the problem which was concerned in this dissertation. Then the chapter 3 described some background knowledge of DOA estimation. Some DOA estimation algorithms were expressed in chapter 4 and we analyzed various array geometries in chapter 5. The chapter 6 showed the simulation of the problem discussed in this dissertation and we draw the conclusion in this chapter. Based on the research of this dissertation, we could get some conclusion.

ESPRIT was the most efficient algorithm in these three algorithms. This was because ESPRIT was proposed in order to promote the computation efficiency from MUSIC, sacrificing a part of accuracy.

MUSIC had the best accuracy in these three algorithms.

In the case of plane array, L Shaped Array (LSA) and Uniform Circle Array (UCA) had acceptable properties in DOA estimation.

Double L Shaped Array (DLSA) had an unexpected ability in signal detection. DLSA showed an amazing adaptability to all kinds of incident angle.

7.2 Future work

It is true that this dissertation is not a perfect research of DOA estimation algorithms or array geometries. There are large number of places where can further the research.

Firstly, we will further the research of DOA estimation. In detail, there will be lots of algorithms of DOA other than MUSIC, Root-MUSIC and ESPRIT, which will be taken into account in future. Moreover, definitely, MUSIC,

Root-MUSIC and ESPRIT have the potential to develop, as some researchers did. MUSIC, Root-MUSIC and ESPRIT are Eigen vector decomposition (EVD) methods, which is only one way to exploit the information of the data, and there are other ideas of processing the data in DOA estimation.

Secondly, the array geometry is a new research area proposed in the last decade. Obviously, there will be new spaces, which are worth to be researched, everywhere in array geometry study. Practically, the simulation of the array directivity is available to be made. Furthermore, some array geometries changed from DLAS is interesting and we can further the research in this area. It is clear that the directivity, accuracy and detection ability are just some aspects of the study of array geometry. Also, it is possible to use differential geometry to analyze the array configuration in the future work.

Thirdly, in this dissertation, idealized antenna models are used, but, in real case, the directivity of the antenna elements and the mutual coupling between them may affect the DOA estimation outcomes. Therefore, we will take account the mutual coupling between elements in the implement of accurate DOA estimation in further research.

In general, the array geometry in DOA estimation, even in beam forming, is an interesting area and it is well worth further research in array geometry.